Study on Hydrodynamic Instability-based Critical Heat Flux Enhancement Mechanism of Nanofluids and Liquid Metal Fin Concept

Seong Dae Park

School of Mechanical & Nuclear Engineering

Graduate School of UNIST

2015

Study on Hydrodynamic Instability-based Critical Heat Flux Enhancement Mechanism of Nanofluids and Liquid Metal Fin Concept

A dissertation

submitted to the Graduate School of UNIST

in partial fulfillment of the

requirements for the degree of

Doctor of Philosophy

Seong Dae Park
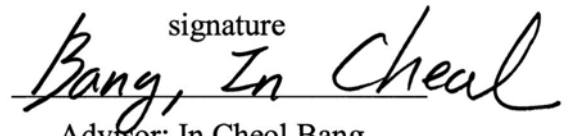
01.16.2015

Approved by

_____

Advisor

Prof. In Cheol Bang

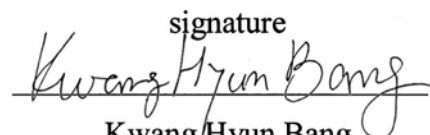# Study on Hydrodynamic Instability-based Critical Heat Flux Enhancement Mechanism of Nanofluids and Liquid Metal Fin Concept

Seong Dae Park

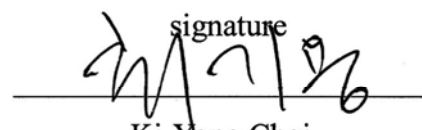This certifies that the dissertation of Seong Dae Park is approved.
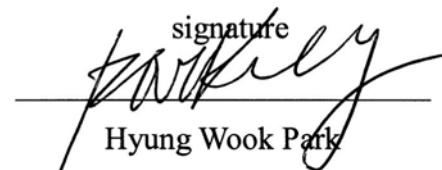
01.16.2015

signature

Bang, In Cheol

Advisor: In Cheol Bang

signature

Kwang Hyun Bang

Kwang Hyun Bang

signature

Ki-Yong Choi

signature

Ji Hyun Kim

signature

Hyung Wook Park

Abstract

In the light water reactors, a number of safety systems have been installed to prevent the progression of the accidents and return to the safety condition. The CFD (core damage frequency) is low enough like $1.0E^{-4}$/RY and $1.0E^{-5}$/RY for OPR-1000, APR-1400 respectively due to the safety systems. However, although the safety systems have been established in the plants, some severe accidents happened. If the prevention of severe accident is absolutely impossible, it is required to terminate the progression of severe accidents through the power cooling system.

While the molten fuel was adequately cooled and certainly retained in reactor vessel in the TMI nuclear accident, the molten fuel was escaped from the reactor vessel in the Fukushima nuclear accident. The different results between TMI and Fukushima accidents give one of the most important lessons that the integrity of reactor vessel should be protected to minimize the spreading of radioactive material. It is called as in-vessel retention (IVR) or in-vessel corium confinement and cooling. One of the effective features for the IVR is an external reactor vessel cooling (ERVC) strategy. In general, ERVC strategy gives sufficient thermal margin for small and medium-sized reactors like AP600 and AP1000. However, it is not certain whether the IVR-ERVC strategy provides enough thermal margin to prevent CHF phenomenon even for large-sized nuclear power plants. In this study, the nanofluid and liquid metal was presented as flooding material to ensure the safety margin to CHF.

Nanofluid is a colloidal with dispersed nanoparticles. It is known that the nanoparticle coated layer induced by boiling was formed on heat surface. One of the most interesting characteristics of nanofluids is their capability to enhance CHF significantly at relatively dilute concentrations due to this layer. In this work, specific pool/flow boiling test facilities were designed for IVR-ERVC test. In pool boiling test, a variety of factors related to CHF were invested. The graphene oxide (3500~5300 W/mK), Al_2O_3 (30 W/mK), SiO_2 (1.3 W/mK) nanofliuds were selected and prepared basis on the thermal conductivity. CHF tests of the pool boiling were conducted to select the prospective candidate for improved IVR-ERVC. The graphene-oxide nanofluid shows the highest enhancement (195 %) in term of CHF value. The effects of the heater inclination on CHF were investigated. The CHF enhancement ratio was decreased as the heater inclination was increased. The coolant contains the boric acid (H_3BO_3, 5000ppm), lithium hydroxide (LiOH, 3ppm) and tri-sodium phosphate (TSP, $Na_3PO_412H_2O$, saturation). These chemicals were added to working fluid to make the real plant situation. Although highly-concentrated chemicals have some influences on CHF enhancement, the graphene oxide nanofluid is dominant factor to enhance the CHF.

After boiling tests, a nanoparticles coated layer was observed on the heater surface. The enhancement of CHF is related to the buildup of a deposition layer of nanoparticles on the heater surface. The main reason of CHF enhancement is explained as increased wettability in many experiments. Reverse results

I

were observed when the graphene oxide was coated on the heater surface. Some models related to improved wettability for nanofluids were limited to explain this unique case. A hydrodynamic instability theory is a traditional model to predict the CHF for pool boiling. Kevin-Helmholtz and Rayleigh-Taylor instabilities were included to establish the theoretical ground in this model. The test heater were designed and prepared to allow direct observation of the Rayleigh-Taylor wavelengths. Higher CHF results have shorter Rayleigh-Taylor wavelengths in all cases. The experimental correlation was presented based on experimental data from observing the Rayleigh-Taylor wavelengths. After analyzing the experimental results and conclusions about pool boiling, the flow boiling CHF tests were designed and conducted.

The test facility was designed to be scaled-down to 1/25 of APR-1400 dimension. Under the ERVC situation, the natural circulation occurs between the reactor vessel outer wall and the surrounding insulation. To simulate this condition, a pump was used to control the mass flux passing over the heater surface. Working fluids are he graphene oxide (3500~5300 W/mK), Al_2O_3 (30 W/mK), SiO_2 (1.3 W/mK) nanofliuds. Graphene oxide nanofluid show the highest CHF enhancement at 50 kW/m^2 mass flux condition. The ratio of the CHF enhancement was about ~80% compared with the case of water under the same conditions. As the mass flux is increased, the ratio of CHF enhancement is also increased. The parameters were the RT wavelength and the advancing contact angle. The effects of these parameters were confirmed with a 3-dimensional hemispherical geometry facility.

Flooding the liquid metal into reactor vessel cavity was proposed and studied to ensure the safe margin for IVR-ERVC strategy. The heat transfer mode is a single-phase heat transfer due to the high boiling point of liquid metal. It allows to remove the decay heat on IVR-ERVC strategy without the concern about CHF. The SWOT (strengths, weaknesses, opportunities, and threats) analysis was conducted to evaluate the IVR-ERVC. Some research approaches were conducted to overcome the weaknesses of liquid metal flooded IVR-ERVC. Improved heat transfer or reduced heat flux was confirmed by experimental results for a small-scaled facility to simulate the boiling phenomena under IVR-ERVC condition. The heat transfer area could be enlarged over 2 times on the basis of the original area for the reactor vessel. This phenomenon was named as "liquid metal fin". The capability of heat removal was determined by some factors. The maximum heat flux was reduced about 3 times compared with that of the case without liquid metal.

A number of power plant has been operated to satisfy energy demand. The nuclear power plants makes the large amount of energy constantly and easily. It is impossible to stop the operation of the nuclear power plants based on this situation. Consequently, it is required to construct and operate more reliable nuclear plants in order to protect the human, public and the environment from radiological hazards. IVR-ERVC strategy is the effective way to terminate the progression of severe accidents. Flooding the graphene oxide nanofluid and the gallium liquid metal could improve the IVR-ERVC strategy.

Contents

List of figures

List of table

Nomenclature

a	maximum amplitude of the wave	[m]
A	heat transfer area	[m^2]
c	specific heat	[Jkg^{-1}K^{-1}]
D	diameter	[m]
f	bubble departure frequency	[s^{-1}]
g	acceleration due to gravity	[m/s^2]
h	latent heat	[J/kg]
I	current	[A]
k	thermal conductivity	[Wm^{-1}K^{-1}]
L	heating element length	[m]
n	nucleation site density	[m^{-2}]
q"	heat flux	[kW/m^2]
R	electric resistance	[ohm]
Q	power	[kW]
S	thermal activity	[$\delta\,(\rho c k)^{1/2}$]
V	voltage	[V]

Greek symbols

φ	particle fraction	[%]
ρ	density	[kg/m^3]
θ	angle	[degree]
ε	porosity	
ρ	density	[kg/m^3]
σ	surface tension	[N/m]
φ	fraction of mass	[%]
λ	wavelength	[m]
δ	thickness	[m]

Subscripts

b	bubble
c	critical
CHF	critical heat flux
d1	1-dimension
d2	2-dimension
f	fluid
fg	vaporization
g	gas
h	heater
KH	Kelvin-Helmholtz
m	mass
p	nanoparticles
po	pore
RT	Rayleigh-Taylor
s	system
th	theoretical
v	volume
w	wire
Z	Zuber

Chapter 1. Introduction

1.1 Background

In-vessel retention through external reactor vessel cooling (IVR-ERVC) is a concept to retain the molten core in the reactor vessel under the event of a severe accident. It has been applied in some advanced light water reactors (ALWRs) such as AP600, AP1000 and APR1400. When the core is melted and relocated into the bottom of the reactor vessel, the IVR-ERVC system begins to flood the reactor cavity to remove the generated decay heat. IVR-ERVC system has some advantages such as preventing the escape of radioactive materials and simplifying the accident scenario. Success of this system could lead to retain the molten fuel in the reactor vessel. IVR-ERVC system could remove the concerns about the ex-vessel progression of a severe accident like the direct containment heating (DCH), ex-vessel fuel-coolant interaction (FCI) and molten core concrete interaction (MCCI) which are complicated and still uncertain[1]. The main heat transfer is boiling in IVR-ERVC system. There should be enough thermal margin to CHF in this system. Improper heat removal leads to the failure of the reactor vessel. The geometry of reactor vessel is down-facing hemisphere. It is unfavorable to remove the heat by boiling on the vessel outer wall. Additionally, there are very interesting phenomena in the corium configuration, which is a focusing effect caused by a thin metallic layer in the corium pool. This layer makes high heat flux on the corresponding vessel outer wall due to the limited radiation heat transfer on the exposed top surface. It makes precarious situation when the thickness of the metallic layer is thin. It leads to a tremendous heat flux which is an incapability to carry out the heat transfer. Therefore, it is essential to obtain an enough safety margin in terms of CHF values. Up to now, a few investigations have been performed to evaluate and increase the coolability of ERVC.

1.2 General literature survey

A few investigations have been performed to evaluate and increase the coolability of ERVC.

Chu et al.[2] presents the results of quenching experiments with a large downward-facing surfaces. The boiling curve was obtained by analyzing the temperature data. The critical heat flux is about 500 kW/m^2. In real plant, the heat flux profile according to the surface of reactor vessel is unique at IVR-ERVC cooling conditions. This condition was not considered in quenching experiments.

Chu et al.[3] summarizes the results of a reactor-scale ex-vessel boiling experiment for assessing the flooded cavity design. The diameter of simulated reactor vessel is about 3.7 m. The boiling process exhibits a cyclic pattern with four distinct phases: direct liquid-solid contact, bubble nucleation and growth, coalescence, and vapor mass dispersion. In this paper, the effectiveness of the flooded cavity

for the central region of the lower head of an AP-600 advanced light water reactor was confirmed with the present design.

Rouge et al.[4, 5] used the SULTAN facility to study the coolability in the large-scale. The tests were performed to evaluate the recirculation mass flow in large systems, and the limits of the critical heat flux (CHF) for a wide range of thermal-hydraulic (pressure, inlet temperature, mass flow velocity) and geometric (gap, inclination) parameters. The empirical correlation for an evaluation was derived from the test results.

A US–Korean International Nuclear Energy Research Initiative (INERI) project had been initiated in which the Idaho National Engineering and Environmental Laboratory (INEEL), Seoul National University (SNU), Pennsylvania State University (PSU), and the Korea Atomic Energy Research Institute (KAERI) determined if IVR is feasible for reactors up to 1500MWe. Rempe et al.[6] presents the summarized results from the first year of a 3-year project. If it is possible to ensure that the vessel lower head remains intact so that relocated core materials are retained within the vessel, the enhanced safety associated with these plants can reduce concerns about containment failure and associated risk.

Yang et al.[7] presents the experimental results about the effects of surface coating and an enhanced insulation structure on the downward facing boiling process and the critical heat flux on the outer surface of a hemispherical vessel. Steady-state boiling tests were conducted in the Subscale Boundary Layer Boiling (SBLB) facility using an enhanced vessel/insulation design for the cases with and without vessel coatings. For the case with thermal insulation, the local CHF limit tended to increase from the bottom center at first, then decrease toward the minimum gap location, and finally increase toward the equator. This behavior differed from the case without thermal insulation. The flow channel was determined when the thermal insulator was installed. The flow path for the two-phase was limited in this situation. The velocity of the two-phase flow would be increased and have a positive effects on the CHF enhancement.

Yang et al.[8] conducted the experiments to investigate the viability of using an appropriate vessel coating to enhance the critical heat flux (CHF) limits during ERVC. Transient quenching and steady-state boiling experiments were performed in the subscale boundary layer boiling (SBLB) facility at the Pennsylvania State University using test vessels with micro-porous aluminum coatings. Local boiling curves and CHF limits were obtained in these experiments. The heat transfer performance of the coatings was found to be desirable with an appreciable CHF enhancement in all locations on the vessel outer surface. The formation of previous coating layer before flooding the coolant in the reactor cavity has some issues. The CHF enhancement should guarantee with an original quality of coating layer. There are some chances to damage the coating layer during the operating period of the plant.

Remp et al.[9] reviewed efforts reported regarding the enhancement of IVR-ERVC in LWRs. In the severe accidents, relocated core materials are retained within the vessel, the enhanced safety associated with these plants can reduce concerns about containment failure and associated risk. Nuclear Regulatory

Commission approving the design without requiring that certain features common to existing LWRs, such as containment sprays, be safety related. ERVC offers the potential to reduce the AP600's construction and operating costs. It is not clear that the ERVC proposed for the AP600 could provide sufficient heat removal for higher-power reactors without additional enhancements.

Theofanous et al.[10] carried out the input parameters regarding the IVR-ERVC strategy in AP600. The assessment includes consideration of bounding scenarios and sensitivity studies, as well as arbitrary parametric evaluations that allow for the delineation of the failure boundaries. The results of the assessment demonstrate that lower head failure is physically unreasonable. Recently, IVR-ERVC system is well known for having the enough thermal margin in small and medium size reactor. This paper contributed to provide this conviction.

Theofanous and Syri[11] provide some experimental results of ULPU series facilities. These facility afford full-scale simulations of the boiling crisis phenomenon on the hemispherical lower head of a reactor pressure vessel submerged in water. Whereas Configuration I experiments (published previously) established the lower limits of coolability under low submergence, pool-boiling conditions, with Configuration II we investigate coolability under conditions more appropriate to practical interest in severe accident management; that is, heat flux shapes (as functions of angular position) representative of a core melt contained by the lower head, full submergence of the reactor pressure vessel, and natural circulation. Additionally, with Configuration III, we examine the effect of a channel-like geometry created by the reactor vessel thermal insulation. Critical heat fluxes as a function of the angular position on the lower head are reported and related to the observed two-phase flow regimes.

Dinh et al.[12] presents the concerns about two-phase flow regimes and characteristics of coolant natural circulation around a reactor pressure vessel (RPV) in in-vessel retention (IVR) scenarios when the external vessel flooding is applied to arrest a hypothetical core melt accident. Target reactor is the AP1000 advanced plant design. This paper presents a synthesis of experimental results obtained in the ULPU-V facility, which simulates the AP1000 reactor geometry.

Park et al.[13] measured the critical heat flux (CHF) on the top part of the reactor vessel lower head external wall. The purpose of this study was to produce experimental data to assess the CHF limits on the top of the external vessel wall for the metal layer and investigate the geometric scaling effect on the CHF. The material of the test section was type 304 stainless steel (SUS304). The CHF results were acquired under an inlet subcooling of 2 and 10 K with mass fluxes between 50 and 400 kg/m2 s. CHF correlations were developed with the data from this study.

Jeong and Chang[14] conducted the test to evaluate the heat removal capability in IVR-ERVC condition. The area of the flow channel and the dimension of the heater width were smaller than those of the ULPU experiments, the general trend of CHF according to the mass flux was similar with that of the ULPU. The SULTAN correlation predicted well this study's data only for the mass flux higher than 200 kg/m^{2}s, and for the exit quality.

1.3 Objectives and scope

This manuscript concentrates on 1) improvement of heat removal capacity using the nanofluid and 2) introduction of innovative IVR-ERVC system with liquid metal flooding condition.

1) To evaluate the limitation of heat removal capacity for IVR-ERVC system when the nanofluid was used as working fluid

2) To establish an experimental correlation about the CHF prediction in IVR-ERVC with nanofluid

3) To conduct the parameter study on gallium liquid metal flooding condition

4) To model the gallium liquid metal IVR-ERVC system to obtain the optimized flooding condition

The introduction of this study is described in chapter 1. General literature survey about the IVR-ERVC system is conducted.

In chapter 2, pool boiling test results and discussion are described. Using nanofluid as working fluid was introduced to improve the thermal limitation of the IVR-ERVC system. Various nanofluid (graphene oxide, Al_2O_3, SiC, SiO_2) was studied to increase the CHF at 10^{-3} vol.%. After boiling test, heater surface characteristics were analyzed to investigate the reasons for CHF enhancement. The effects of the coolant chemical condition were studied. The dispersion stability of nanoparticles was evaluated to determine the application of nanofluid in the nuclear power plant.

In chapter 3, modified hydrodynamic CHF prediction model was presented based on the experimental results. The surface wetting is improved when the nanoparticles were deposited. However, the case of graphene oxide nanofluid is different in comparison with the cases of other nanofluids. Modified hydrodynamic CHF prediction model was established in order to apply the correlation in all nanofluid cases.

In chapter 4, flow boiling test results and discussion are described. Although the flow was generated by natural convention in real IVR-ERVC system, the flow rate is relatively high due to the larger structure scale and a significant amount of heat. To simulate the flow condition, a pump was used in this test. The bubble behavior was analyzed to predict the CHF in flow boiling test. The hydrodynamic instability information obtained pool boiling tests was used to predict the CHF.

In chapter 5, the application of liquid metal was investigated to improve the IVR-ERVC system. The CHF issues are caused from locally high heat flux on the reactor vessel under the severe accidents. When the liquid metal was flooded in surrounding of reactor vessel, the maximum heat flux could be reduced. Overall consideration to apply the liquid metal was described in this chapter. The experimental results show the prevention of CHF occurrence clearly.

The conclusions and recommendations are described in chapter 6.

Chapter 2. POOL BOILING CHF EXPERIMENTS

2.1 Introduction

The concept of the in-vessel retention (IVR) for the molten core has been adopted in the advanced light water reactors (ALWRs) such as AP600, AP1000, and APR1400. One of this concept is In-vessel retention through external reactor vessel cooling (IVR-ERVC). The heat removal of ERVC is restricted by thermal limit called by critical heat flux (CHF). Besides, the power capacity of the nuclear power plants has been increasing for the economics. This trend causes the decrease of the thermal safety margin. The flooded water is obtained from the plant itself. In APR1400, flooded water comes from the reactor coolant system (RCS) or the in-containment refueling water storage tank (IRWST). The water in RCS and IRWST contains the boric acid (H_3BO_3, 5000ppm), lithium hydroxide (LiOH, 3ppm) and tri-sodium phosphate (TSP, $Na_3PO_412H_2O$, saturation). These chemicals have their own functions such as neutron absorption, pH control and capturing fission gas under proper concentrations in solution to nuclear applications, respectively. The nanoparticles would be suspended in this coolant to enhance the CHF margin. There are some candidate as dispersed nanoparticles. These candidates should get the stable dispersion characteristics in the coolant. The purpose of this study is to report the integral effects of the nanofluid and chemicals on CHF limits to evaluate the nanofluid in IVR-ERVC system.

2.1.1 Inclination effect

The first to correlate the effect of orientation on q_{CHF}'' was established by Vishnev[15]. His correlation was developed for cryogenic fluids based on the helium data of other researchers. This are established according to which the critical boiling mode changes with the orientation of the hot surface.

Quenching experiments investigating transient pool boiling from the underside of inclined and downward facing flat surfaces in saturated water were performed[16, 17]. Inclination angles investigated are 0 °, 5 °, 10 °, 15 °, 30 °, 45 ° and 90 ° (vertical). While transition boiling heat flux increased as the inclination angle was increased, nucleate boiling heat flux decreased. The values of q_{CHF}'' and q_{min}'' and the corresponding wall superheats are correlated as functions of the inclination angle. In addition, the steady-state q_{CHF}'' data of other investigators for saturated helium and nitrogen are correlated as a function of inclination angle.

2.1.2 Additives effect

Kwark et al.[18] studied the effects on pool boiling heat transfer of aqueous solutions of boric acid (H_3BO_3) and sodium chloride (NaCl) as working fluids. The pool boiling tests were conducted using 1

x 1 cm^2 flat heaters at 1 atm. The critical heat flux (CHF) increased compared to boiling pure water. At the end of boiling tests it was observed. The boric acid and NaCl coatings disappeared after repeated boiling tests on the same surface in pure water. The flooding water of reactor cavity is the coolant. The coolant always includes the Boric acid and sodium chloride. Additional CHF enhancement could be expected.

Jeong et al.[19] conducted the CHF test and analyzed the wettability of the heated surface under pool boiling of surfactant solutions and nanofluids has been investigated. Tri-sodium phosphate (TSP, Na_3PO_4) solutions (0.01, 0.05, 0.1, 0.3, 0.5, 0.8 wt.%) and aluminum oxide (Al_2O_3) nanofluids (0.5, 1, 2, 4 vol.%) were prepared for experiments. Stainless steel heated strips were quenched in the prepared solutions. Contact angles of pure water and the solutions on the quenched surface and fresh surface were measured. Surfaces deposited TSP and nanoparticle could affect surface energy of the strips and enhance hydrophilicity of the surfaces. Several implications of the experimental results on the pool boiling CHF model and CHF enhancement using TSP and NF were discussed to explain the effects caused by deposited materials.

Milanova and Kumar[20] investigated the effect of nonofluid at different acidity. LiOH included in the coolant to control the potential of hydrogen. If the coolant is acidic, the corrosion of the plant structure will be accelerated. Although the potential of hydrogen has an influence on CHF, controlling the pH was not considered due to complicated effects.

Lee and Chang[21] conducted the pool boiling CHF tests under atmospheric pressure with SA508 test heater. SA508 is the material of the reactor pressure vessel in a nuclear power plant. Therefore, the CHF behavior of SA508 material is important for the reactor pressure vessel integrity. It showed very higher CHF value and the test heater surface was changed significantly. This test heater surface change is due to corrosion of SA508, and the rate of corrosion increases with boiling time. Additives like TSP, Al_2O_3 and CNT nanoparticles are also tested, but they did not show the CHF enhancement effect. In case of TSP, it showed CHF decrease effect due to preventing effect on SA508 corrosion. Before flooding the coolant in the reactor cavity, this corrosion layer would be already formed on the surface of the reactor vessel. The effects of nanofluid and TSP could influence the CHF enhancement individually.

2.1.3 Nanofluid effect

Nanofluids were used to form a coating layer on a heater surface. Nanofluids are colloidal dispersions of nanoparticles suspended in traditional heat transfer fluids. Since You et al.[22] introduced a new way to enhance the pool boiling CHF value using nanofluids which have nanoparticles suspended in water, many pool boiling experiments have been conducted with a variety of nanofluids. One of the most interesting characteristics of nanofluids is their capability to enhance the critical heat flux (CHF) significantly[23, 24]. Nanofluid is made of typical particle materials. Materials of nanoparticles include

metals (e.g., silver, copper, gold), metal oxides (e.g., titania, alumina, silica, zirconia), and carbon allotrope (e.g., carbon nanotube, graphite, fullerene and graphene). The carbon allotrope materials received a lot of attentions recently because of the own unique geometry and the excellent thermal conductivity. So far, alumina has been proposed as a candidate of coating materials to enhance the safety margin due to its well-known characteristics for dispersion and surface deposition[25]. Here, the graphene-oxide nanosheets were selected as nanomaterials dispersed in the water and chemical solution for nuclear application. During boiling, a thin nanoparticles-deposited layer was formed on the heater surface immerged in the nanofluid. It is well known that the coating is physically induced by microlayer-evaporation below boiling bubbles[26]. A good point of the nanofluid-induced coating technique is that the coating is sustainable through self-healing process because nanoparticles could be coated onto the heated surface once boiling occurs or as long as boiling is kept. This removes a concern on the durability of a coating layer during the life time of the nuclear power plant as long as 40 or 60 years[27]. Therefore, this process could enhance the credibility of ERVC by self-healing a part of the coating structure damaged by unexpected reasons. If the nanofluid is applied to the ERVC, a good way to reduce the functional and economic matter of the nanofluid coolant is to adopt the separately concentrated nanofluid storage tanks[28].

2.2 Experimental apparatus

A schematic diagram of the experimental apparatus is shown in Fig. 2-1. The pool boiling facility consists of a rectangular vessel (100 mm × 50 mm × 120 mm), copper electrodes, Teflon cover, a reflux condenser, a 1 kW DC power supply, a data acquisition system, a hot plate and a standard resistor. A concentration of nanofluid is maintained by the Teflon cover and the reflux condenser. The heating method on test heater is based on joule heating through the wire. The material of heating wire is nickel-chrome (80/20 composition, L=55 mm, R=0.49 mm). The new pure wire was replaced in every test.

2.3 Test procedure and experimental uncertainty

Equation (2-1) and (2-2) were used to calculate the average heat flux. In order to reduce the uncertainty in the heat flux measurements, it is required to consider the system resistance of the test electrodes and wires. The same heating time with increasing heat flux was maintained for consistency. A stepwise power escalation was initiated, with increments of 50 kW/m^2 heat flux. Each power step lasted one minute, until a new steady state was achieved. This process was applied equally during each test.

$$R_h = V / I - R_s \qquad (2\text{-}1)$$

$$q'' = I^2 R_h / \pi D_h L_h \qquad (2\text{-}2)$$

Equation 2-3 is composed of voltage, current, and heat transfer area. The maximum uncertainty in the heat transfer area is ±1%. The uncertainty for voltage measurements is ±0.03%. This uncertainty is inherent to the power supply. The uncertainty of the current is ±0.01%, due to the inherent properties of the standard resistor. The system resistance (R_s) is constant. The resistance of the heating element (R_h) is calculated using Eq. (2-2). The uncertainty of R_h is included in the uncertainty for both the voltage and current values. The uncertainty of heat flux is ±1%.

$$\frac{\Delta q''}{q''} = \sqrt{\left(\frac{\Delta V}{V}\right)^2 + \left(\frac{\Delta I}{I}\right)^2 + \left(\frac{\Delta\left(\pi D_h L_h\right)}{\left(\pi D_h L_h\right)}\right)^2} \qquad (2\text{-}3)$$

Ggraphene oxide nanofluids are prepared from graphite. In this work, graphite used is manufactured by Sigma Aldrich Corporation (graphite powder, size<45μm). Modified Hummers method is used in preparing the graphene and graphene oxide nanofluids[29]. The process of manufacture is divided to pre-oxidation, oxidation, and reduction. At the pre-oxidation process, graphite powder (2 g) is mixed with H_2SO_4 (3 ml, 80 °C), K_2S_2O (1 g) and P_2O_5 (1 g). The produced dark blue mixture is cooled at room temperature for 6h. At the oxidation process, the pre-oxidized graphite power (1 g) is mixed with H_2SO_4 (23ml, 0 °C) and $KMnO_4$ (3 g). This compound is mixed with distilled water (140 ml), H_2O_2 (30 %, 2.5 ml). The graphene oxide nanofluids manufactured through the above processes is yellow-brown dispersion. Graphene oxide powder (5 mg) was dispersed into distilled water (10 ml). After centrifuge the this fluid at 3000rpm for 10min, graphen oxide (5 ml), N_2H_4 (5 μl) and NH_4OH(35 μl) are added. Graphene nanofluid is prepared by using centrifugation at same condition.

2.4 Results and discussion

The main effects of the heater inclination on CHF are related to coalescence phenomena of bubbles which are sweeping along the heater surface due to the buoyancy force. The heat is removed from a heater surface by early departures due to coalescence of bubbles flowing over the heated surface with bubbles growing on the surface. Bubble-sweeping along the heater surface becomes the more dominant factor when the heater inclination approaches to the vertical arrangement. Therefore, the bubbles crowding and bubbles coalescences near the vertical region prevent the water supply to the heated surface resulting in decrease of the CHF limits compared to relatively horizontal arrangement of heater.

The experimental results for CHF enhancements under saturated temperature at atmospheric pressure are shown in Fig. 2-2. CHF limits for water are consistent with the conventional correlations considering

effects of heater inclination such as Eq. (2-4) and (2-5) which are Vishnev's and El-Genk and Guo's correlation. Vishnev correlated the effects of heater orientation on pool boiling CHF based on liquid helium data of Lyon. This correlation is still used most widely. El-Genk and Guo[3] developed the correlations according to test fluids such as water, liquid nitrogen and liquid helium.

$$q''/q''_{0^o} = (190-\theta)^{0.5}/190^{0.5} \qquad (2\text{-}4)$$

$$q'' = C_{CHF}(\theta)\rho_g h_{fg} \left[\sigma(\rho_f - \rho_g)g/\rho_g^2\right]^{1/4} \qquad (2\text{-}5)$$

$$C_{CHF,water}(\theta) = 0.034 + 0.0037(180-\theta)^{0.656}$$

$$C_{CHF,liquid-nitrogen}(\theta) = 0.033 + 0.0096(180-\theta)^{0.479}$$

$$C_{CHF,liquid-helium}(\theta) = 0.002 + 0.0051(180-\theta)^{0.633}$$

Figure 2-3 shows the representative pool boiling phenomena of water and graphene-oxide nanofluid at a heat flux condition as high as 80% CHF. There are no outstanding differences in boiling phenomena apparently shown between both fluids. The observations show the efforts of the present work to physically figure out the reason why CHF is varied and affected.

The enhancement of CHF limits was observed in all nanofluids. The effect of heater orientation is similar to a general trend that the horizontal orientation of the heater gives higher values compared to vertical arrangements in terms of vapor escaping path due to buoyancy. This trend is also shown in all cases of nanofluids such as SiO_2, Al_2O_3 and graphene-oxide. However, the ratio of enhancement is different. The graphene-oxide nanofluid shows the highest enhancement in term of CHF value while the SiO_2 shows the lowest CHF limit. This trend is also observed in all angles of heater inclination. It was confirmed that the graphene-oxide nanofluid with forming relatively ordered porous structures during boiling showed higher CHF performance compared to the SiO_2 and Al_2O_3 nanofluid. The morphology of deposition structures and CHF limits are previously reported.

Figure 2-4 shows the experimental results for effects of heater orientation and chemicals on CHF limits. An interesting finding is that highly-concentrated chemicals have some influences on CHF enhancement regardless of whether the graphene oxide nanoparticles were included in a test fluid or not. Based on the effects of single chemical, major contribution among chemicals is achieved by TSP and boric acid. In the chemicals, Tri-sodium phosphate has a strong influence on the boiling behavior. Tri-sodium phosphate (TSP) is a surfactant. When the TSP added in the fluid, the surface tension is decreased. The reduction of surface tension will influence the activation of nucleate sites, bubble growth and dynamics thus influence the boiling heat transfer coefficient. As the results of that, the cases with

TSP have relatively low gradient in a CHF enhancement as a function of heater angle in Fig. 2-4. The case with the highest CHF enhancement ratio was observed when all chemicals were dissolved together in the grapheneoxide nanofluid. Deposition layers of nanomaterials and chemicals on heaters were also observed through the current experiments as reported in the literature. To characterize the deposition layers in terms of CHF enhancement mechanisms, the static contact angle of each heater surface was measured like in Fig. 2-5. The static contact angle was measured three times on the other sites of a heater wire. The uncertainty of the measurement is less than 2%. It means that the uniform coating layer was formed on the heater surface. The degree of the static contact angle is affected by the deposited materials on the heater surface. Such change of contact angle means the variation of surface characteristics such as wettability (surface roughness, porosity) and nucleation sites. The nanomaterials and chemicals affect the CHF by changing the surface characteristics like the surface wettability based on the deposition layers and a modification of the Taylor wavelength due to different bubbles escaping path or hydrodynamic instability.

Table 2-1 shows thermal conductivity, viscosity and pH of test fluids. Thermal conductivity is nearly unchanged. The major factors determining thermal conductivity of nanofluid are a mixture concentration and the thermal conductivity of particles. Although graphene oxide has high thermal conductivity, the low concentration of the nanofluid in this work has marginal effects. The more materials are added to graphene-oxide nanofluid, the higher viscosity the fluid has. The viscosity of working fluid is related to a pump power. The viscosity of graphene oxide nanofluid was same with one of distilled water due to its low concentration as we checked. The pH values depend on the chemicals surely. The thermophysical properties are closely linked to practical problems of engineering when we consider a conceptual nanofluid injection system. Say, if we consider an application of the nanofluid to the ERVC, the marginal viscosity change means that the required time to fill the cavity with flooding coolant is not delayed.

Figure 2-6 shows a conceptual nanofluid injection system for the ERVC including a position of a storage tank and a flow path of nanofluids. Nanofluid is maintained in a separated tank from the reactor coolant system (RCS). To set up a separated tank is an easiest way to meet the functional and economic requirements. It enables to easily maintain and monitor a quality of nanofluids. If a severe accident would occur, nanofluid would be injected to the reactor vessel outer through the RCS and then a coating layer would be formed on the vessel outer surface. Therefore, there is a concern on whether nanofluid can keep its dispersion stability. It is necessary to check the dispersion stability in two different environments. First is that only nanoparticles are dispersed in the distilled water. The condition is corresponding to the situation that nanofluid is stored in the tank. Second is that some chemicals are dissolved with nanofluid in the RCS and the vicinity of vessel. If there are some interactions between the chemicals and nanoparticles, aggregation of nanoparticles can occur. It causes the dilution of nanofluid. Conclusively, effective coating layer for CHF enhancement would not be obtained.

Zeta potential as the potential difference between the dispersion medium and the stationary layer of fluid attached to the dispersed particle was measured in order to secure the stability or check the compatibility with nuclear coolant chemicals. It represents surface charge making the repulsion force between particles to prevent the agglomeration. The results of dispersion stability are shown with variation of zeta potential according to pH change in Fig. 2.7.

The Zeta potential was increased with increasing pH value regardless of the chemicals. If the absolute value of measured potential is over 30mV, the dispersion stability is generally considered as a stable state (no sedimentation). However, some results are under the reference value at all pH ranges in the tests. The pH of graphene-oxide nanofluid is 7 as shown in Table 2-1. The zeta potential of graphene oxide nanofluid is about -35 mV at pH 7, which means that the fluid is considered to have good dispersion stability. The test fluid containing all the chemicals in the graphene oxide nanofluid had the alkaline pH 8.24. The absolute value of the zeta potential corresponding to pH 8.24 is less than 30mV (about -24mV). The aggregation of nanoparticle and sedimentation were not immediately observed in the present work. It is critical when the aggregation occurs as soon as nanofluids meet the chemicals. But the aggregation was observed in the mixture after several hours. It is enough to remain the stable condition of nanofluid. There is a flow caused by natural circulation. The flow could be strongly operative to maintain a stable state.

2.5 Conclusion

In present study, an experimental study has been conducted to investigate the viability of using graphene-oxide nanofluid under various coolant chemical environments to enhance CHF during ERVC. Pool boiling CHF experiments were carried out for the thin-wire heater at 0, 30, 60 and 90 degrees of heater inclination angle under saturated temperature of atmospheric pressure. The dispersion stability of graphene-oxide nanofluid in the chemical conditions of the flooding water that includes boric acid, lithium hydroxide (LiOH) and trisodium phosphate (TSP) was checked in terms of surface charge or zeta potential before the CHF experiments. Finally integral effects of graphene-oxide nanosheets and chemicals on CHF limits were investigated.

The following conclusions are obtained.

(1) Graphene-oxide nanofluids were stable under ERVC coolant chemical environments and enhanced CHF limits up to about 40% at minimum at 90 degree of angle (vertical orientation) and about 200% at maximum at 0 degree of angle (horizontal orientation) in comparison to pure water .

(2) After the CHF, a thin coating/deposition layer was observed on the heater surface. It is induced by microlayer dryout below boiling bubbles. This coated layer modifies the surface conditions/characteristics to affect CHF limits. The complex deposition of the nano-materials and

11

chemicals makes differences in enhancement.

(3) The graphene oxide nanofluid was maintained under a stable dispersion condition. It is expected that there would be no serious problems to build the coating layer on the vessel outer surface when graphene oxide nanofluid would be mixed with boric acid, lithium hydroxide (LiOH) and tri-sodium phosphate (TSP).

(4) The kind of nanoparticle suspensions is known to make a self-healing coating effect because the self-coating can be achieved as long as boiling or micro-layer evaporation occurs.

Table 2-1 Measurements of thermophysical properties of graphene-oxide nanofluids

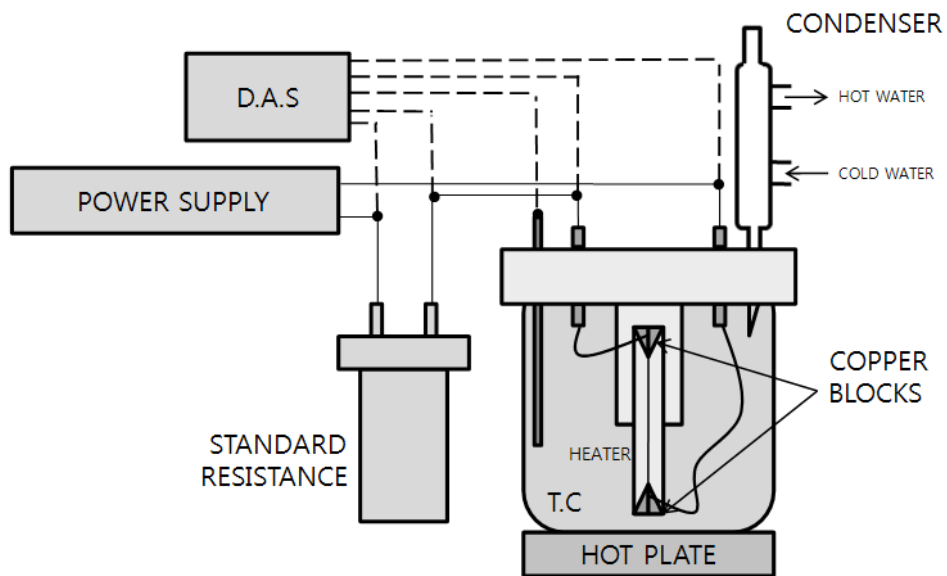| fluid	Thermal conductivity (W/mK)	Viscosity (N_sec/m2)	pH
Distilled water	0.588	1.01	7
LiOH	0.587	1.01	11.47
TSP	0.590	1.07	12.31
Boric Acid	0.589	1.08	4.72
LiOH + TSP + Boric Acid	0.592	1.12	8.31
Graphen oxide (GO) fluid	0.595	1.01	7
GO + LiOH	0.589	1.01	11.54
GO + TSP	0.596	1.06	12.22
GO + Boric Acid	0.593	1.09	4.47
GO + LiOH + TSP + Boric Acid	0.598	1.14	8.24

*LiOH(3ppm), Boric acid(5000ppm), TSP(saturation)

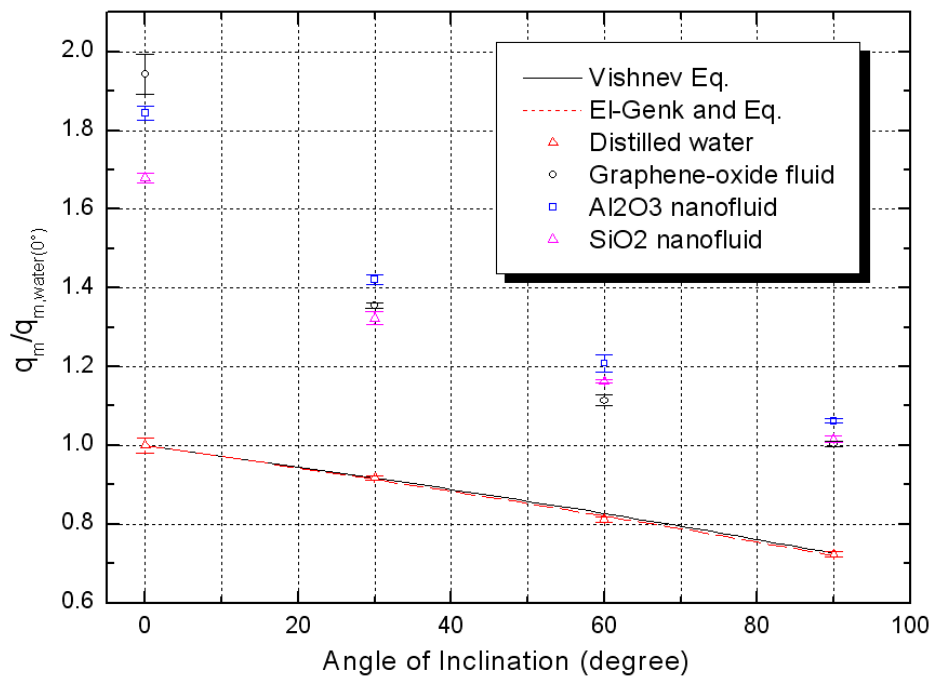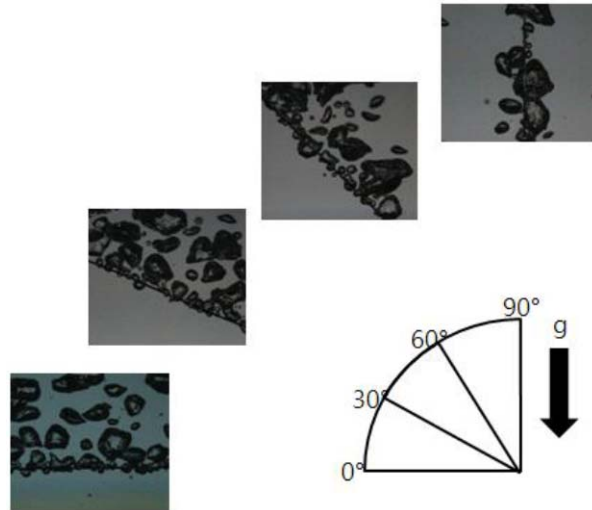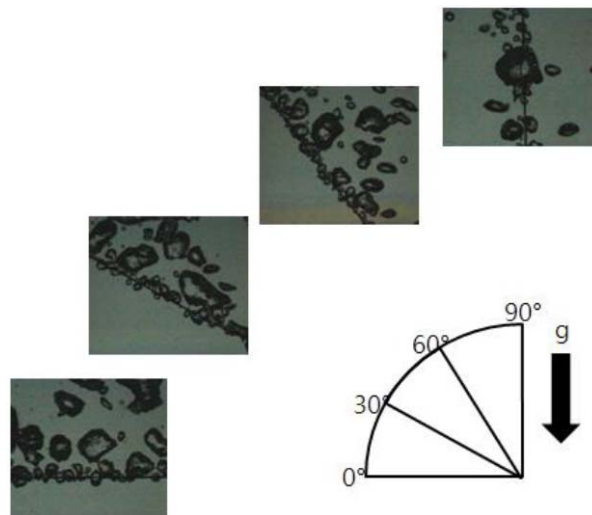Fig. 2-1 Schematic diagram of the test facility

Fig. 2-2 Effects of heater orientation on CHF limits

(a) Boiling phenomena of water at 80% CHF for water
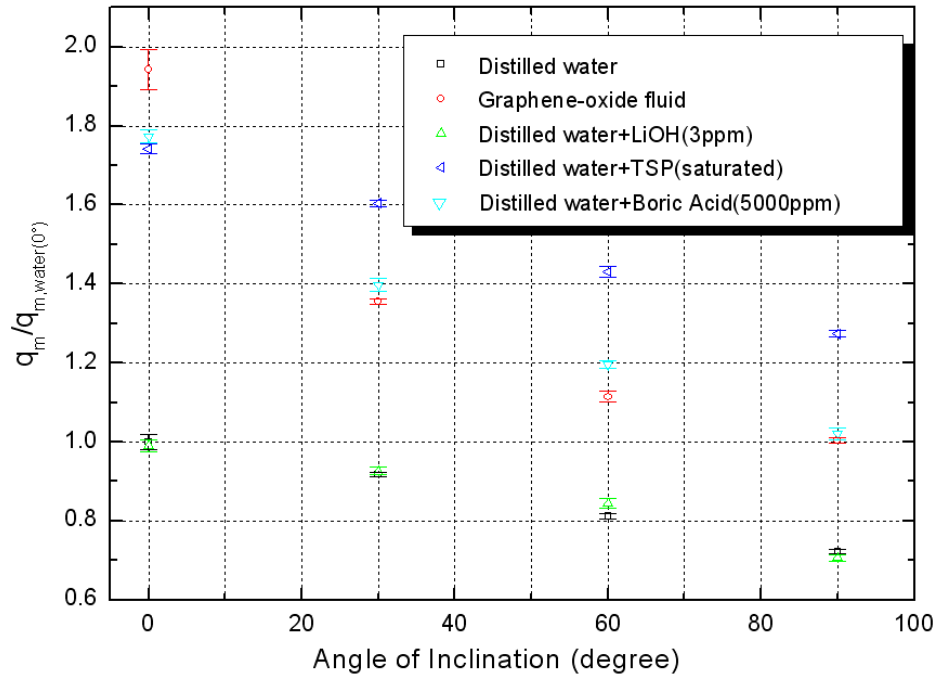

(b) Boiling phenomena of graphene-oxide nanofluid at 80% CHF for water
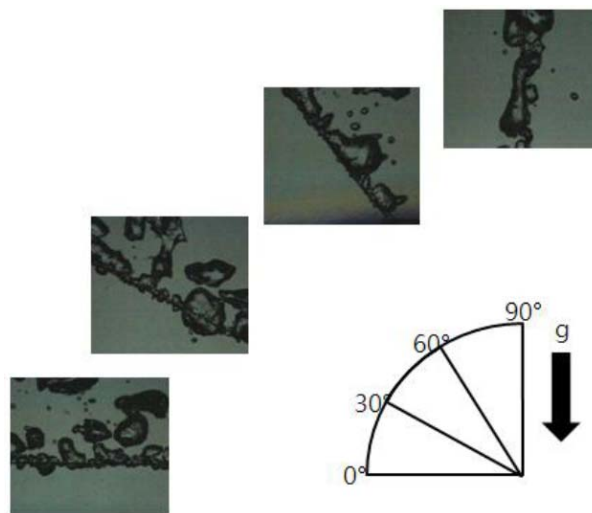
(c) Boiling phenomena of graphene-oxide nanofluid at 80% CHF for graphene-oxide nanofluid

Fig. 2-3 Effects of heater orientation on pool boiling phenomena

(a) Base fluid : distilled water
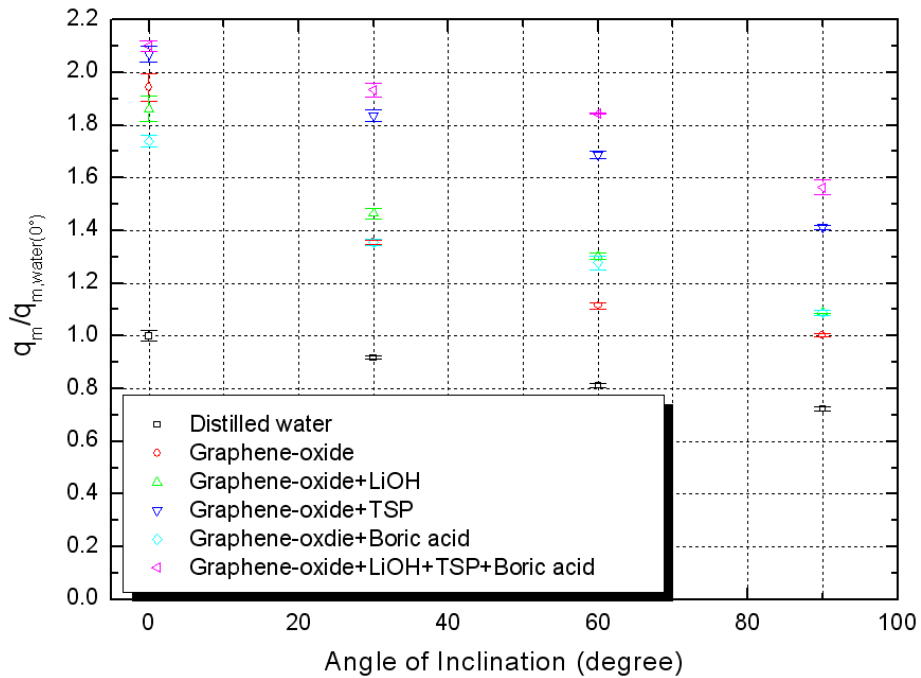
(b) Base fluid : graphene oxide nanofluid

Fig. 2-4 Effects of chemicals on CHF as a function of the heater angle

17

(a) Bare, 65°

(b) GO, 78°   (c) Al2O3, 21°   (d) SiO_2, 49°

(e) LiOH, 60°   (f) TSP, 22°   (g) Boric acid, 24°

(h) GO+LiOH, 45°   (i) GO+Boric acid, 40°   (j) GO+TSP, 20°

(k) GO+LiOH+Boric acid+TSP, 22°

Fig. 2-5 Effects of surface coating/depositions of nano and chemical materials on static contact

angle (wire surface vs. water droplet)

Fig. 2-6 A conceptual nanofluid injection tank and dispersion environments in APR1400

(a) Graphene oxide nanofluid

(b) Graphene oxide nanofluid+Boric Acid+ LiOH+TSP
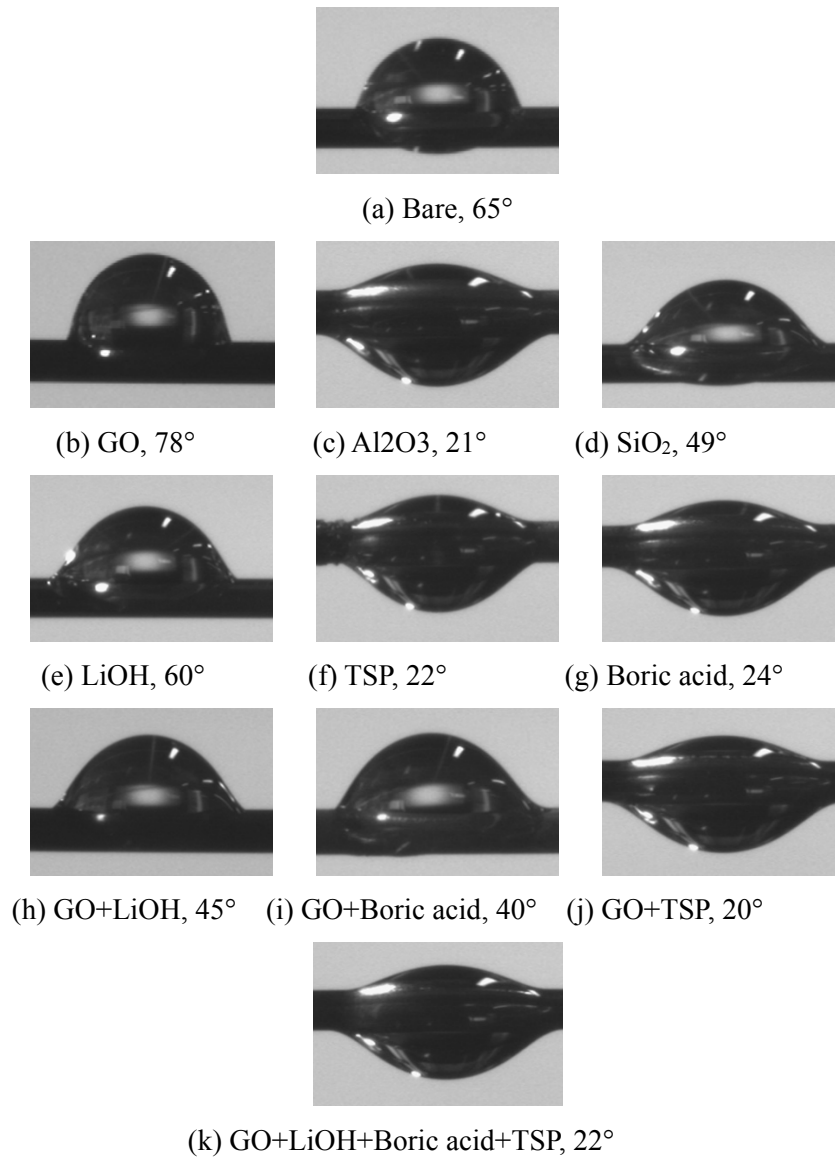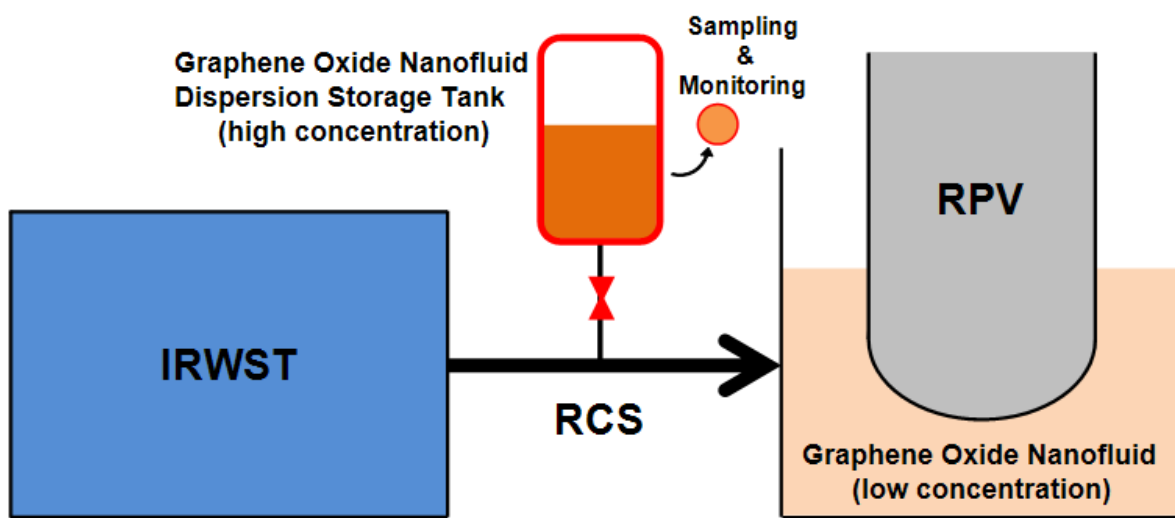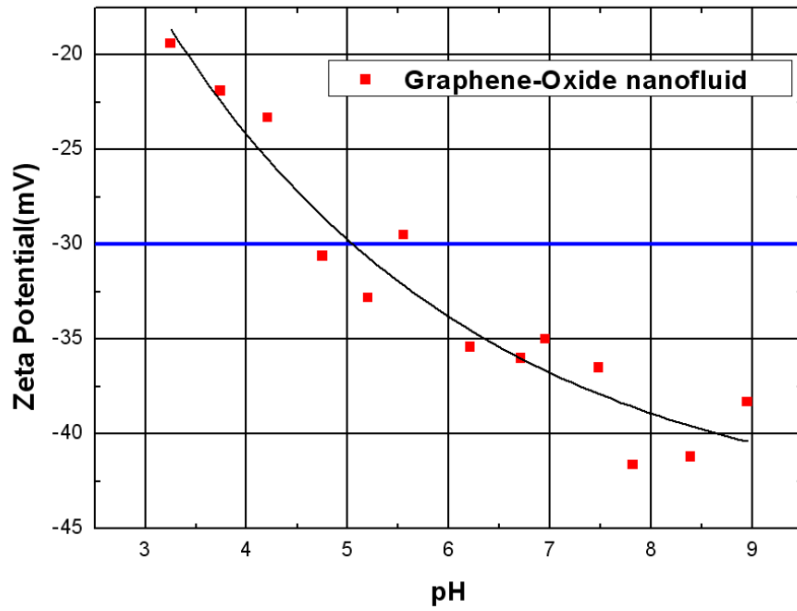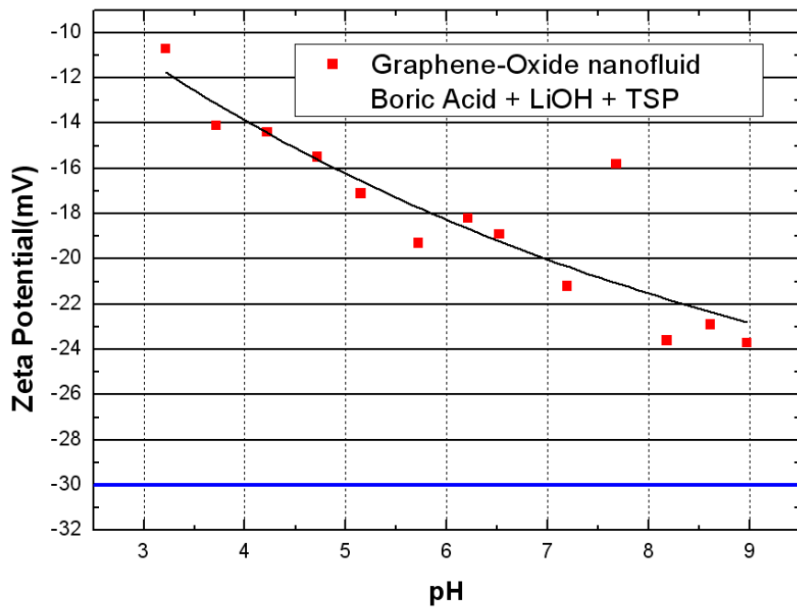
Fig. 2-7 Curve of zeta potential as a function of pH varied
by adding a small amount of HCl and NaOH solution.

Chapter 3. MODIFIED HYDRODYNAMIC CHF PREDICTION MODEL

3.1 Introduction

Phase change by boiling is a highly efficient heat transport mechanism, which accommodates large heat fluxes with relatively low driving temperature differences. During high heat flux boiling, the formation of a vapor film on the surface of the heating element leads to inefficient heat transfer across the superheated surface. This phenomenon is known as critical heat flux (CHF), which is the thermal limit for phase-change nucleate boiling heat transfer. Researchers have examined the phenomenon of CHF by proposing CHF prediction models based on hydrodynamic instability theory.

Kutateladze[30] studied critical heat flux in a similar process, upstream gas behavior in a liquid pool. When the velocity of gas reaches a critical value, continuous flow ceases. This change is related to Kelvin-Helmholtz instability. After performing dimensional analysis, he proposed the following model to predict CHF. In this model, the CHF depends upon the Kutateladze number, Ku.

$$Ku = \frac{q''}{h_{fg}\rho_g^{1/2}\left[\sigma\left(\rho_f - \rho_g\right)\right]^{1/4}} \approx \text{constant} \quad (3\text{-}1)$$

Zuber[31] developed a CHF prediction model based on liquid-vapor interface instability. This instability includes Kevin-Helmholtz and Rayleigh-Taylor instabilities. Zuber considered that vapor jets determine CHF, as a result of the liquid-choking phenomenon when the velocity of vapor escaping from the heating element surface reaches a critical value. Zuber suggested the following model based on hydrodynamic instability.

$$q''_z = \frac{\pi}{24}\rho_g^{1/2}h_{fg}\sqrt[4]{\sigma g\left(\rho_f - \rho_g\right)} \quad (3\text{-}2)$$

Vapor escape is a discontinuous phenomenon, however. It does not have a cylindrical shape. Furthermore, the model includes no consideration of the heating element surface condition. Variables like surface roughness and a coating layer on the heating element surface clearly influence CHF during boiling[32, 33]. Representative approaches to predicting CHF based on other parameters of the phenomenon include a macrolayer dryout theory[34, 35], a hot/dry spot theory[36, 37], and a bubble interaction theory[38, 39].

Nanofluids, which are colloids of nanoparticles in a base fluid such as water, are known to significantly enhance the occurrence of CHF, and so the reasons for enhanced CHF have been explored

specifically for nanofluids[40, 41, 42, 43]. The enhancement of CHF is related to the buildup of a deposition layer of nanoparticles on the heating element surface while boiling nanofluids. The main reason behind the enhancement of CHF is explained as increased wettability in many experiments that observe the contact angle, which indicates the degree of wetting ability on the nanoparticle-coated heating element surface[44].

In this study, CHF experiments were conducted to test a CHF prediction model for nanofluids based on hydrodynamic instabilities.

3.2 Experimental apparatus

A schematic diagram of the experimental apparatus is shown in Fig. 3-1. The pool boiling apparatus consists of a rectangular vessel (100 mm × 50 mm × 120 mm), copper electrodes, a Teflon cover, a reflux condenser, a 1 kW DC power supply, a data acquisition system, a hot plate and a standard resistor. The Teflon cover and reflux condenser are included to maintain nanofluid concentration. Heat is generated through joule heating of the heating element wire. The wire heating element is of nickel-chrome composition (80/20 ratio, L = 55 mm, D = 0.49 mm).

3.3 Test procedure and experimental uncertainty

The heating element was replaced with a new, pure wire for each test. Equation (3-4) and (3-5) were used to calculate the average heat flux. In order to reduce the uncertainty in the heat flux measurements, it is required to consider the system resistance of the test electrodes and wires. The same heating time with increasing heat flux was maintained for consistency. A stepwise power escalation was initiated, with increments of 50 kW/m^2 heat flux. Each power step lasted one minute, until a new steady state was achieved. This process was applied equally during each test.

$$R_h = V / I - R_s \qquad (3\text{-}4)$$

$$q'' = I^2 R_h / \pi D_h L_h \qquad (3\text{-}5)$$

Equation (3-5) is composed of voltage, current, and heat transfer area. The maximum uncertainty in the heat transfer area is ±1%. The uncertainty for voltage measurements is ±0.03%. This uncertainty is inherent to the power supply. The uncertainty of the current is ±0.01%, due to the inherent properties of the standard resistor. The system resistance (R_s) is constant. The resistance of the heating element

(R_h) is calculated using Eq. (3-4). The uncertainty of R_h is included in the uncertainty for both the voltage and current values. The uncertainty of heat flux is ±1%.

$$\frac{\Delta q''}{q''} = \sqrt{\left(\frac{\Delta V}{V}\right)^2 + \left(\frac{\Delta I}{I}\right)^2 + \left(\frac{\Delta(\pi D_h L_h)}{(\pi D_h L_h)}\right)^2} \qquad (3\text{-}6)$$

Three trials of pool boiling tests were conducted for each nanofluid to obtain the CHF value with distilled water as a base fluid. A nanoparticle coating layer on each heating element was formed by boiling the nanofluid. The heating elements with coating are prepared to observe a change of Rayleigh-Taylor instability. These test heating elements were prepared under the same conditions as CHF test to obtain the coated heating elements, but without reaching CHF. Table 3-1 shows the thermal properties and predicted CHF values for both distilled water and R-123 base fluids. The R-123 refrigerant eases the examination and measurement of the distance between the bubbles formed on the heating element surface without burnout of the heater due to its relatively lower CHF value compared to distilled water.

When CHF occurred on the heating element, a vapor film formed, which caused a temperature increase on the surface compensating for the relatively low heat transfer. This temperature increase for nanofluids is relatively large compared with distilled water because of high CHF value. The heating element wire is usually damaged, as suddenly elevated temperature passes the melting point of the wire material. This makes observing bubble behavior during film-boiling impossible. R-123 refrigerant was used to maintain the integrity of both the coating layer and the heating element itself. Using R-123 maintains the integrity of the heating element both before CHF and during the phase of film boiling. After CHF occurs, the heat flux is controlled to decrease to a minimum heat flux at the film boiling region. The transition from a film boiling to a nucleate boiling gives insight in understanding the enhanced incidence of CHF in nanofluids.

Two different experiments were conducted for each nanofluid. One was a CHF test to obtain the limit of heat transfer for boiling. The other was an observation test to examine bubble behavior on the heating element surface. The final surface condition of the heating element in the CHF test was identical to the initial condition of the heating element in the observation test. Total boiling time, which corresponds to the heat flux, was controlled to keep the coating conditions for each nanofluid. This complex procedure was necessary because nanoparticles have poor dispersion stability when suspended in R-123 refrigerant. The heat flux level and incidence of CHF were carefully controlled to minimize damage to the coating layer and measure the Rayleigh-Taylor wavelength.

3.4 Result and discussion

The Zuber model is well known in hydrodynamic instability theory. This model applies to almost pure fluids because Eq. (3-2) is based on the thermo-physical properties of fluids. In the current work, there was an error of about 10% between the CHF results for bare wire in distilled water and the Zuber equation.

It has been shown that there is no significant change in the properties of dilute nanofluids compared with a base fluid[44]. However, the occurrence of CHF in nanofluids was enhanced in comparison with distilled water. Figure 3-2 presents the CHF enhancement ratio for nanofluids. Each of the nanofluids has a different value. The CuO nanofluid shows the largest CHF enhancement of about 160%. The lowest CHF enhancement took place in the ZnO nanofluid, measured at 90%. This enhancement is closely related to the buildup of a deposit layer of nanoparticles on the heating element surface during boiling[14]. Although the chief factors contributing to this deposition are not clear, roughly three factors must be in play: the properties of the dispersed particles (size, shape, zeta-potential, concentration, etc.), the properties of the heating element surface (roughness, electrical/magnetic characteristics, etc.), and the properties of the base fluid (vapor/liquid density, surface tension, etc.) The morphologies of deposit layers formed on the heating element surface from different nanoparticle materials during nucleate boiling are shown in Fig 3-3.

So far, explanations for the mechanism of CHF enhancement in nanofluids have been focused on improved surface wettability. Reverse results were reported when graphene/graphene oxide materials were deposited on a heating element surface[45]. These researchers tried to interpret the CHF enhancement using hydrodynamic instability theory by measuring the distance between the droplets appearing on the surface. The wavelength change corresponds to the CHF enhancement tendency for all of the tested nanofluids. This means that the hydrodynamic limit model for a bare surface, based on Rayleigh-Taylor instability wavelengths, can be extended to a surface with a nanoparticle coating layer.

Liter and Kaviany[46] suggested and studied a modified hydrodynamic instability CHF prediction model for porous heating surfaces. They explained the effect of modulated wavelength on CHF for a porous coating layer using the following Eq. (3-7) and (3-8).

$$\frac{q''_{CHF}}{\frac{\pi}{24}\rho_g^{1/2}h_{fg}[g\sigma(\rho_f-\rho_g)]^{1/4}}=\left(\frac{9}{2\pi}\frac{\lambda_{RT,c}}{\lambda_m}\right)^{1/2}=\frac{3[\sigma/g(\rho_f-\rho_g)]^{1/4}}{\lambda_m^{1/2}} \qquad (3\text{-}7)$$

$$q''_{CHF}=\frac{\pi}{8}h_{fg}\left(\frac{\sigma\rho_g}{\lambda_m}\right)^{1/2} \qquad (3\text{-}8)$$

Polezhaev and Kovalev[47] investigated the effect of porous structure on CHF. The test fluids for boiling were water, ethanol, and Freon-113. The experimental data matched well with the model in Eq. (3-9). They derived the numerical model from thermal properties of the fluids, the porosity of the surface, and the measured breakthrough pore radius. Interestingly, Liter and Kaviany show that porosity can be converted to the wavelength term. Equation (3-9) can then be presented as the simplified Eq. (3-10)

$$q''_{CHF} = 0.52 \varepsilon^{2.28} h_{fg} \left[\frac{\sigma \rho_f \rho_g}{\left(\rho_f + \rho_g\right) r_{po}} \right] \qquad (3\text{-}9)$$

$$q''_{CHF} = q''_Z \frac{\sqrt{\lambda_{bare}}}{\sqrt{\lambda_{porous}}} \qquad (3\text{-}10)$$

The onset of CHF based on the hydrodynamic limit is due to the instability of vapor columns. The porous layer could change the critical distance between vapor columns rising from the heater and thus modify the critical instability wavelength. A similar phenomenon was observed in droplet formation on the nanoparticle-coated surface. This formation is closely related to the departure of bubbles from the surface. However, the wavelength was measured indirectly by observing the opposite fluid. During pool boiling, bubbles depart from the heating element surface, since the heating element is immersed in the boiling liquid. So, one needs to know the distance between these bubbles in order to analyze the CHF effects in terms of Rayleigh-Taylor wavelength on the surface.

The test heating elements were designed and prepared to allow direct observation of the Rayleigh-Taylor wavelengths. The surprising results are shown in Fig 3-4. The observed distance between the bubbles is different for each nanoparticle-coated surface. All of the nanoparticle-coated surfaces have a shorter average distance between bubbles than the bare surface's bubbles. Fluids with high CHF enhancement exhibit short Rayleigh-Taylor wavelengths and these two data correlate for all the nanofluids tested. A short wavelength allows the vapor to prevent the formation of a bulk of vapor by venting the vapor evenly across the heating element surface. Shorter wavelengths also increase wettability by allowing the liquid to break through the developing vapor film, which also enhances CHF.

Figure 3-5 plots the observed Rayleigh-Taylor wavelengths versus CHF for each nanofluid with constant heat flux. The vapor films under confined liquid cover the heated surface with well-known Rayleigh-Taylor wavelength instability due to the different density between vapor and liquid once film boiling commences, beyond CHF. This is the origin of the hydrodynamic instability-based CHF prediction model of Zuber. The Rayleigh-Taylor wavelength instability due to different density of the liquid and vapor is used as the critical factor in determining the Kelvin-Helmholtz instability and CHF

occurrence. The Rayleigh-Taylor wavelengths reported in this work are not exactly matched with Eq. (3-7) because of the different heating element geometries. Our heating element geometry was a cylindrical wire of ~0.5 mm diameter. Equation (3-7) is based on a finite plate heating element geometry. The wavelength is dependent on the heating element geometry described in Eq. (3-9) to Eq. (3-11).

$$\lambda_{d1,RT} = \frac{2\pi\sqrt{3}}{\sqrt{\dfrac{g\left(\rho_l - \rho_g\right)}{\sigma}}} \quad \text{for 1-D flat heating element geometry} \tag{3-11}$$

$$\lambda_{d2,RT} = \sqrt{2}\lambda_{d1,RT} \quad \text{for 2-D flat heating element geometry}$$

$$\lambda_{d1,RT} = \frac{2\pi\sqrt{3}}{\sqrt{\dfrac{g\left(\rho_l - \rho_g\right)}{\sigma} + \dfrac{2}{D_h^2}}} \quad \text{for 1-D cylindrical geometry}[48] \tag{3-12}$$

$$\lambda_{d1,RT} = \frac{2\pi\sqrt{3}}{\sqrt{\dfrac{g\left(\rho_l - \rho_g\right)}{\sigma} + \dfrac{4}{D_h(D_h + 2a)}}} \quad \text{for 1-D cylindrical geometry}[49] \tag{3-13}$$

While previous studies used a two-dimensional plate heater[30, 45], a thin cylindrical heating element was used in this study to explore the CHF enhancement mechanism for nanofluids. The wavelength due to Rayleigh-Taylor instability is dependent on the heating element geometry. The different geometries limit comparison between this work and previous studies. To compensate for this concern, a relative value was calculated from data relating to the CHF enhancement and reduced wavelength. Figure 5 shows the effects of a geometrically determined wavelength on CHF for nanofluid boiling on a horizontally oriented, cylindrically shaped coated wire heating element. When the wavelength decreases, the CHF increases. The overall trend conforms to existing models. In these models, the bubble diameter is considered simply as a function of Kelvin-Helmholtz wavelength, $\lambda_{KH} = \pi D$. The relation between the Kelvin-Helmholtz and Rayleigh-Taylor wavelength is described by $\lambda_{KH} \propto \lambda_{RT,c}$. These parameters are directly proportional with each other. The major parameters considered in most hydrodynamic instability models could be replaced with the Rayleigh-Taylor wavelength. The experimental correlation could be established by combining the reduced Rayleigh-Taylor wavelength with the Zuber equation as shown in Eq. (3-12) and (3-13). λ_{th} is the wavelength calculated from theoretical background. In this work, the CHF value for the bare heating element is close to the CHF value predicted from the Zuber equation. The wavelength for the bare heating element (λ_{bare}) is identified with the theoretical wavelength used in the Zuber CHF prediction model (λ_{th}).

$$q''_Z : q''_{CHF} = \left(\frac{\lambda_{th}}{\lambda_{bare}} \right)^n : \left(\frac{\lambda_{th}}{\lambda_m} \right)^n \quad (3\text{-}14)$$

$$q''_{CHF} = q''_Z \left(\frac{\lambda_{bare}}{\lambda_m} \right)^n \propto \left(\frac{\lambda_{bare}}{\lambda_m} \right)^n \quad (3\text{-}15)$$

Figure 3-6 shows the comparison between the measured data and the proposed model. The enhancement of CHF for nanofluids was predicted as a function of the reduced Rayleigh-Taylor wavelength. The value of n as related in Eq. (3-13) is 3. This value is obtained from a best-fit curve for the observed Rayleigh-Taylor wavelengths. This value is higher than that of the modified hydrodynamic instability model proposed by Liter and Kaviany. One might postulate that the diameter of bubbles is half of the Rayleigh-Taylor wavelength in the original hydrodynamic instability model. This means that the relation between bubble diameter and Rayleigh-Taylor wavelength is linear. However, the relation is not linear in our tests, as shown in Fig. 3-4. Suppose that there are two cases with different Rayleigh-Taylor wavelength at constant heat flux. Bubbling behavior might be observed on the vapor film covering the heating element surface as shown in Fig. 3-4. Isolated bubbles formed and detached from the heating element surface. The total amount of the heat transfer is estimated by calculating the average bubble volume from both the nucleation site density and the bubble diameter. The total volume of generated vapor is the same in terms of the energy balance equation, as shown in Eq. (3-14) and (3-15). The Rayleigh-Taylor wavelength for the first case is a half size of the second case. The number of bubble departure sites, which were originally called "vapor jet sites," increases. The number of sites is doubled with a one-dimensional heater surface. This number quadruples with a two-dimensional heater surface. On the other hand, the radius of the bubble is reduced by about 21% and 37% with a one-dimensional and two-dimensional heater surface, respectively. The bubble departure frequency is assumed to be equal. Additionally, the relation between the bubble diameter and the reduced wavelength influences the area portion of evaporating vapor on the heater surface. In a hydrodynamic instability model, the area portion is a constant $\pi/16$ regardless of the Rayleigh-Taylor wavelength. However, the reduced Rayleigh-Taylor wavelength enables the area portion of an evaporating vapor per unit area to grow because of this non-linear relation. This change would affect the critical velocity for escaping bubbles from the heater surface. Ultimately, CHF could be enhanced by delaying liquid choking phenomena due to Kelvin-Helmholtz instability.

$$Q = Aq'' \quad (3\text{-}16)$$

$$q'' = \frac{\pi D_b^3}{6} \rho_g h_{fg} fn \qquad (3\text{-}17)$$

Although the n-value in Eq. 13 has been defined as 1/2 in previous studies[2], the value is set as 3 in this work. This value is not essential because it does not emerge from the theoretical background. However, considering the change of the bubble diameter, the area portion of an evaporating vapor and the velocity of escaped vapor, which are induced by the reduction of the Rayleigh-Taylor wavelength, the n-value must be changed to fit the parameters that are determined and changed by a hydrodynamic instability model.

We observed the bubble behavior on the heater surface in the film boiling. When the nanoparticles are coated on the heater surface, the distance between the separated bubbles are short in comparison with that of the bare surface case. This distance were quantitatively evaluated for every case. In the original hydrodynamic model, the distance between the bubbles or vapor columns was determined by the Rayleigh-Taylor instability. This Rayleigh-Taylor instability is important factor to estimate the critical vapor velocity. CHF phenomenon is triggered by the liquid choking in the vapor up streaming path as shown in Fig. 3-7. The critical velocity could be expressed in Eq. (3-18) and (3-19) based on the heat balance and fluid properties. It is impossible to directly observe the Kelvin–Helmholtz instability. The Rayleigh-Taylor wavelength was measured as an alternative factor to replace the Kelvin–Helmholtz wavelength. The Rayleigh-Taylor wavelength is proportional to the Kelvin-Helmholtz wavelength. If the Rayleigh-Taylor wavelength was reduced, allowable critical vapor velocity is increased. It means that a greater amount of the vapor was generated on the heater surface and removed from the heater surface without the liquid chocking phenomena. This is the CHF enhancement.

$$q''_{CHF} = \dot{m}_g h_{fg} = \rho_g u_{g,c} \frac{A_g}{A_h} h_{fg} \qquad (3\text{-}18)$$

$$u_{g,c} = \left(\frac{2\pi\sigma}{\rho_g \lambda_{KH}} \right)^{1/2} \qquad (3\text{-}19)$$

$$\lambda_{KH} \propto \lambda_{RT} \qquad (3\text{-}20)$$

3.5 Conclusion

To explore the effects of nanoparticle coating induced by boiling on a hydrodynamic instability model, pool boiling CHF tests were conducted with a variety of nanofluids. The correlation was established based on experimental data from observing the Rayleigh-Taylor wavelengths. The relation between the reduced wavelength and the enhanced CHF was studied based on a theoretical model of hydrodynamic instabilities. The change to the Rayleigh-Taylor wavelength influences the bubble diameter, the portion of the heating element area covered by evaporating vapor and the velocity of the escaped vapor.

The following results are obtained.

✓   The CHF was improved 90-160% for nanofluids compared to distilled water.

✓   The change of the Rayleigh-Taylor wavelength was observed on the nanoparticle-coated surfaces.

✓   The change in the Rayleigh-Taylor wavelength correlates with the CHF enhancement.

Table 3-1. Thermal properties and predicted CHF of distilled water and R-123

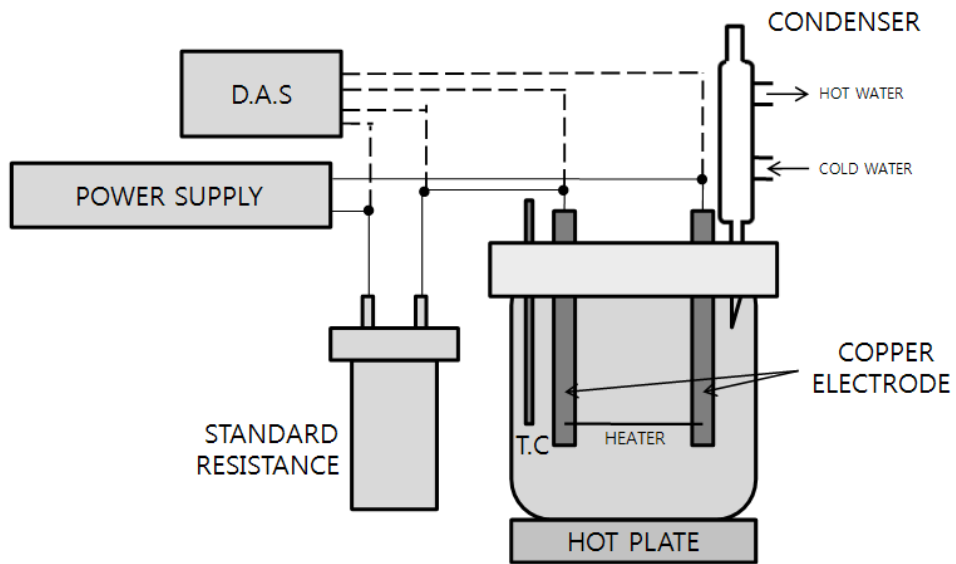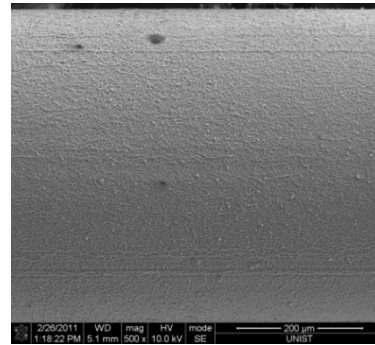|	Boiling Temperature (°C)	Latent Heat (kJ/kg)	Thermal Conductivity (W/mK)	Surface tension (N/m)	Density(kg/m^3) vapor/liquid	CHF (kW/m^2)
Distilled water	100	2257	0.668	0.059	0.6/958.1	1100
R-123	27.8	171	0.081	0.015	5.8/1463	200

Fig. 3-1 Schematic diagram of the testing apparatus
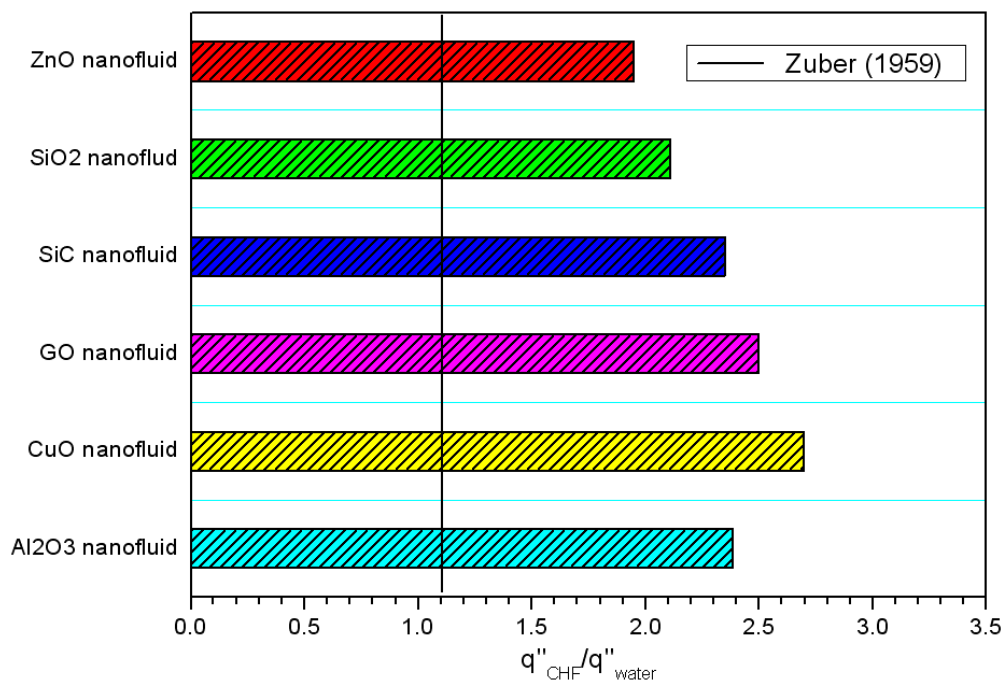
Fig. 3-2 Results of CHF enhancement for each test fluid compared with the Zuber Equation
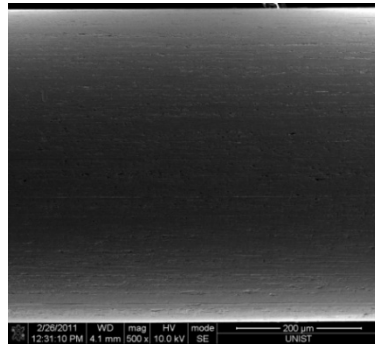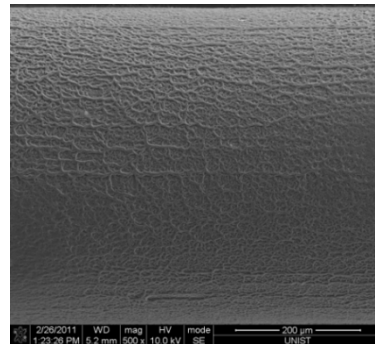
(a) Bare wire   (b) ZnO coated wire
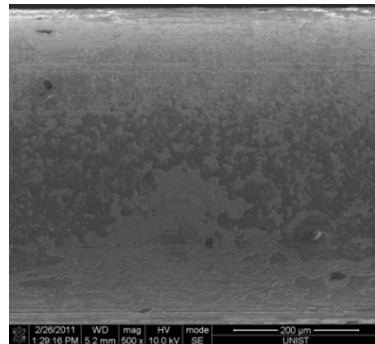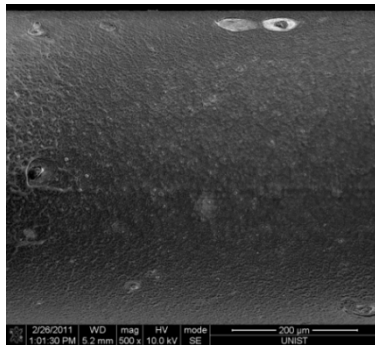
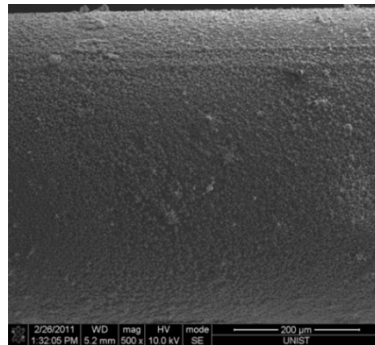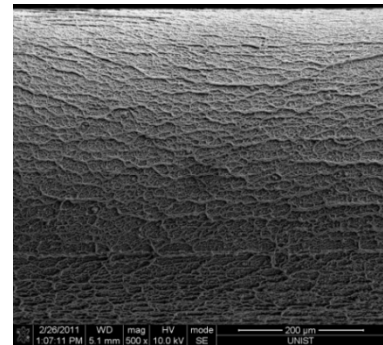(c) SiO$_2$ coated wire   (d) SiC coated wire

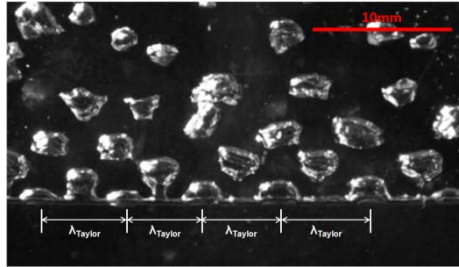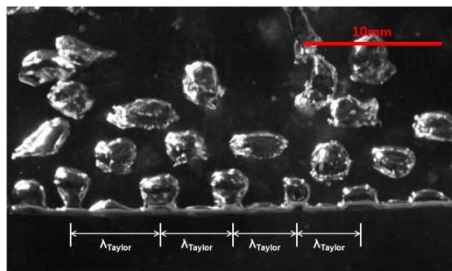(e) Al$_2$O$_3$ coated wire   (f) GO coated wire   (g) CuO coated wire
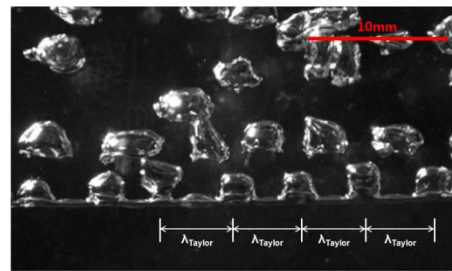
Fig. 3-3 SEM images of test heater surface after boiling in test fluids

(a) Bare wire (~6.4mm)

(b) ZnO coated wire (~5.8mm)   (c) SiO$_2$ coated wire (~5.6mm)
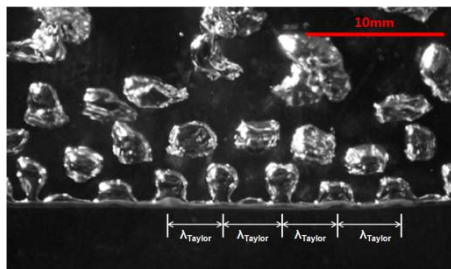
(d) SiC coated wire (~5.2mm)   (e) Al$_2$O$_3$ coated wire (~5.2mm)
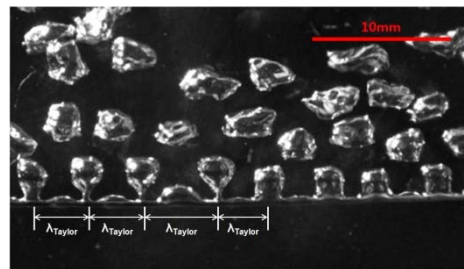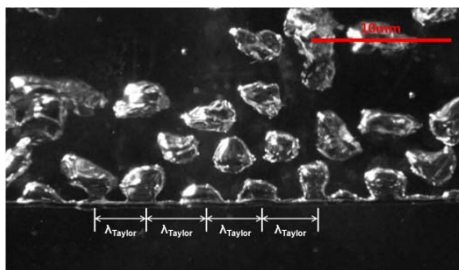
(f) GO coated wire (~4.8mm)   (g) CuO coated wire (~4.5mm)
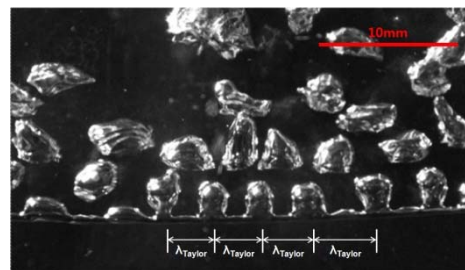
Fig. 3-4 Rayleigh-Taylor wavelength on surfaces
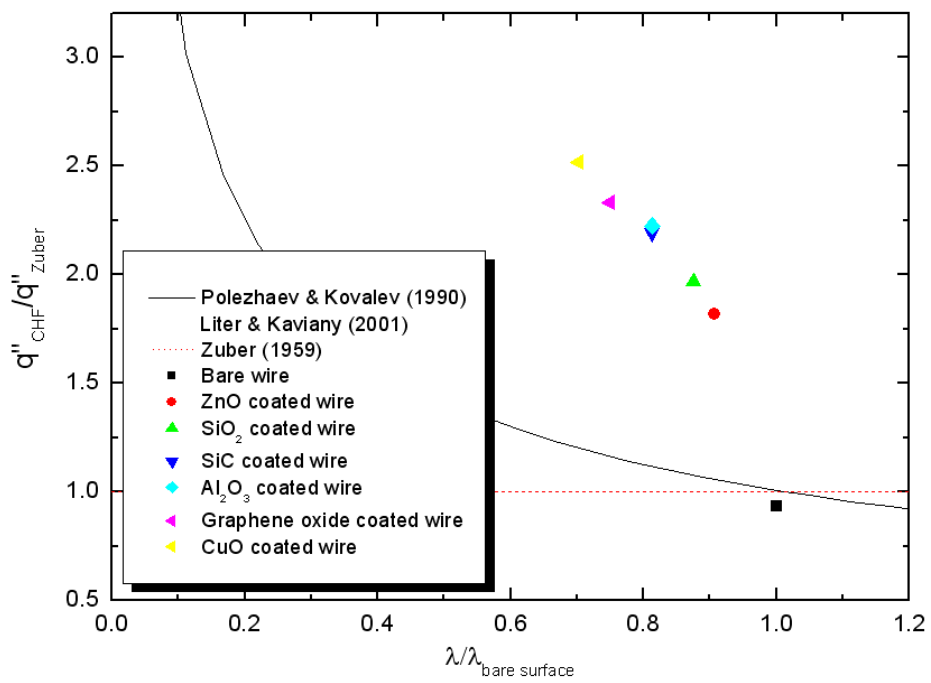
Fig. 3-5 Effects of a geometrically determined critical instability wavelength
(Liter and Kaviany's model with modulation wavelength).

Fig. 3-6 Comparison of theoretical models, experimental data, and best-fit curve

Fig. 3-7 Trigger phenomenon of CHF in a hydrodynamic instability model

Chapter 4. FLOW BOILING CHF EXPERIMENTS

4.1 Introduction

In this chapter, nanofluids were used to build a coating layer on a heated surface simulating the vessel's outer surface. It is a simple method to form the coating layer. It is well known that the coating layer is physically induced by microlayer-evaporation below boiling bubbles. An advanta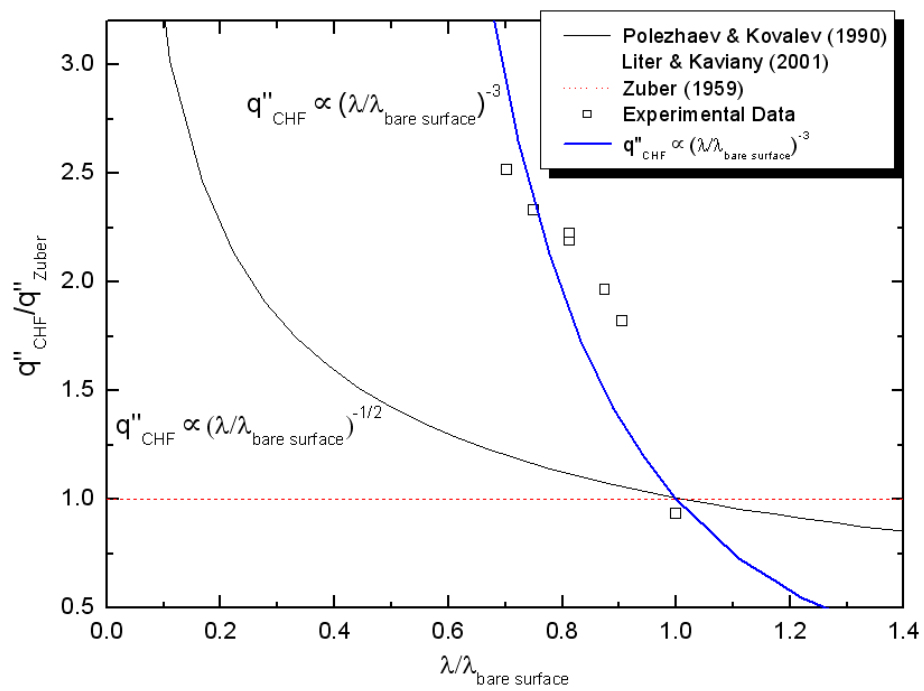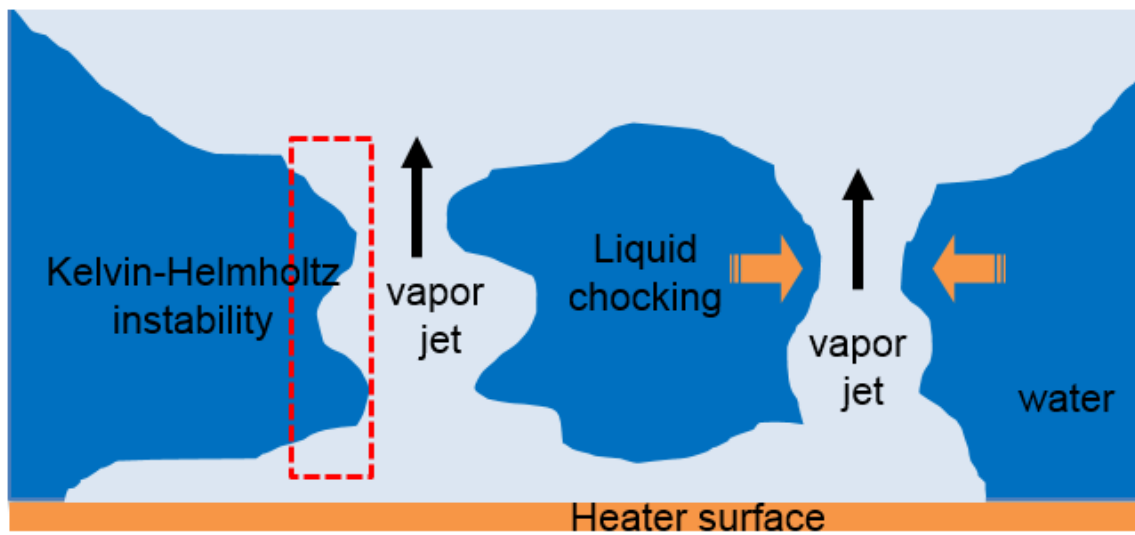ge of the nanofluid-induced coating technique is that the coating is sustainable through the self-healing process because nanoparticles can be coated onto the heated surface once boiling occurs or as long as boiling is kept[50]. This approach removes the problem concerning the durability of a coating layer during the IVR-ERVC strategy. Therefore, this process could enhance the credibility of nanofluid application in IVR-ERVC system by self-healing. The graphene series material with a high thermal conductivity was selected as a coating material. In order to check whether the graphene oxide nanofluid is suitable for the ERVC applications, the critical heat flux (CHF) on the reactor vessel external wall was measured using the small scale two-dimensional slide test section.

4.2.1 Additives effect

Lee et al.[51] studied the effects of tri-sodium phosphate (TSP) and boric acid on CHF enhancement were studied. Both TSP and boric acid are used to control pH in nuclear power plants. TSP is a kind of surfactant, and several surfactants, include TSP, have been reported to have an effect on enhancement of heat transfer. Nothing has yet been reported for the case of boric acid. CHF experiments were performed with mass flux ranging from 100-500 kg/m^{2}s and inlet subcooling temperature of 50 ^{o}C under atmospheric pressure. The test section was a vertical circular SS316 tube having an inner diameter of 10.98 mm. Its heated length was 224 mm, and it was heated by a heat flux control system using DC electricity. Fluids in the test loop were plain water, TSP solutions, and boric acid solutions. TSP solutions had three concentrations (0.2, 0.4, 0.6%), and boric acid solutions had four concentrations (0.2, 0.4, 0.6, 0.8%). In the case of TSP, 21.4% enhancement of CHF was observed at the inlet subcooling temperature of 50 ^{o}C and extremely low mass flux (100 kg/m^{2}s). In the case of boric acid, 12.4 % enhancement of CHF was observed at inlet subcooling temperature of 50 ^{o}C and extremely low mass flux 100 kg/m^{2}s.

Jeong et al.[52] Surfactant effect on CHF (critical heat flux) was determined during water flow boiling at atmospheric pressure in closed loop filled with solution of tri-sodium phosphate (TSP, $Na_3PO_412H_2O$). TSP was added to the containment sump water to adjust pH level during accident in nuclear power plants. CHF was measured for four different water surfactant solutions in vertical tubes, at different mass fluxes (100 ~ 500 kg/m^{2}s) and two inlet subcooling temperatures (50 ^{o}C and 75 ^{o}C). Surfactant

solutions (0.05 ~ 0.2 %) at low mass flux (100 kg/m²s) showed the best CHF enhancement. CHF was decreased at high mass flux (500 kg/m²s) compared to the reference plain water data. Maximum increase in CHF was about 48 % as compared to the reference data. Surfactant caused a decrease in contact angle associated with an increase of CHF from surfactant addition.

Kim et al.[53] performed the critical heat flux (CHF) experiments using a 2-D curved test section with tri-sodium phosphate (TSP: Na_3PO_4) and boric acid (BA: H_3BO_5). The CHF values of TSP solution, BA solution, and TSP + BA solution were enhanced by as much as 50 % for all experimental conditions except the condition of 150 mm radius with BA solution. The enhancement can be explained by decreased contact angle (enhancement of wettability). This CHF enhancement could provide additional thermal margin for the IVR-ERVC strategy.

4.1.2 Nanofluid effect

Although CHF enhancement, most of nanofluids tests was conducted with pool boiling condition, some tests were reported with forced flow condition. Even if flow rate condition is different, relatively high CHF enhancement results for nanofluids were presented in comparison with the case of distilled water. The formation of nanoparticle coating layer is not interrupted by forced flow. The CHF enhancement characteristics for nanofluids still appear. Table 4-1 shows the test condition of flow boiling with nanofluid.

Kim et al.[54] studied the effect of the alumina nanoparticles on CHF in the flow boiling condition at low pressure. Previously, the research on nanofluids had been focused on the pool boiling. The flow condition is more suitable when applying the nanofluid in practical devices. The results of this study firstly reported about the potential of nanofluids to enhance the CHF in flow condition. The wettability of nanoparticles coated surface was improved in comparison with one of the bare surface. High surface wettability mitigates the propagation of the hot spot.

A variety of nanofluid (alumina/water, zinc-oxide/water and diamond/water) were used to perform the CHF test in flow condition[55]. The parametric studies about the mass flux, nanoparticle material, and concentration on the flow boiling were conducted to determine the major factor on the CHF enhancement. The highest CHF enhancement was observed at high mass flux in all cases. After the CHF test, a substantial amount of nanoparticles were found to precipitate on the heater surface. The conclusion of this paper is that the CHF enhancement is associated with the wettability.

Kim et al.[56] explored the possible mechanism underlying CHF enhancement via application of the alumina nanofluid at low flow and low pressure. The CHFs of the alumina nanofluids were enhanced about 60% compared with the case of the distilled water due to the enhanced wettability of the liquid film on the heated surface. The CHF enhancement trend for nanofluid also applied to a low mass flux. This flow condition is similar to natural circulation condition for IVR-ERVC system. When local dry

out occurs, rewetting takes place readily owing to the effects of nanoparticle deposition, ultimately leading to enhanced CHF.

Vafaei and Wen[57] investigated the critical heat flux of subcooled flow boiling of alumina nanofluids in single microchannels. As the nanofluid concentration increases, more particles were observed on the surface. In the conclusion, this coating layer contributes to the explanation of CHF enhancement. It is also related to the improved wettability.

Lee et al.[58] performed the CHF test in flow boiling of alumina and silicon carbide nanofluids at low flow conditions. The subcooling parameter was considered to determine the CHF enhancement for each nanofluid. The wettability of the nanoparticle coated surface was estimated by measuring the contact angle. The CHF enhancement occurred because of the improved wettability of the liquid film on the heater surface due to the nanoparticle deposition.

4.2 Experimental apparatus

A schematic diagram of the experimental apparatus is shown in Fig. 4-1. Figure 4-2 show the detailed test section without the insulation. The visible windows are attached to make it possible to analyze the behavior of the bubble on the heater surface. The material of the test section is stainless steel 304. The actual reactor vessel is made by SA508 or SA533 material which is carbon steel. The oxide layer could be easily formed on this material. In this work, the modified heater surface characteristics induced by nanofluid were studied in terms of CHF enhancement. When the oxide layer was formed on the heater surface, many parameters should be considered comprehensively. Additionally, some parameters are coupled very closely in order to investigate the effects individually. Stainless steel material was selected to prevent the formation of oxide layer on the heater surface. The radius of curvature is 100mm which is a 1/25 scale down of the APR-1400 design. The heater shape is a quarter-circle. The dimension of each part in the test section simulated the APR-1400 based on scale law[9]. It is shown in Fig. 4-3. The heater was designed to produce different heat flux level by controlling the thickness of the stainless steel 304. The proper heater thickness was varied to design the optimized electrical resistance. Figure 4-3 shows the generated heat flux ratio according the inclination angle of reactor vessel. The magnitude of wall heat flux for APR1400 is estimated by the MAAP4 results[59]. The top point (inclination angle 80~90º) is designed to generate the highest heat flux considering the focusing effect which is caused by thin metallic layer. There is uncertainty to determine the thickness of the metallic layer. The configuration of the molten fuel in the reactor vessel is under the transient process. There is a potential to form the 3 layer configuration due to carbon. To compensate the issue, the geometry was designed to produce relatively high heat flux. The minimum gap effect of APR-1400 was also evaluated in this test facility. These designs are shown in Fig. 4-4. It was designed so that the overall heat load increased linearly by increasing the output power of the power supply in all region of the heater.

4.3 Test procedure and experimental uncertainty

In this test, direct joule heating was used to generate heat in the test section. A heat flux was calculated using Eq. (4-1). As shown in Fig. 4-2, the stainless steel 304 was welded using copper electrodes which are connected to a power supply. The voltage between the both sides of the test section (stainless steel 304) was directly measured when the electricity flowed. The exact electrical resistance of the test section was obtained using Ohm's law under a condition in which we were fully aware of the current and voltage. The effective area is limited to the part of the stainless steel 304 in contact with the water. The other side was insulated to prevent heat loss. In addition, the test section, as a whole, was surrounded by insulation. Thermocouples were attached onto the outside of the heater surface to estimate the occurrence of the CHF phenomenon.

$$q'' = \frac{V^2}{RA_{eff}}$$

(4-2)

Under the ERVC situation, the natural circulation occurs between the reactor vessel outer wall and the surrounding insulation. To simulate this condition, a pump was used to control the mass flux passing over the heater surface. Table 4-2 shows the experimental conditions of this study. The maximum mass flux is estimated as 350 kg/m^{2}s in AP1000 nuclear power plant. The design of AP1000 nuclear power plant was focused on the passive system. IVR-ERVC system was originally included in this concept. The design of flooding system and geometry of insulator were optimized. However, IVR-ERVC system was adopted later in APR1400. The capability to form the natural circulation flow is weak in comparison with AP1000. The maximum mass flux was presented as 200kg/m^{2}s[11]. The CHF is proportional to the mass flux. It is more reasonable that CHF test would be conducted under a low mass flux and low subcooling condition. The low mass flux conditions such as 50 and 100 kg/m^{2}s were selected to test the thermal limit of simulated IVR-ERVC system.

The main components of the test facility system include an overhead liquid reservoir (working fluid storage and prevention of countercurrent), a surge tank (working fluid storage), a magnet turbine pump (the working fluids were circulated by a pump with a variable speed driver), a pre-heater to control the inlet temperature of the working fluid, a flow meter to confirm the flow mass rate of the working fluid (the uncertainty of the flow mass rate was less than ± 4 %), a test section, a DC power supply and a condenser for cooling the working fluid. Two piezoresistive transmitters were installed at the inlet and exit of the test section in order to monitor the pressure at the inlet and exit of the test section. Also, the thermocouples were installed in order to monitor the temperature of the test section part, the inlet and outlet of the test section, the tank and the condenser outlet. An Agilent data acquisition system was used

to read the instrument outputs and translate them into physical parameters. A computer was used to sample all the data periodically and to monitor the experiment. After flooding working fluid in test facility, degasing process was conducted to eliminate the non-condensable gas by heating up to 95℃. A stepwise power escalation is initiated. About 50 kW/m² heat flux was increased in each step. Each power step lasts a minute until a new steady state is achieved. This process was equally applied in all tests. The new test heater was replaced in every test to make the initial surface condition. Figure 4-5 shows the heat loss in heated test facility. Original heat was generated by electrical heating. The circulated fluid obtained the heat through the test section. Some portion of obtained heat was used to increase the test section itself. The heat balance test was conducted at specific condition (mass flux: 100kg/m²s, subcooling: 10 K). The thermal insulator was tightly packed to reduce the thermal heat loss. About 8% was estimated as heat loss in this test facility.

4.4 Results and discussion

In this study, the CHF tests were conducted with a test section at the specific mass fluxes such as 50 kg/m²s and subcooling condition of 10 K under atmospheric pressure. Working fluids are SiO_2, SiC, graphene oxide, Al_2O_3. We already obtained the CHF enhancement trend for each nanofluid with the pool boiling CHF tests. It is required to confirm that CHF enhancement trend is applied in all CHF tests regardless of flow condition. Figure 4-6 shows the result of the CHF tests. The highest CHF enhancement was observed when the graphene oxide nanofluid is used as working fluid regardless of the flow condition. Nanoparticle coating layer was observed on the heater surface after CHF tests. The static contact angle was measured for each cases as shown in Fig. 4-7. The behavior of the generated vapor was influenced by this contact angle. If the contact angle is relatively high, the diameter of generated bubble would tend to be large. However, the liquid supply will be enhanced. These phenomena is theoretically in conflict. We observed the bubble behavior on the heater surface by using the high speed camera. The bulk vapor was periodically generated ash shown in Fig 4-8. The thickness of this vapor is related to CHF enhancement. The CHF enhancement is inversely proportional to the thickness of this vapor.

The CHF occurred in the upper region of the test section in all test cases. It is reasonable that the fluid flowing at this position has the highest enthalpy with the bulk vapor. Additionally, the effects of the minimum gap in the test facility are not critical to the CHF. It is confirmed that the engineered design revision of reactor insulation avoids the early CHF issues. The CHF was enhanced as the mass flux increased. The CHF limits for water are relatively higher than the results obtained at KAIST and ULPU configuration II under the same test conditions. The reason of this increase is caused by the unique channel design related to the minimum gap. The cross sectional area of the channel varies due to the minimum gap. It increases the flow instability which is the leading positive effect on CHF. The

small scale test facility was used to measure the thermal limit on the upper region of the heater. Therefore, the instability effect was stronger in the upper region of the heater. Furthermore, the effects of the geometric scale were studied by varying the dimension of the curvature radius[60]. The variation of CHF result according to the curvature radius was caused by the different exit quality and the position of the two-phase boundary. In this work, the curvature radius is far smaller than one of the KAIST and ULPU configuration II. There is a potential to increase the CHF due to the small scale geometry. The CHF limit was enhanced when the graphene oxide nanoparticles were dispersed in the working fluid in the wide range of flow condition. This enhancement ratio increased as the mass flux is increasing as shown in Fig. 4-9. This trend is attractive to IVR-ERVC system. The additional thermal margin could be acquired by just adding the graphene oxide nanoparticles to the flooding water without severe economic concerns. The initial surface condition of each test is clean. This clean condition is kept by replacing with a new heater. After the flow boiling experiments, build-up layers are observed on the heater surface as shown in Fig. 4-10. Figure 4-10 shows the SEM images of heater surface after CHF tests were completed. The case of the bare heater surface shows the plain surface without contaminants. The SS304 has high resistance to form the oxide layer on the surface. A few minutes was spent to take the CHF test. It is a short time to form the pollutant on the heater surface. Graphene oxide nano particles are deposited on the heater surface induced by boiling in nanofluid. It is easily estimated that the coating layer is composed with only graphene oxide nanoparticles. After CHF tests, the roughness was measured by the confocal laser scanning microscope. The roughness (Ra) of both bare surface and graphene oxide coated surface is 0.182 μm and 1.275 μm respectively. This coating layer has been already reported in other related research results. The build-up mechanism of the coating layer is that the nanoparticles are deposited on the dried surface which is the spot where the bubbles departed from the heater surface. The nanoparticle coating layer was formed due to the evaporation of the thin liquid microlayer on the heater surface. The nanoparticles contained in the microlayer were deposited on the heater surface.

So far many studies have presented that the main cause of CHF enhancement was the improved wettability of the nanoparticle coated heater surface. The wettability of the surface is estimated by measuring the static contact angle on the heater surface using a sessile drop test. Generally, the contact angle of the nanoparticle coated heater decreased in comparison with the non-coated or bare heater surface. As the result, the inconsistency relationship between the contact angle and the CHF value was acquired from measuring the contact angle. Although the contact angle is relatively increased, the CHF is enhanced in comparison with the case of the uncoated heater in distilled water. The CHF tests were conducted under a pool boiling condition. In this work, the present flow condition is high quality on adjacent heater surface. This condition was estimated as the annular flow region in the two phase flow map. In this region, the CHF or the liquid film dryout (LFD) is determined by the thickness of the liquid film covering the heater surface. The mechanism is shown in Fig. 4-11. Numerous bubbles are generated

and detached from the heater surface. Two phase flow with high quality makes the hydrodynamic instability. There is a chance to form the local dry out region caused by this instability. The high wetted surface aids to supply liquid to the dried region. Ultimately, the CHF phenomenon is delayed. This mechanism has been studied to explain the CHF enhancement for nanofluid under the flow condition. In this study, there is no improvement on wettability due to the coating layer. The present result of the unimproved wettability shows that it is limited to explain the CHF enhancement by supplying the liquid more.

To avoid the CHF or sustain the nucleate boiling, rapid heat removal is essential on the dried region. Ultimately, CHF phenomenon occurs due to the inadequate heat removal from a heated surface. The CHF could be enhanced by supplying more liquid to the dried region or venting the vapor rapidly from the dried region. In this work, the wetting characteristics of the heater surface were analyzed by measuring the static contact angle. The result of the static contact angle was increased in comparison with one of the base surface. It means that the CHF enhancement mechanism is limited as the result of unimproved wettability. The observation of the changed hydrodynamics wavelength is limited with the present test facility at designed condition. The conduction heat transfer through the heater itself could be considered as additional CHF enhancement mechanism. This heat transfer process could delay overheating the heater surface. The effect of the CHF enhancement is expected. The parameter which is related to this effect has been defined as thermal activity in Eq. (4-2) [62].

$$S = \delta \sqrt{\rho_h c_h k_h} \qquad\qquad (4\text{-}2)$$

The thermal activity can be strengthened when a material with high thermal conductivity coats the heater surface. The coating thickness is an important parameter when estimating or calculating the value of the thermal activity. The ordinary material of nanoparticles is a metallic or oxide component. The thermal conductivity of these materials is not superior in comparison with the material of the heater. Table 4-3 shows the value of each parameter according to the heater material based on the thermo-physical properties. Although the thermal conductivity of the graphene allotropy is excellent, the thickness of the coating layer is several micro-meters. The increase of the thermal activity was not initially considered in explaining the CHF enhancement. However, the result of the thermal activity is different. Figure 4-12 shows the heat dissipation result on the unheated test heater surface at room temperature and atmospheric pressure. 50 μl of the heated distilled water (80 $^{\circ}$C) was dropped on the upward heater surface. A change in temperature distribution was observed by using an IR camera as shown in Fig. 4-12. The heat transfer occurs more rapidly when the graphene oxide was coated on the surface. This characteristic is applied to the heat transfer during the boiling on the dried region. Thermal activity can delay the bubble formation resulting in hot spot. Thus, CHF can be delayed and enhanced

without improved wettability. Fortunately, the heat transfer area on the surface could be easily controlled because the graphene coated heater surface had an un-wetted characteristic. The results of the thermal activity can be directly compared with the heaters.

4.5 Conclusion

In this work, the CHF tests were conducted to investigate whether the additional thermal margin could be obtained in the IVR-ERVC strategy by using graphene oxide nanofluid. The test conditions was selected for a low mass fluxes at 10 K subcooling. The design of the test section simulates the APR-1400 nuclear power plant according to a scale law. The size of the test section is scaled-down to 1/25.

The following results were obtained.
(1) When graphene oxide nanofluid was used as a base fluid, the CHF enhancement is the highest in comparison with distilled water and other nanofluids.
(2) A thin coating layer without showing any improved wettability was observed on the heater surface for graphene oxide nanofluid.
(3) The rapid heat dissipation was observed on garphene coated heater surface. This phenomenon was caused by the improved thermal activity.

Table 4-1. Overview of CHF experiments on flow boiling using nanofluid

	Heater Dimension (mm)	Subcooling (K)	Mass Flux (kg/m²s)	Pressure (MPa)	Nanofluid	Concentration (volume%)	Max. CHF enhanceemnt (%)
Kim et al. (2008)	D =8.7 (I.D) L = 240 L/D = 27.6	<20	1000 1500	0.1	Al₂O₃/water	0.01	30% (for 1500kg/m²s)
Kim et al. (2009)	D =6.35 (I.D) L = 100 L/D = 15.7	<20	1500 2000 2500	0.1	Al₂O₃/water ZiO/water Diamond/water	0.001 0.01 0.1	53%, 53%, 38% (for 0.1v%, 2500kg/m²s)
Kim et al. (2010)	D =10.98 (I.D) L = 500 L/D = 45.5.	25, 50	100 200 300	0.1	Al₂O₃/water	0.001 0.01 0.1	70.24% (for 0.01%, 50℃, 100 kg/m²s)
Vafaei and Wen (2010)	D =0.510 (I.D) L = 306 L/D = 600	60~70	650 900 1120 1370 1630	0.1	Al₂O₃/water	0.001 0.01 0.1	51% (for 0.1%, 650kg/m2s)
Lee et al. (2012)	D=10.98(I.D) L=500 L/D=45.5	25, 50	100 150 200 250	0.1	Al₂O₃/water SiC/water	0.01	15% (for 50℃, 200 kg/m²s) 42% (for 25℃, 150 kg/m²s)

Table 4-2. Test condition for CHF experiment

Test matrix	
Heater radius(mm)	100
Test section gap size(mm)	20
Heating method	DC heating
Circulation method	Forced circulation
Pressure (kPa)	101.3
Mass flux(kg/m2s)	50, 100
Inlet subcooling(K)	10
Minimum gap point(degree)	56.6
Working fluid	distilled water, graphene oxide nanofluid

Table 4-3. Thermo-physical properties of the heater and materials

	ρ_h (kg/m^3)	c_h (J/kgK)	k_h (W/mK)	$\sqrt{\rho_h c_h k_h}$
SS304	8030	500	16.2	~255
Graphene	~2230	~710	490	~2814
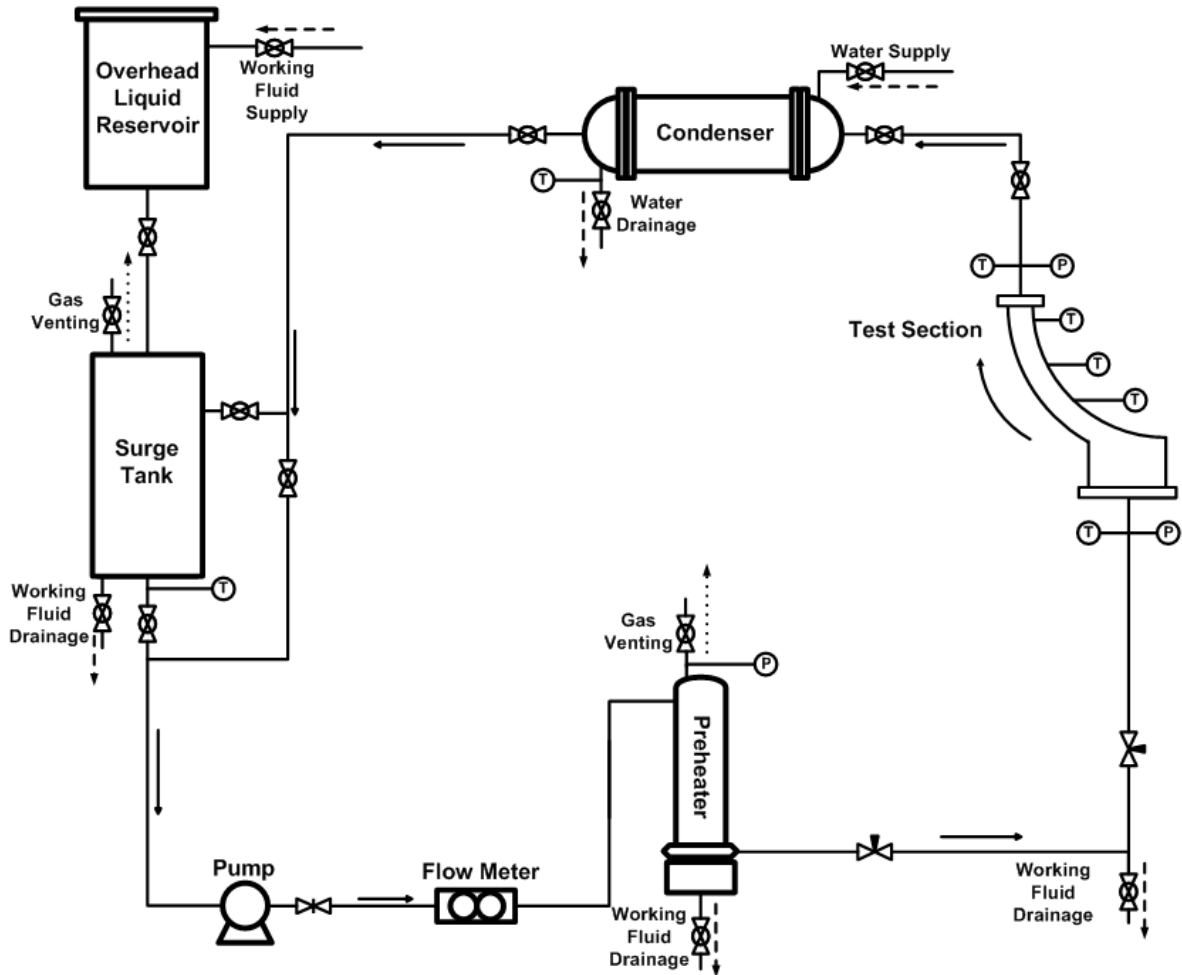
Fig. 4-1 Schematic diagram of the experimental loop
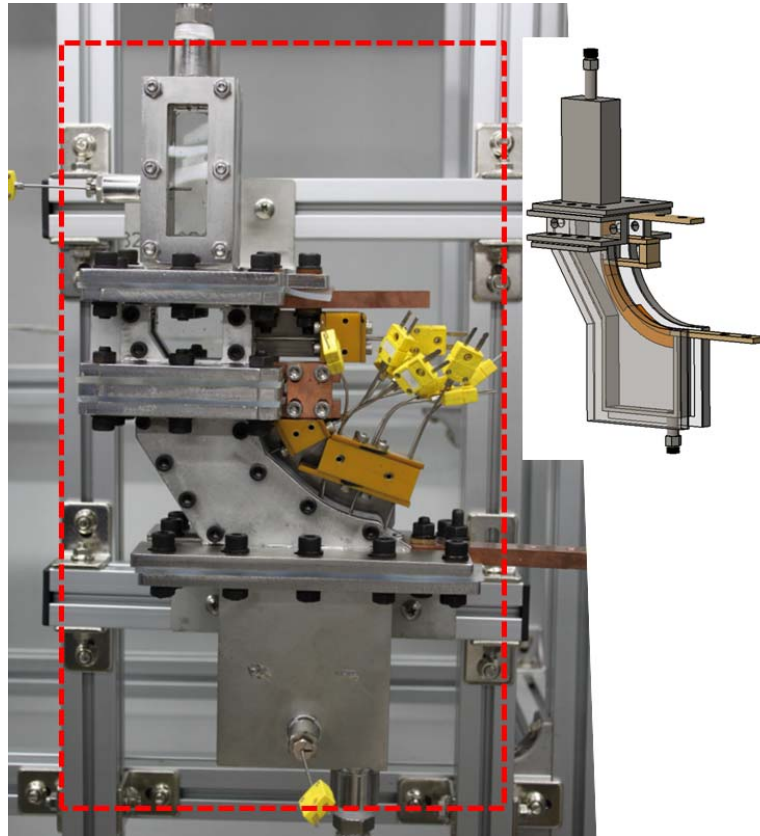
Fig. 4-2 Geometry of test section on front view
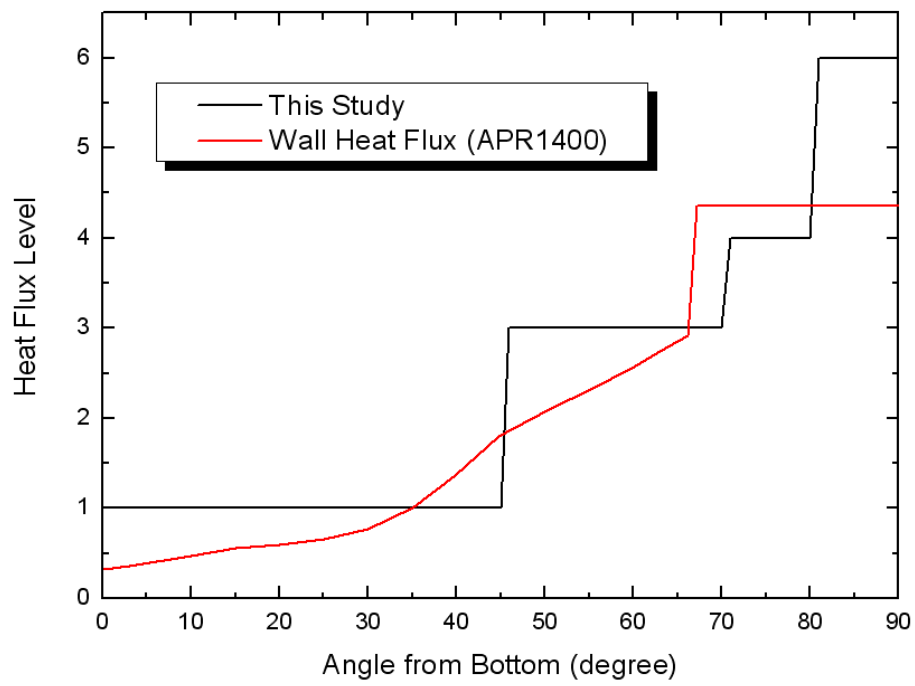
Fig. 4-3 Heat flux distribution of the test heater section

Flow direction
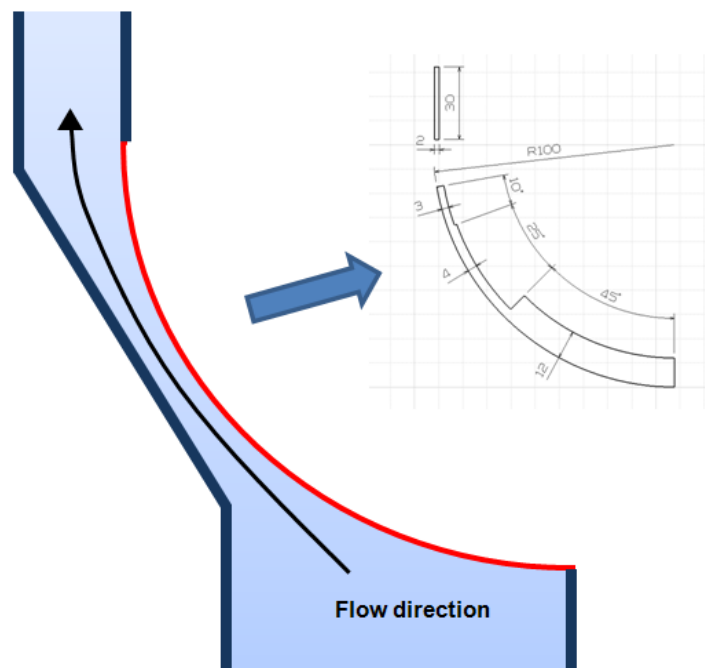
Fig. 4-4 Flow channel of test section and heater geometry view
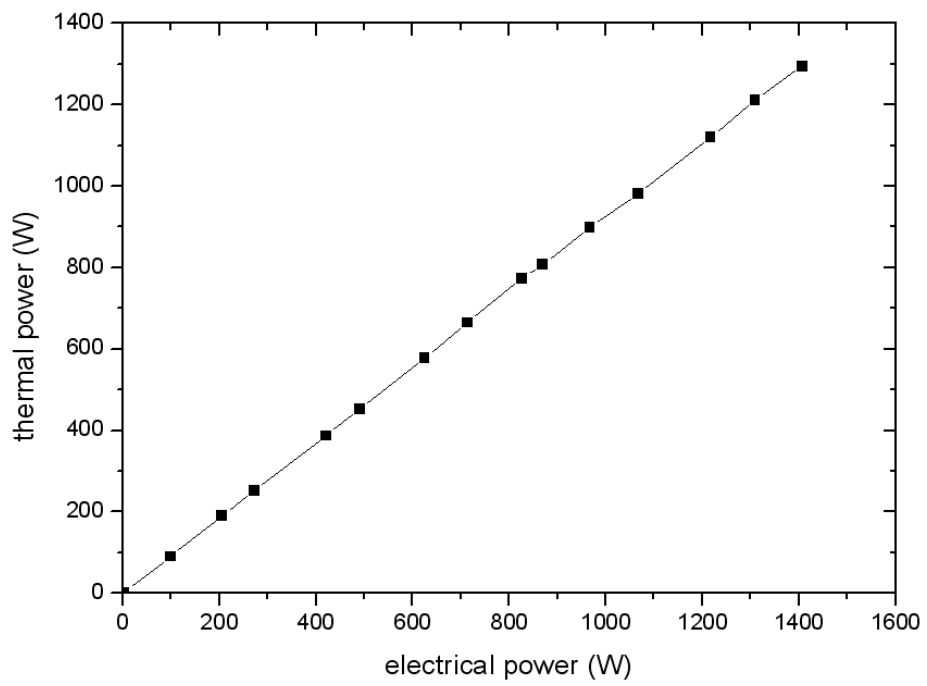
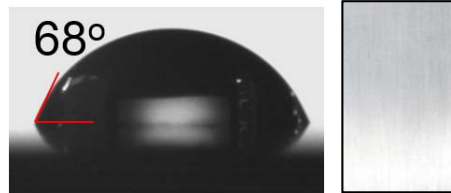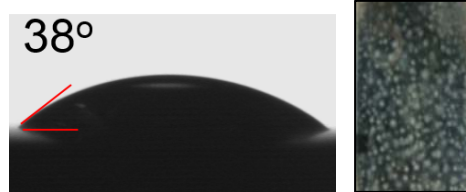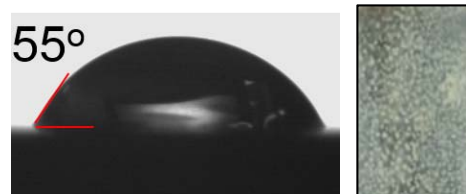Fig. 4-5 Result of heat balance test between the thermal power and electrical power.
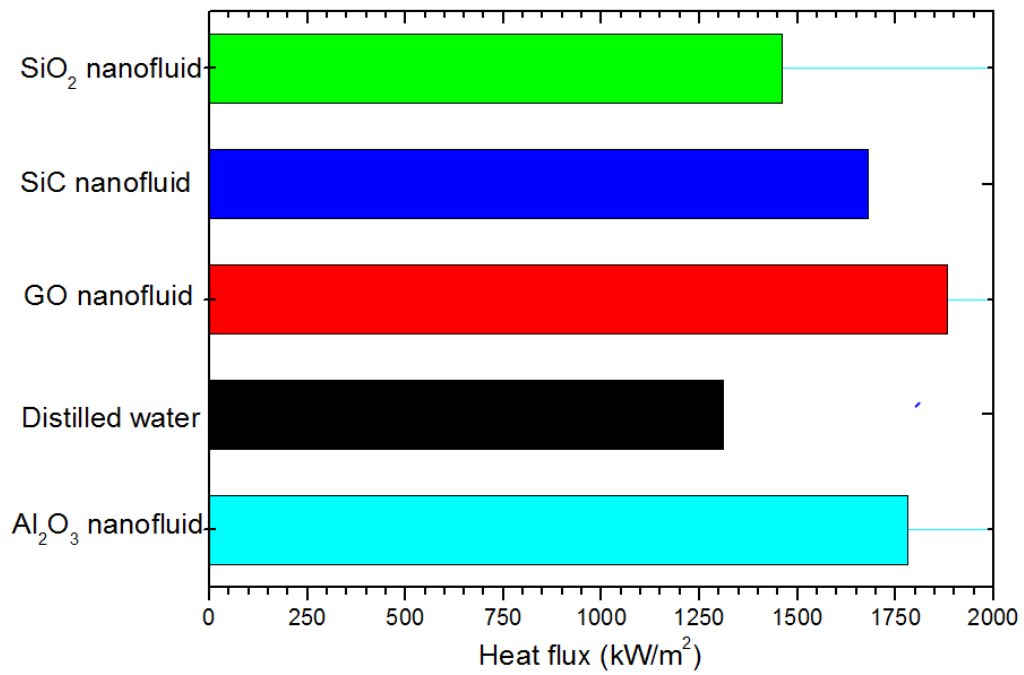
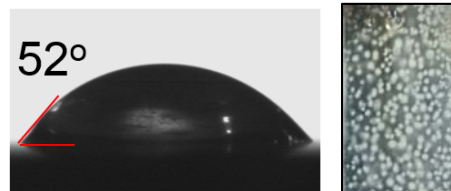Fig. 4-6 CHF results at subcooling 10K and 50 kg/m^{2}s condition
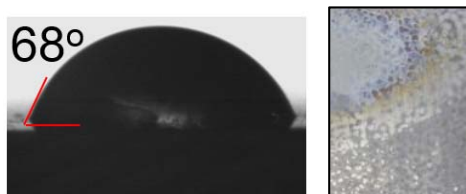
(a) Bare surface

(b) SiO_2 nanoparticle coated surface
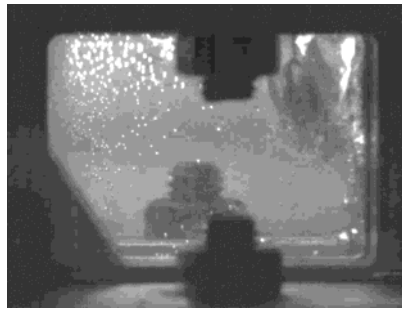

(c) SiC nanoparticle coated surface

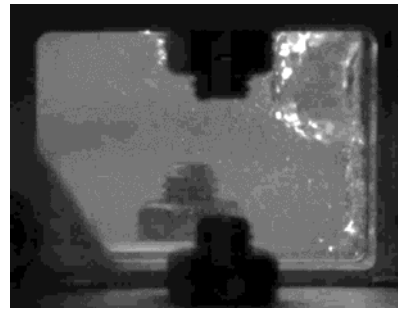(d) Al_2O_3 nanoparticle coated surface

(e) Graphene oxide particle coated surface
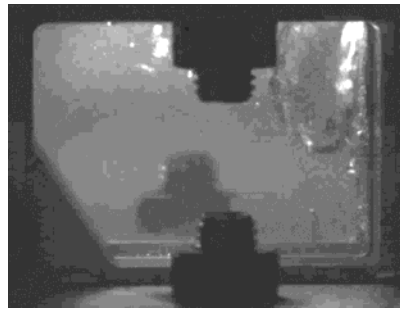
Fig. 4-7 Static contact angle and coated surface

(a) Distilled water

(b) SiO2 nanofluid

(c) SiC nanofluid
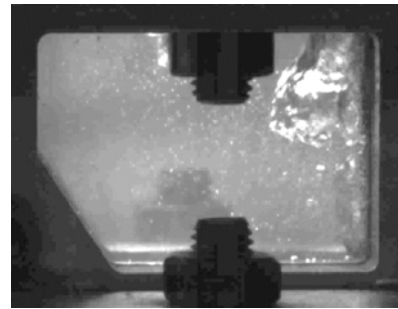
(d) Al2O3 nanofluid

(e) Graphene oxide nanofluid

Fig. 4-8 bubble behavior on the heater surface
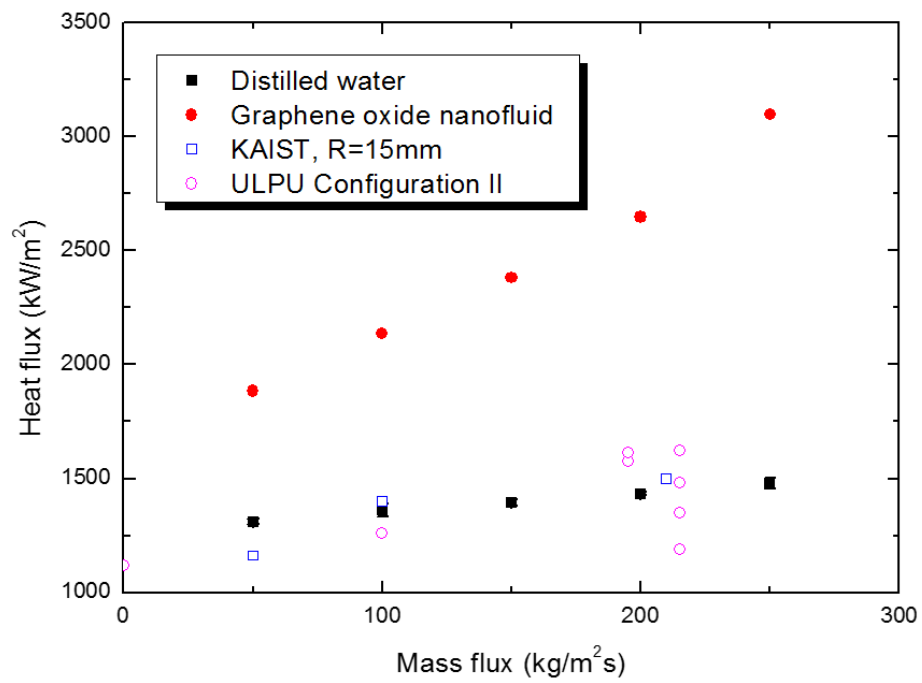
Fig. 4-9 CHF results according to mass flux at subcooling 10K condition.
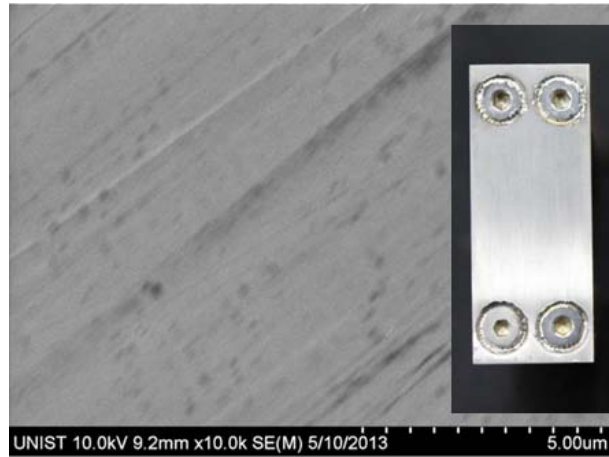
(a) Bare heater surface
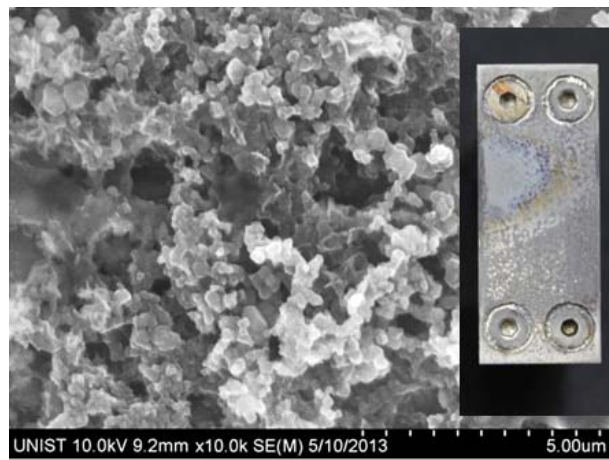
(b) Graphene oxide coated heater surface

Fig. 4-10 SEM image on heater surface after the CHF test
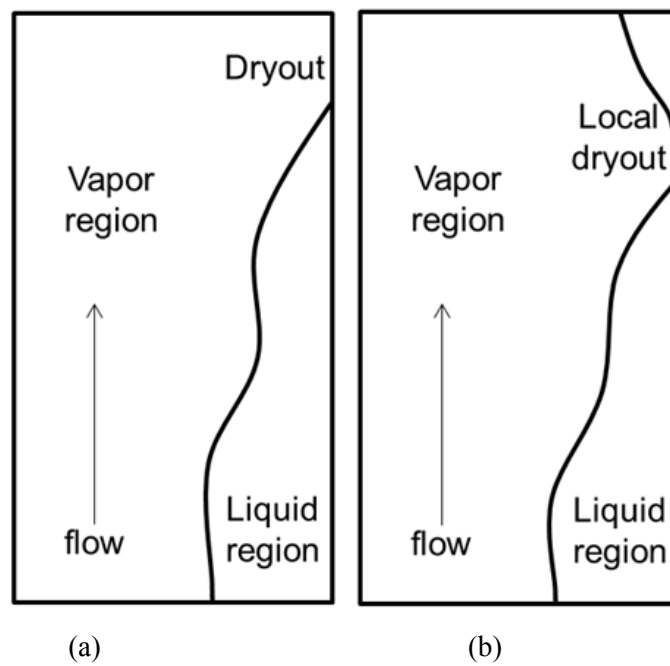
Fig. 4-11 CHF mechanism in the vertical geometry (a) Normal LFD (b) Local dryout due to hydrodynamic instability
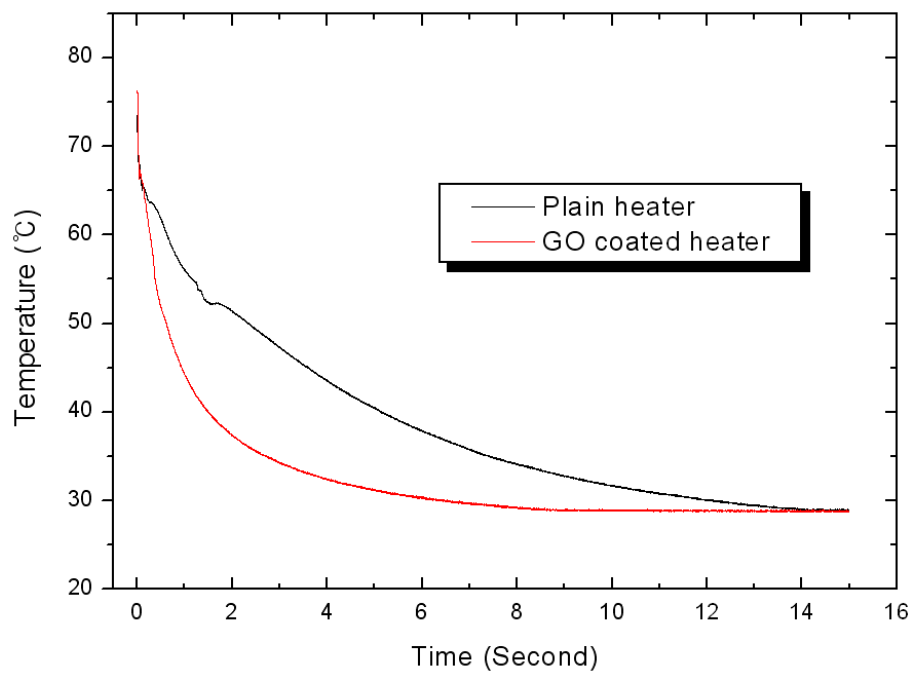
Fig. 4-12 Temperature change on the heater surface with a droplet (80℃, 50μl)

(a) Bare heater surface

(b) Graphene oxide coated heater surface

Fig. 4-13 Temperature distribution images on the heater surface with a droplet (80℃, 50μl)

Chapter 5. GALLIUM LIQUID METAL FLOODING SYSTEM

5.1 Introduction

In the light water reactors, a number of safety systems have been installed to prevent the progression of the accidents and return to the safety condition. However, although the safety systems have been established in the plants, some severe accidents happened due to the human errors and unexpected natural disasters. The repres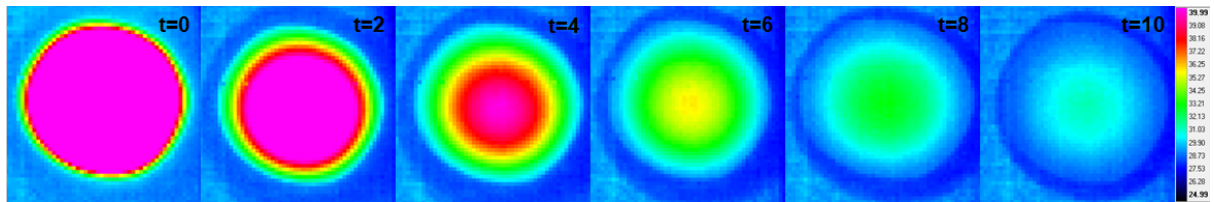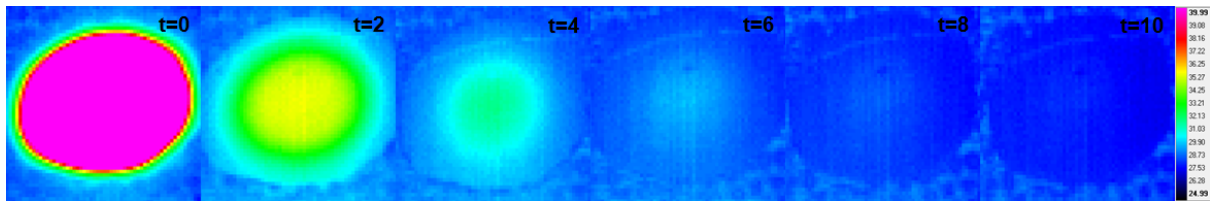entative examples of severe accidents are TMI[63] and Fukushima nuclear accidents[64]. There are a lot of reports analyzing the accidents to compare each other. There are many differences about the reactor type, generating capacity, containment building and causes of accident as well as accident progression. The most noticeable difference may be on the final location of the molten fuel. If the proper cooling systems could not be applied, the core material could be relocated to the bottom of reactor vessel. It is the natural movement of the corium which is the molten core material under severe accident condition. In the TMI nuclear accident, this corium was adequately cooled and certainly retained in reactor vessel. The progress of accident was finished in this step. When the proper cooling was not adopted under a severe accident, the corium could escape from the damaged reactor vessel. While the behavior boundary of radioactive materials was limited in reactor vessel in TMI accident, Fukushima nuclear accident caused even secondary damage such as ground water contamination which might occur with corium melt-through. The severe accidents really make difficult issues to deal requiring tremendous time and cost. The different results between TMI and Fukushima accidents give one of the most important lessons that the integrity of reactor vessel should be protected to minimize the spreading of radioactive materials through the broken boundary. It is called as in-vessel retention (IVR) or in-vessel corium confinement and cooling. One of the effective features for the IVR is an external reactor vessel cooling (ERVC) strategy. The effectiveness of IVR-ERVC has been studied for decades by many researcher[9, 10]. This strategy has been adopted for the light water reactors such as Loviisa VVER, AP600, AP1000, and APR1400 through external reactor vessel cooling (ERVC). The main heat removal mechanism of IVR-ERVC condition is boiling heat transfer on the outer surface of reactor vessel. The function of this system is determined by the limitation of boiling aside from material issues related to temperature, stress, fatigue and creep. The limitation of boiling is critical heat flux (CHF). When CHF occurs, the heated surface is covered with vapor film. A few of CHF studies have been carried out with test facilities simulating the flow geometry and conditions of IVR-ERVC.

Table 5-1 shows the applied mitigation strategies depending on the reactor type. The mitigation strategy can be divided into two types such as in-vessel corium cooling and ex-vessel corium cooling according to the position of the corium. In general, ERVC strategy gives sufficient thermal margin for small and medium-sized reactors like AP600 and AP1000. However, it is not certain whether the IVR-ERVC strategy provides enough thermal margin to prevent CHF phenomenon even for large-sized

nuclear power plants which have a large-power capacity around 1500 MWe. One of the advantages of ERVC strategy is to prevent the release of radioactive materials from the reactor vessel during the severe accidents. It also simplifies the accident scenario by eliminating the direct containment heating (DCH), ex-vessel fuel-coolant interaction (FCI) and molten core concrete interaction (MCCI) which are complicated and still uncertain. The recommendations for increase of CHF include porous coating on the vessel outer surface, increasing the reactor cavity flood level and streamlining the gap between the vessel and the vessel insulation.

Flooding the liquid metal into reactor vessel cavity was proposed conceptually by Park and Bang[65] to prevent CHF itself. Predicted heat flux, in particular, at the outer zone of reactor vessel with focusing effect of metal layer of corium formed in the inner vessel is beyond the critical heat flux under normal ERVC conditions of boiling heat transfer. Therefore, when the liquid metal is flooded into the cavity instead of normal water flooding for ERVC, the heat transfer mode is changed from two-phase of water to single-phase heat transfer of liquid metal. Although the heat was ultimately removed by boiling of water coolant in an additional inventory, the integrity of reactor vessel could be protected by reducing the focusing effect causing CHF occurrence. In this work, the UNIST liquid-metal experimental facility was designed and established to evaluate the concept of the liquid metal-based ERVC in terms of the improved heat transfer without CHF issues.

5.2 Experimental apparatus

Figure 5-1 shows the test section of liquid metal-based IVR-ERVC. The simulated decay heat was generated from the cartridge heaters which was inserted in the heated object. The material of the heated object was copper   which was used to manufacture the desired geometry. 10 kW electric power is applied to this object via cartridge heaters. The refrigerant-123 is used as working fluid because CHF phenomenon can be studied at limited heat flux condition of the current facility capacity. R-123 has low boiling point (27.6 $^{\circ}$C) and about 8 times lower than predicted CHF value of water. Therefore, it is possible to simulate the IVR-ERVC phenomena and compare differences between typical ERVC and liquid-metal ERVC strategies more realistically. The diameter size of the simulated vessel is 0.14 m. Gallium is used as liquid metal coolant. The melting point of this liquid metal is about 30 $^{\circ}$C while its boiling point is about 2400 $^{\circ}$C. The available temperature range of this metal is wide enough to operate as the heat transfer medium in a liquid phase. The thermal conductivity of gallium is about 50 times greater than one of water at 30 $^{\circ}$C. This liquid metal is considered as a potential candidate for IVR-ERVC strategy with liquid metal.

As shown in Fig. 5-2, the experimental facility consists of test section, condensers, power controller, and data acquisition system. The input power was calculated by using the current and voltage indicated on the display of power controller. The temperature data were obtained from embedded thermocouples.

Sudden temperature jump is estimated as CHF phenomenon. When the maximum temperature is beyond the design limit of material, the power could be automatically shut down to prevent the damage of cartridge heaters and heated object. The embedded thermocouples were located in 10, 20, 40, 60, 80, and 90 degrees on the basis of stagnation point which is the lowest point on the heated surface. The temperature data obtained from these thermocouples are used to calculate the local heat flux and heat transfer coefficient on the surface of heated object.

5.3 Test procedure and experimental uncertainty

The first step for the test is to make the saturated and steady state for coolant at low heat flux condition. The first stage of heat flux is 10 kW/m^2. After reaching the steady state condition, a stepwise power escalation was initiated with increments of 10 kW/m^2 heat flux. Each power step lasted 10 minutes until a new steady state was achieved. In the liquid-metal test run, the filling height of liquid metal was 0.03, 0.06 m as shown in Fig. 5-3.

Equation (5-1) expressed the heat transfer rate which is composed of the heat flux and the heat transfer area. The heat flux (q_1") was calculated based on Fourie's law. Some thermocouples are imbedded in the copper heated object as shown in Fig. 5-4. Heat flux (q_2") on the surface was important to determine the CHF value or thermal margin to CHF. The maximum uncertainty of the thermal conductivity is 0%. This value is a variable corresponding to the temperature. Temperature change was reflected. The uncertainty for the temperature is 1K. A K-type thermocouples were used. The uncertainty of the dimension like x, R is 0. 1 mm. This value is based on the manufacturing tolerance. The uncertainty of heat flux is ±3.4%.

$$\int_A Q = q''\Delta A$$
$$q_1''\Delta A_1 = q_2''\Delta A_2 \tag{5-1}$$

$$\frac{\Delta q''}{q''} = \sqrt{\left(\frac{\Delta k}{k}\right)^2 + \left(\frac{\Delta T}{T}\right)^2 + \left(\frac{\Delta x}{x}\right)^2 + \left(\frac{\Delta R}{R}\right)^2} \tag{5-2}$$

5.4 Results and discussion

Table 5-2 shows the thermal properties of liquid metals which have been considered as nuclear coolants for fast reactor conventionally. The first priority considered to apply a liquid metal in ERVC strategy is to check whether a liquid metal has the low melting temperature and the high boiling temperature. The other requirement is on whether it is chemically stable or not. And the desirable liquid

metal has good thermal properties for the heat transport. In particular, among those, the melting temperature is much of concern during the procedure of flooding in the reactor cavity and the period exposed to the air. If the liquid metal is solidified during an injection from the storage tank of a liquid metal to the reactor cavity, the ERVC strategy itself can be failed. After flooding the reactor cavity successfully with the liquid metal, the desirable natural circulation flow could be stably formed in a liquid metal pool as long as there are no solidified layers formed. Although liquid metal is used as a flooding material to remove the uncertainty of the CHF limit, the similar phenomenon can occur if the boiling point of a liquid metal is low or close to operating temperature of the liquid metal pool. When core melts and deposits on the bottom of reactor vessel, the temperature of a liquid metal directly contacting with the reactor vessel is very high due to the decay heat. It is checked through the thermal-fluid analysis in this work. Based on the above-mentioned requirements, the promising candidate among the liquid metals considered in nuclear applications. Gallium has the enough low melting point of ~29.7 ^{o}C to ensure to maintain liquid state within the containment building. Even though the overall thermal properties of Na are superior to those of gallium, there are no chemical reactions between gallium and water[66].

As coolants, liquid metals should be stored to maintain liquid state in the storage tank which has heating and heat shield system. The melting point of gallium is 29.76 °C. Gallium can be maintained as the liquid state in the storage tank without much heat required because the containment building-inside temperature usually is higher than a room temperature. But, the high temperature gallium has relatively lower viscosity. Therefore, the additional heating systems to the gallium storage tank and injection pipes can enhance the flooding velocity and guarantee the liquid state.

The location of the storage tank in the ERVC system is important in terms of passive safety. The requirements for the storage tank could be summarized as follows.

✓ The storage tank should be located near the reactor.
✓ The storage tank should in a higher position than that of a reactor cavity.
✓ The capacity of the storage tank should be designed in a minimum covering the gallium inventory required for full flooding of the reactor cavity.

The first is required to immediately respond to severe accidents. To meet this, there should be enough space to install the storage tank near the reactor. Therefore, the concept about this space could be considered from the design stage of the new power plant in order to consider a liquid metal in the ERVC strategy while a storage tank for operating nuclear power plants should be portable. The second is required to operate the ERVC system under the event of the station black-out. The ERVC system should be designed to inject the liquid metal into the reactor cavity by the gravity without any external power. This passive concept is a lesson learned from the Fukushima nuclear accident caused by a natural

disaster. This concept is shown in Fig. 5-5, 5-6. Gallium has much higher viscosity than water so that filling up the cavity takes longer as long as everything else is same. Therefore, in order to accelerate the injection rate of the liquid metal, locating the storage tank in upper position, replacing the injection pipe with large diameter, and pressurizing the storage tank to increase the pressure difference between the inner storage tank and the reactor cavity are required. The last one is required to reduce the stress added on the structure. The density of gallium is about 5 times heavier than that of water. The gallium storage tank causes the big loads on the supporting structures. The most fundamental way to reduce the load is to design the storage tank in a minimum capacity for full flooding of the cavity. And the high cost of gallium compared to water requires the minimization of tank capacity.

In the typical ERVC system, the borated water could be considered as the ultimate heat sink which is defined as in general, a virtually unlimited supply of water that can be used by nuclear reactor to cool vital systems and the primary containment. The decay heat generated in corium is removed through the outer reactor vessel wall by the boiling heat transfer under natural convection. The heat removal on the outer reactor vessel wall is restricted by the thermal limit of CHF. The space outside the reactor vessel is filled with the liquid metal to avoid the thermal limit that occurs in water. The main function of gallium in ERVC system is to perform the heat transfer without CHF issue only between the reactor vessel and the ultimate heat sink, if we assume only to consider the ERVC system, not considering the containment overpressure due to steam. A gallium pool can also play a role to store the heat by its specific heat capacity without phase changes before the heat is transferred to the ultimate heat sink. To enhance the safety of the reactor vessel from the viewpoint of the heat storage or extended heat transfer area or lowering heat fluxes, flooding a large amount of liquid metal into the reactor cavity is positive. Liquid metal plays a role as the heat transfer and storage medium in the ERVC system. The borated water is still used as the ultimate heat sink in the system. Of course, competitions between economics and safety should be considered at the same time.

The decay heat generated in corium is transferred between the reactor vessel and liquid metal. Then the heat is considered to be ultimately dissipated by boiling in the surface facing borated water in the present work. The heat removal capacity of the system depends on the relative configuration between liquid metal and borated water. The possible configuration of both gallium and borated water could be considered with two types depending on whether or not the direct contact occurs with each other. This concept is shown in Fig. 5-5 and 5-6.

In the first configuration named as a side cooling in this work, two fluids are separated by the block structure. When LOCA occurs, the cavity would be flooded with water from the broken pipe and spray cooling systems. In the gallium flooding system, a gallium layer is situated below a water layer due to the density difference. Therefore, it is expected that there are no significant effects related to water previously existing in the cavity. The sufficient heat transfer area between liquid metal and borated water could be provided. Additionally, the area can be enlarged by attaching the fins on the block

structure surface, for example. It ensures the safety of the reactor vessel and decreases the temperature of liquid metal in the ERVC system.

In the second configuration named as an upper cooling in this work, the cavity is flooded with both borated water and gallium in the same reactor cavity space which is not separated like the first configuration. As the result, two layers of the fluids are naturally formed by the different density. The application of a liquid metal in ERVC strategy can be easier and simplified in terms of structuring. However, large amounts of liquid metal are required to flood the reactor cavity in the present system. Another disadvantage is that the heat transfer area between liquid metal and borated water is small compared with the first configuration because utilization of the space around the reactor vessel is limited. This concept of upper cooling could be applied immediately to operating nuclear power plants through the some design changes such as installation of gallium storage tank. In the current study, the feasibility of the gallium-based IVR-ERVC system is evaluated by using the CFD analysis for two configurations.

Heat was ultimately removed by vapor formation regardless of flooding the liquid metal as shown in Fig. 5-7. However, when the liquid metal was flooded as the new IVR-ERVC concept, vapor generation was decreased in comparison with typical IVR-ERVC system in which the surface of heated object was directly facing with the R-123 coolant because the heat transfer area was enlarged via liquid metal filled in the cap structure. The small-size bubbles merged into larger bubbles along with the heated surface. When the surface of heated object is directly exposed to the coolant, the surface temperature is quickly changed due to bubbles behavior. The formation of larger bubbles or higher void fraction is considered as an indicator of critical heat flux condition causing critical damage on the reactor vessel. Figure 5-8 shows the temperature history form a thermocouple. This thermocouple is embedded near the surface of the copper heated object. When the heat load is over 1000 W, there is a unique phenomenon which is temperature jump. It means that the bulk vapor film was suddenly formed on the heater surface. The heat transfer coefficient deteriorated and the surface temperature was increased to compensate the heat transfer coefficient. This is CHF. In the liquid metal system, new heat transfer phenomena could be expected and the CHF phenomenon could be prevented. Although the larger bubbles were formed on the surface of cap structure, heat also could be dissipated more quickly through the liquid metal itself. This heat dissipation phenomenon can prevent the local temperature rise or hot spot of heated object. Even though the enlarged heat transfer area is considered as the main factor to prevent CHF, delayed temperature response can contribute to enhancing critical heat flux.

The experimental results are compared with CFD analysis. The geometry for CFD analysis was a hemispherical shape. The geometry consists of SS cartridge heaters, cooper heated object, gallium liquid metal, and SS cap structure. The cartridge heaters were used to simulate the decay heat. The boundary condition for CFD was determined by considering realistic situation. Volumetric heat source was applied in the domains indicating the cartridge heaters. The cooling surface was set to have the constant temperature (32°C) to simulate the boiling phenomena. In the experimental condition, the

contact resistance between the cartridge heaters and heated object is present. Wetting characteristics of liquid metal should be also considered because the contact condition between the liquid metal and structure is major factor to determine the heat transfer. In CFD simulation, there is no contact resistance in all interfaces. As the result of this setting, the temperature of CFD analysis is lower than one of experimental results about 5 K in the same position. It does not seriously affect to prediction of the local heat flux because overall temperature rise in the object are equally applied.

The liquid metal system was originally considered to prevent the CHF. Figure 5-8 shows the heat flux profile along the heated surface depending on the flooding conditions. After relocation of the corium into the bottom of reactor vessel in the severe accidents, the thin metallic layer is expected to be formed on the top of corium pool resulting in the focusing effect. The temperature of this layer is very high due to the poor radiation heat transfer. High heat flux to outer vessel wall is predicted due to this conduction layer. The focusing effect was reflected in the present work by controlling the location of cartridge heaters. When the heated surface was exposed to the coolant without the liquid metal, high heat flux was generated at top region of hemispheric (Z-axis: 0 m). However, when the liquid metal was flooded, this focusing effect was reduced. The reduction ratio is very noticeable when the heat flux condition is high. This result is surely owing to the enhanced heat transfer of flooded liquid metal. The heat transfer modes should be considered to understand the heat transfer characteristics induced by flooded liquid metal. The heat source is decay heat regardless of flooding conditions. The generated heat is transferred through the reactor vessel by conduction. The heat is removed by boiling on the outer surface of reactor vessel in the original IVR-ERVC strategy. On the other hand, the heat is also transferred to the liquid metal by convection. The top surface of flooded liquid metal might be directly facing with water coolant depending on a design option of flooding. Most of heat is finally removed by boiling on the outer surface of container to hold the liquid metal on flooding state.

Figure 5-11 shows the temperature distribution result of CFD analysis. The temperature of top region for flooded liquid metal is relatively lower than the temperature of other region. It means that the amount of heat transfer is negligible. This estimation is valid when the flooding height is enough high. If the flooding height is small, the exposed surface is maintained at high temperature. Active boiling heat transfer takes place on this surface. Two important insights could be obtained by analyzing temperature gradient. The traditional fluid has the constant ambient temperature. However, the high temperature gradient exists in the liquid metal because the thermal conductivity of liquid metal is high. It is caused by low Prandtl number of the liquid metal. Other insight is that the temperature of outer surface for reactor vessel is higher when the liquid metal was flooded. The medium of liquid metal layer exists between the reactor vessel and coolant. The overall heat transfer coefficient would be reduced due to the increased heat transfer resistance. The maximum temperature is about 150 $^{\circ}$C in the case of bare condition. About 30 $^{\circ}$C is increased in temperature when the liquid metal was flooded. The negative effect related to the temperature rise would enhance the ablation phenomenon inner surface of reactor

vessel. The remained thickness of reactor vessel becomes thinner when the temperature of outer surface is increased. It is expected that the reduced thickness is not a serious concern because the inner temperature reaches the melting point of reactor vessel regardless of flooding liquid metal. Reduction of thickness can be relatively lowered according to the temperature difference between the inner and outer surfaces of reactor vessel.

5.5 Conclusion

The present work found that significant reduction of focusing effect by liquid metal and extended surface area guarantee enough margin of successful IVR-ERVC without CHF issue even for large-sized power reactors. Improved heat transfer or reduced heat flux including large drop of focusing effect was confirmed by experimental results for a small-scaled facility to simulate the boiling phenomena under IVR-ERVC condition. The scaled facility uses R-123 and Gallium. The heat transfer area is enlarged up to 2 times compared to the original area of the reactor vessel. This effect is also named as "liquid metal fin".

Table 5-1 Corium cooling strategy for each reactor type

Reactor type	Power (MWe)	Cooling type
EPR	1,700	Ex-vessel corium cooling
APWR	1,600-1,700	Ex-vessel corium cooling
ESBWR	1,600	Ex-vessel corium cooling
ABWR	1,400-1,600	Ex-vessel corium cooling
AES-2006	1,150	Ex-vessel corium cooling
AP600	600	In-vessel corium cooling
AP1000	1,000	In-vessel corium cooling
SWR1000	1,000	In-vessel corium cooling
APR1400	1,400	In-vessel corium cooling or Ex-vessel corium cooling

Table 5-2 Main thermal properties of liquid metals as nuclear coolants

	Na	Pb	LBE	Ga
Atomic Weight	22.997	207.21	208	69.723
Melting Point (°C)	97.8	327.4	123.5	29.76
Boiling Point (°C)	892	1737	1670	2204
Density (kg/m^3)	880	10500	10300	6095
Specific Heat(J/kg-K)	1300	160	146	381.5
Thermal Conductivity (W/m-K)	76	16	11	29
Viscosity (cP)	0.34	2.25	1.7	1.810
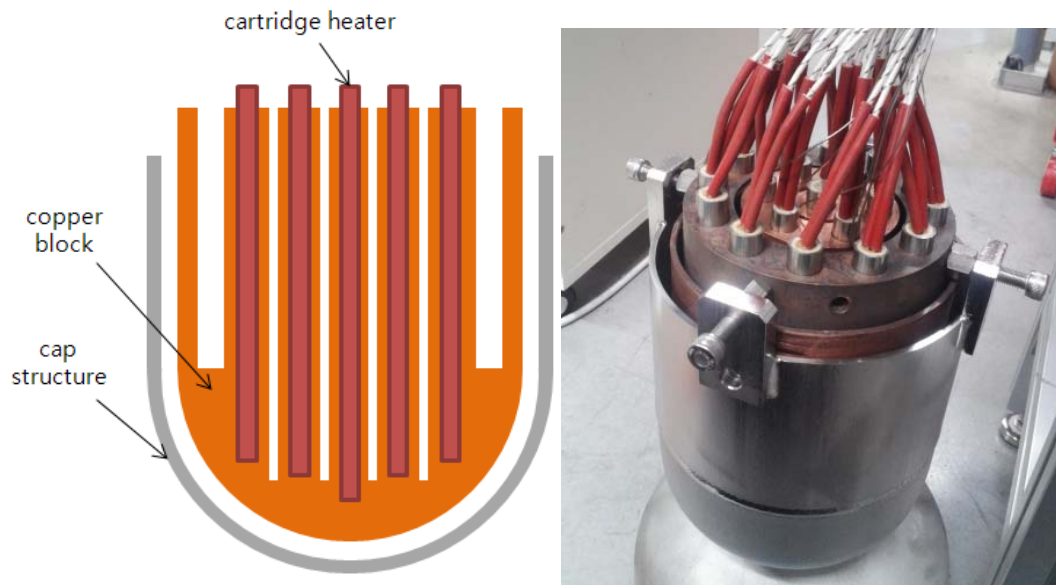
Fig. 5-1 Test section of Ga liquid metal IVR-ERVC
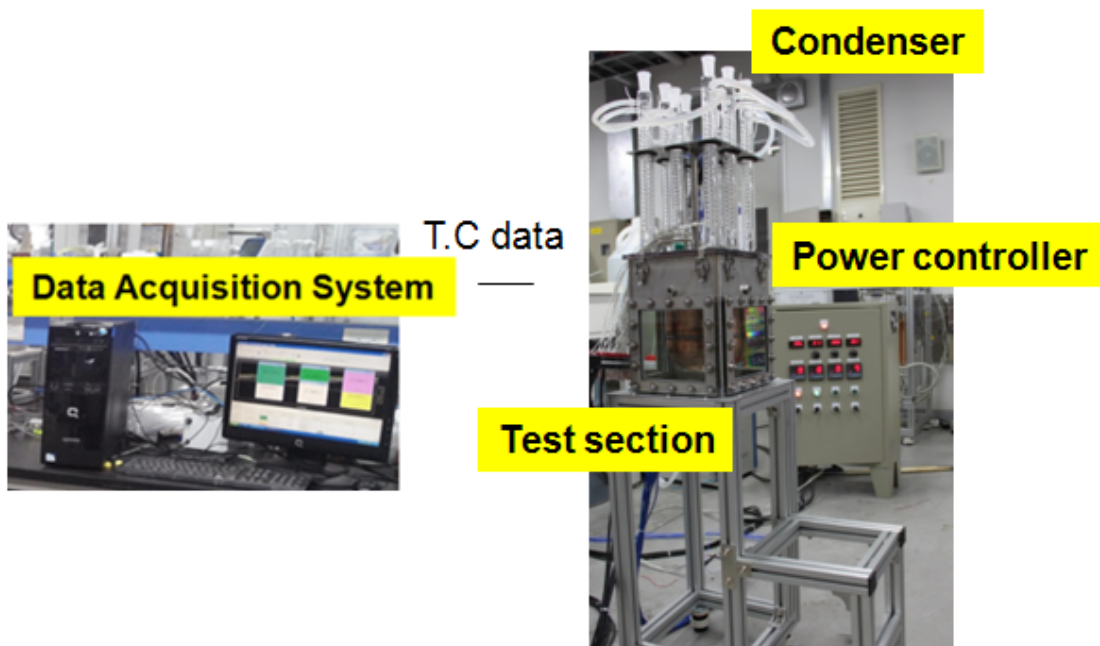
Fig. 5-2 Test facility for IVR-ERVC with liquid metal

(a) Case 1   (b) Case 2   (c) Case 3
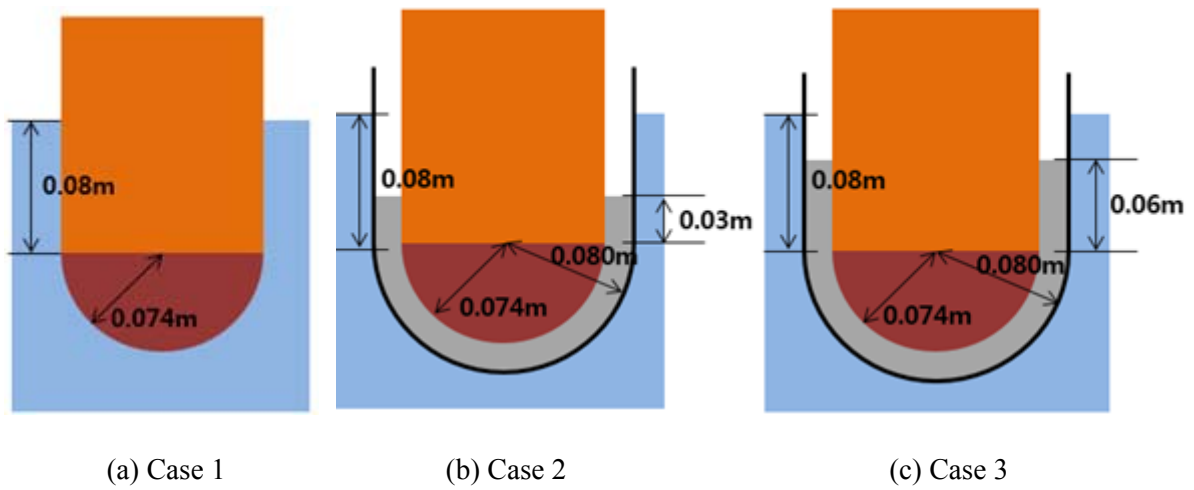
Fig. 5-3 Liquid metal flooding condition
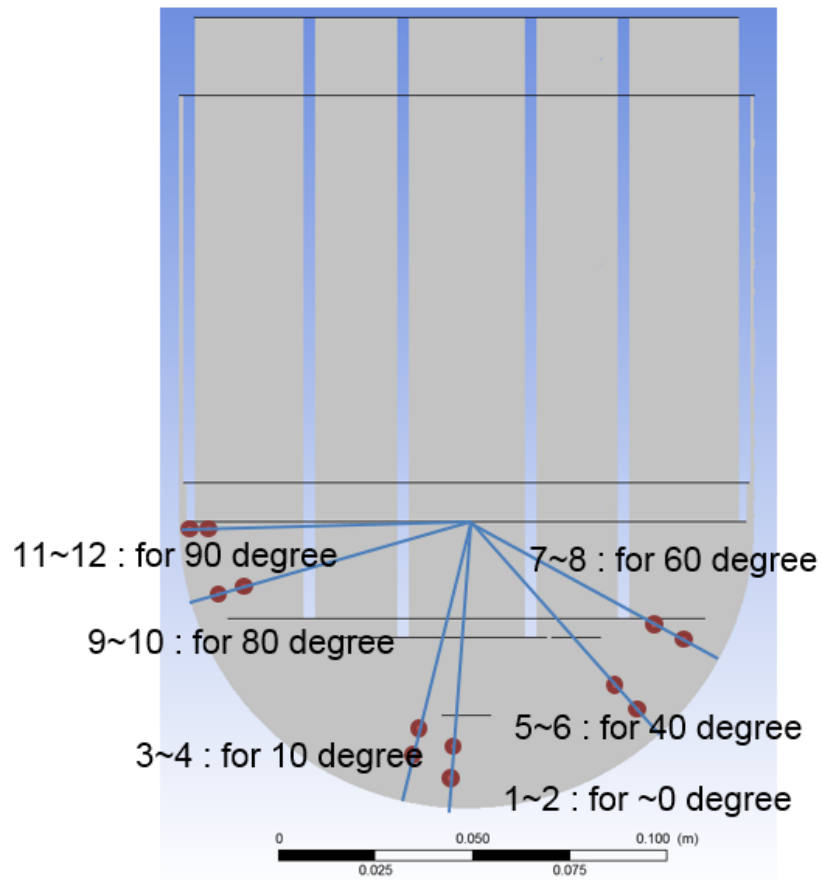
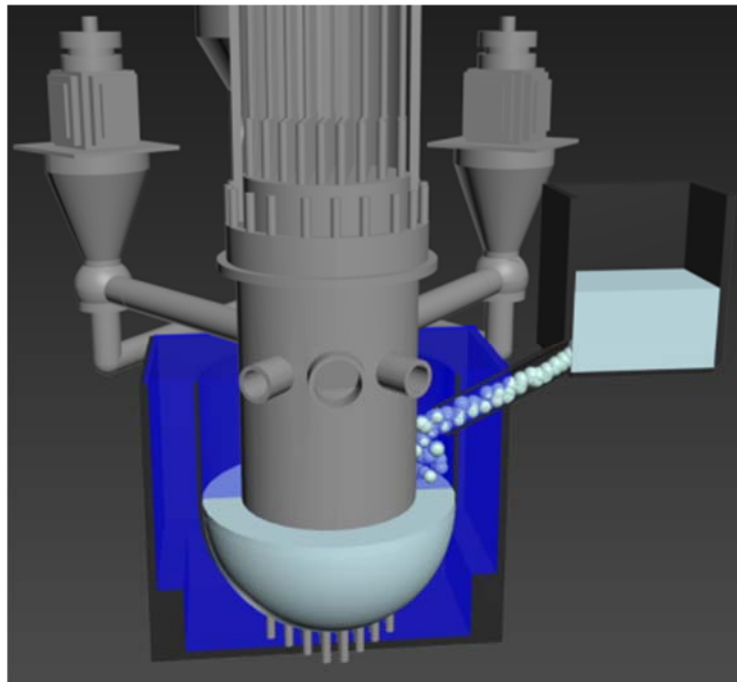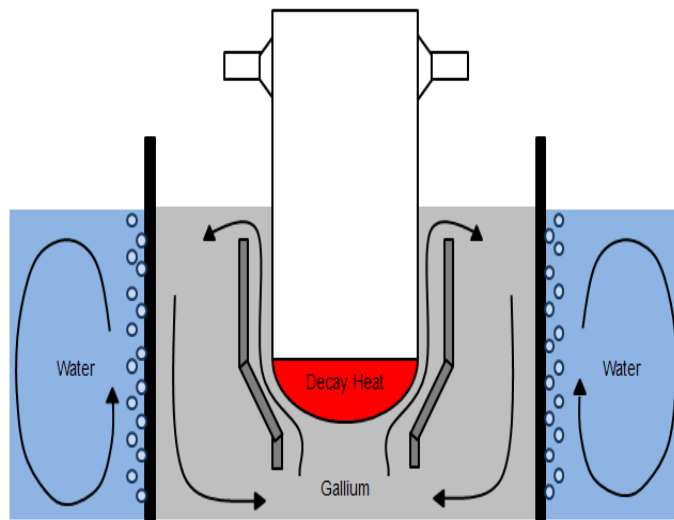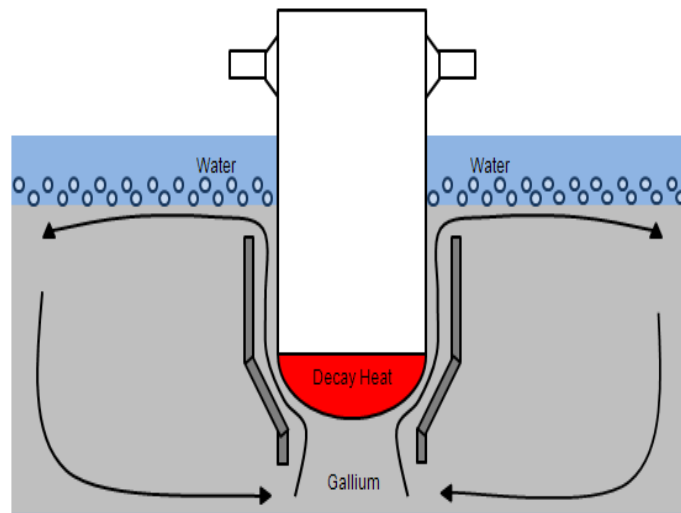Fig. 5-4 Location of embedded thermocouples

Fig. 5-5 IVR-ERVC Concept of Gallium Injection and Storage Tank

(a) Side cooling concept

(b) Upper cooling concept

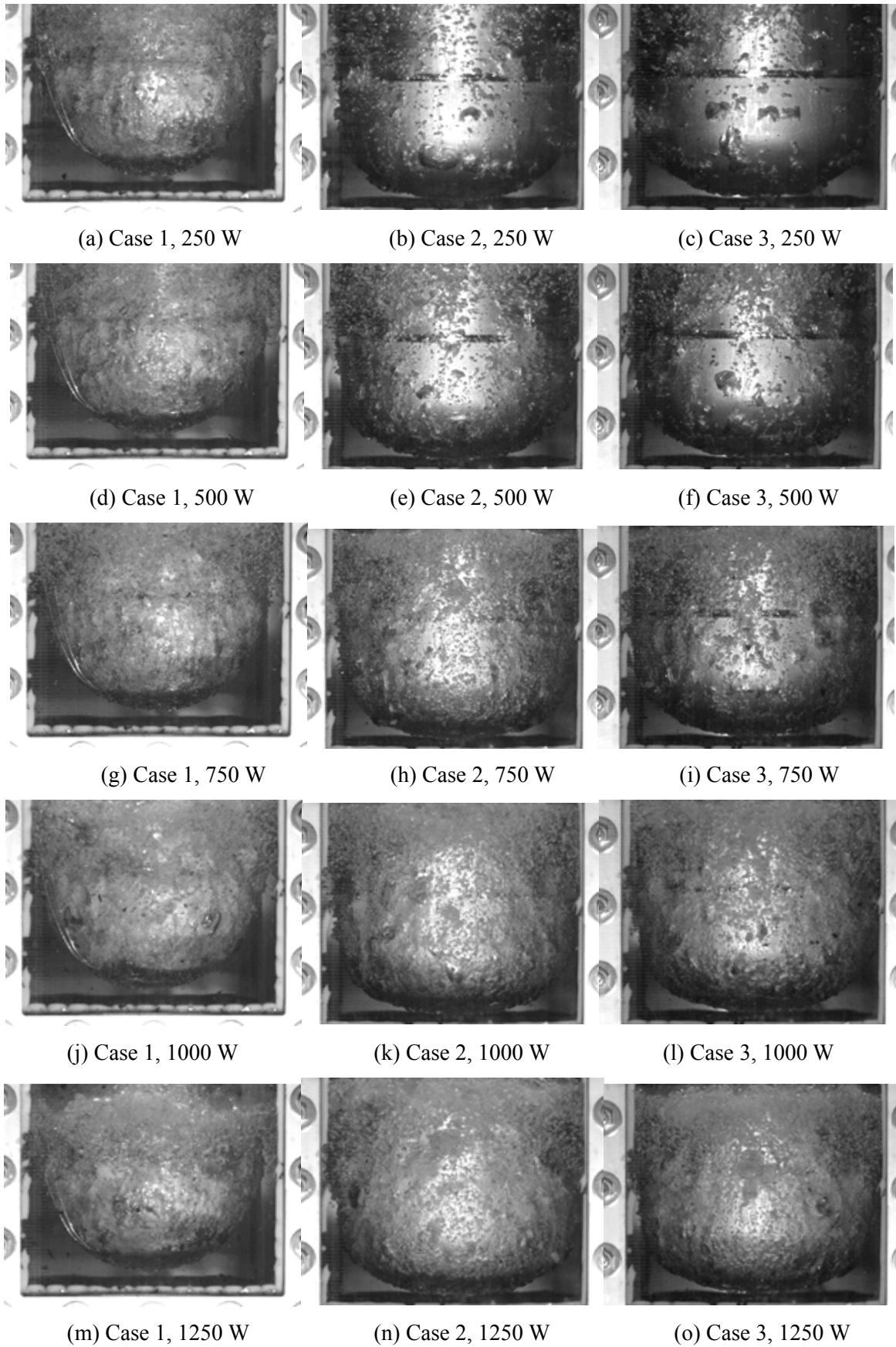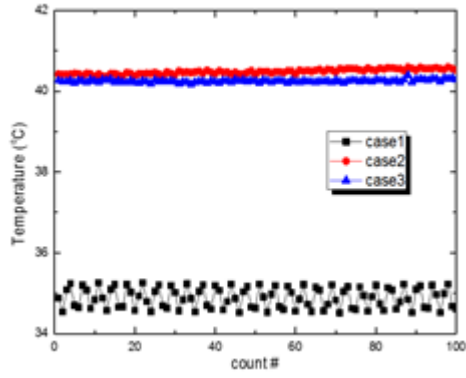Fig. 5-6 Configuration with liquid metal and borated water

(a) Case 1, 250 W   (b) Case 2, 250 W   (c) Case 3, 250 W

(d) Case 1, 500 W   (e) Case 2, 500 W   (f) Case 3, 500 W

(g) Case 1, 750 W   (h) Case 2, 750 W   (i) Case 3, 750 W

(j) Case 1, 1000 W   (k) Case 2, 1000 W   (l) Case 3, 1000 W

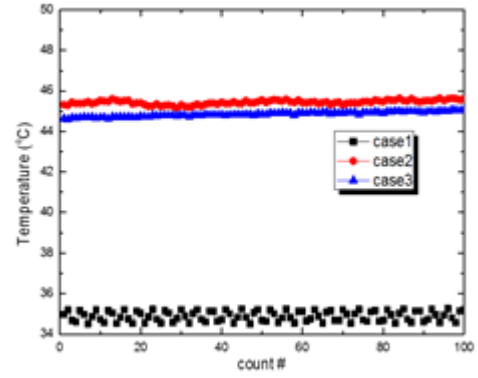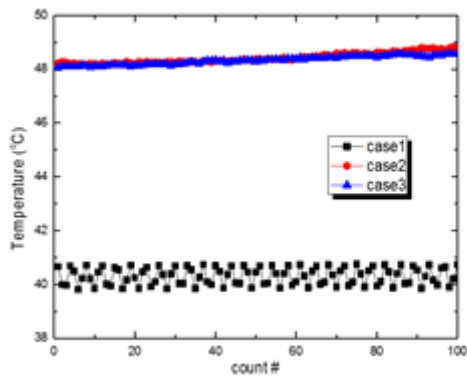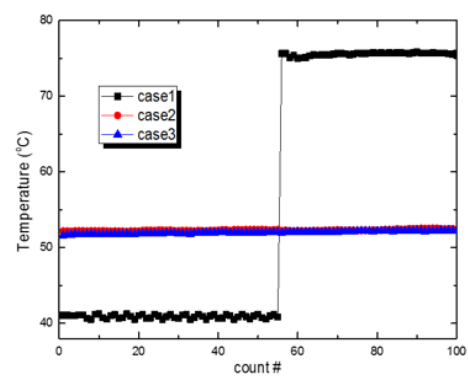(m) Case 1, 1250 W   (n) Case 2, 1250 W   (o) Case 3, 1250 W

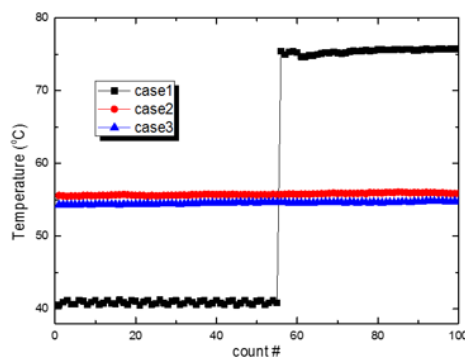Fig. 5-7 Vapor behavior on the heated surface

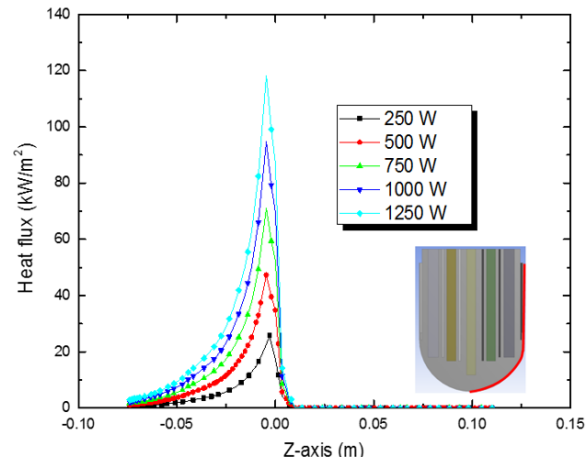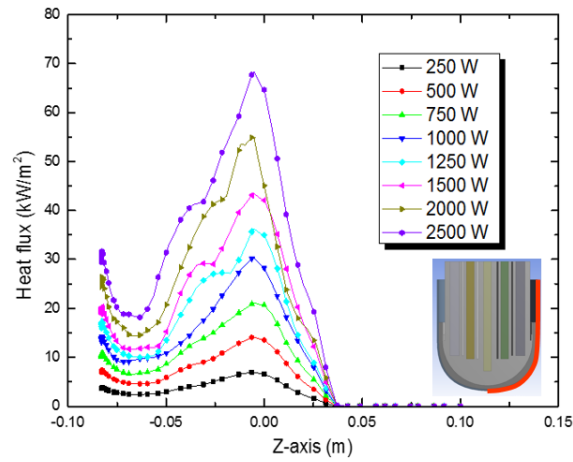(a) 250 W   (b) 500 W

(c) 750 W   (d) 1000 W

(e) 1250 W

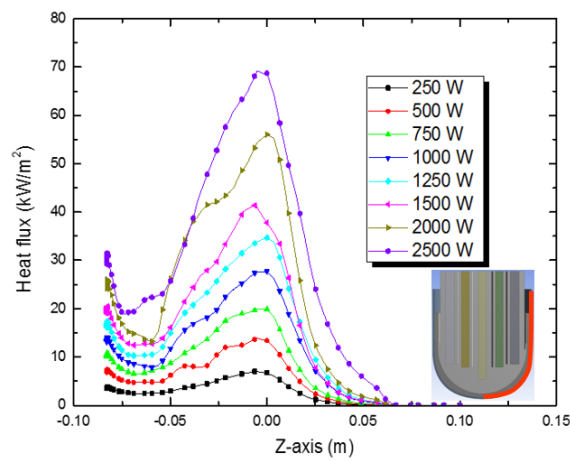Fig. 5-8 Temperature history according the power condition

(a) Case 1

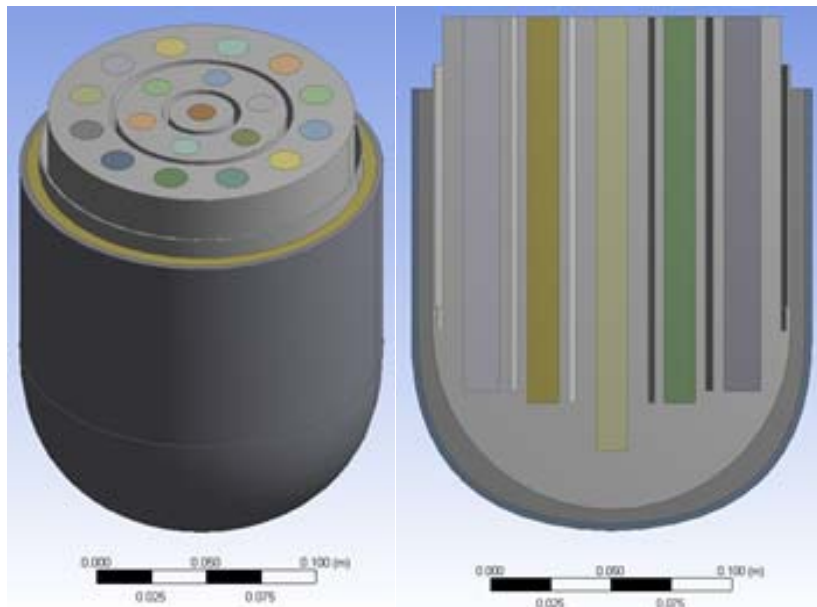
(b) Case 2

(c) Case3

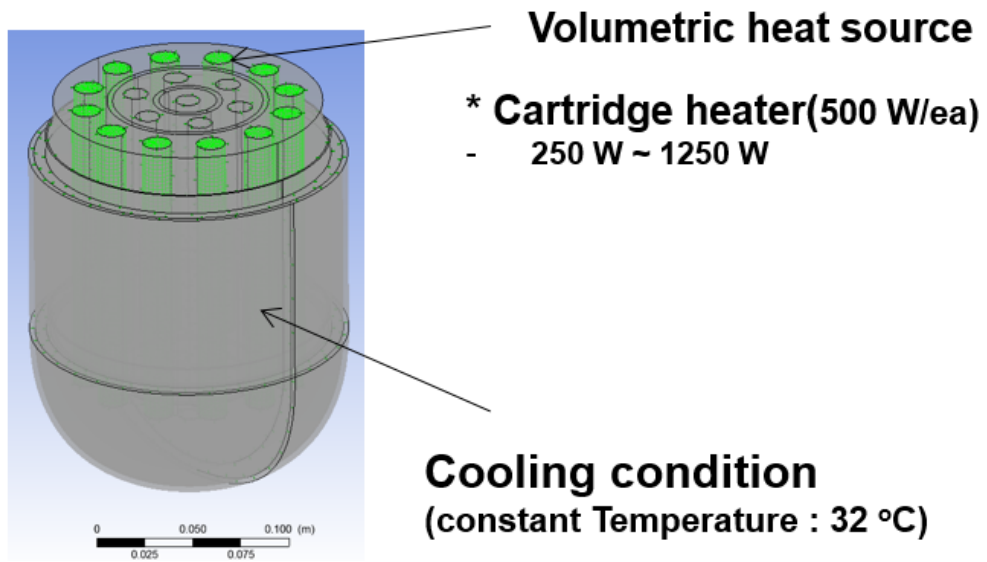Fig. 5-9 Heat flux profile on the boiling surface

Fig. 5-10 Geometry of test section for CFD analysis
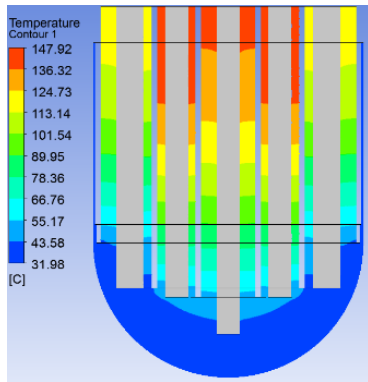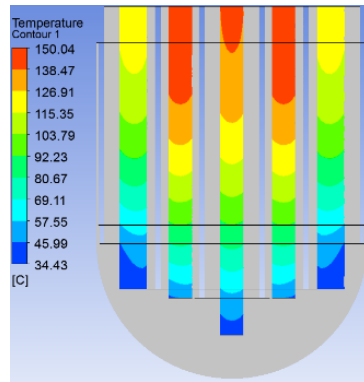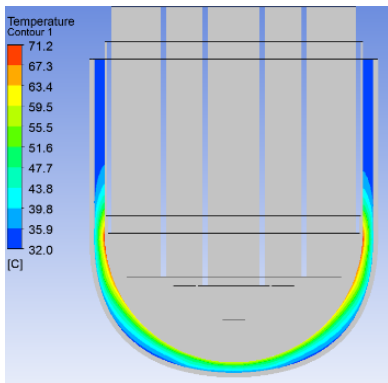
Fig. 5-11 Boundary condition in CFD
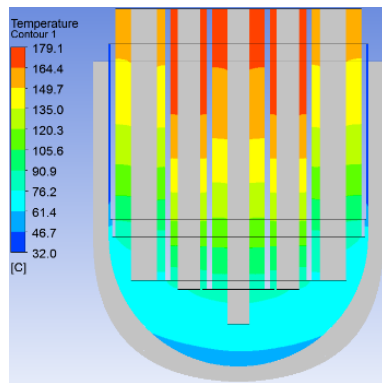
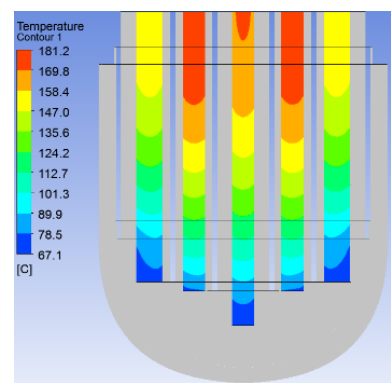(a) Copper domain   (b) Heater domain

(c) Gallium domain   (d) copper domain   (e) Heater domain

Fig. 5-12 Temperature distribution on test section

Chapter 6. CONCLUSIONS AND RECOMMENDATIONS

6.1 Conclusions

6.1.1 CHF enhancement of nanofluis

Nanofluids was studied to improve the thermal margin to CHF in IVR-ERVC system. Nanofluids with low concentrations can significantly enhance the pool/flow boiling CHF. In this work, various nanofluid was used as working fluids; graphene oxide, SiO_2, Al_2O_3, SiC nanofluid. The nanoparticle coated layer was formed on the heater surface.

Modified hydrodynamic instability model was established to predict the CHF for nanofluid in the pool boiling tests. The wetting characteristicof heating surface is not improved for graphene oxide nanofluid. It is not general case. The RT wavelength was observed to explore the unique CHF enhancement for graphene oxide nanofluid. This instability model could be related to flow boiling condition.

Graphene oxide nanofluid is superb candidate to improve the IVR-ERVC system. The enhancement ratio is the highest in all cases. The graphene oxide nanofluid has the good dispersion stability.

6.1.2 CHF enhancement of gallium flooding system

The application of IVR-ERVC system could be limited in a high power reactor due to the CHF phenomenon. To eliminate this issue, we propose using the liquid metal replacing the coolant. The liquid metal has high boiling point. The integrity of the reactor vessel could be ensured by flooding the liquid metal in surrounding the reactor vessel. The heat transfer area could be enlarged over 2 times on the basis of the original area for the reactor vessel. This phenomenon was named as "liquid metal fin".

6.2 Recommendations

Flooding the liquid metal would be attractive to improve the cooling capacity of IVR-ERVC system. There are not enough study results about this concept. Although we present the experimental results about the prevention of CHF phenomenon, responses to various accidents and further studies are needed to be utilized. Using the nanofluid is simple but powerful to improve the IVR-ERVC system. However, there are a large uncertainty based on the CHF enhancement data conducted in the different conditions with same nanofluid. The best way to improve the IVR-ERVC system is to take the two methods simultaneously. When using this way, we can expect a high thermal margin to secure the plant safety under a severe accident.

References

1. Oh, S.J.; Park, J.W.; Effectiveness of external reactor vessel cooling (ERVC) strategy for APR1400 and issues of phenomenological uncertainties. *In: WorkshopProceedings on Evaluation of Uncertainties in Relation to Severe Accidents and Level,* **2005**, 2

2. Chu, T.Y.; Bainbridge, B.L.; Simpson, R.B.; & Bentz, J.H.; Ex-vessel boiling experiments: laboratory-and reactor-scale testing of the flooded cavity concept for in-vessel core retention Part I: Observation of quenching of downward-facing surfaces. *Nuclear engineering and design*, **1997**, 169, 77-88.

3. Chu, T.Y.; Bentz, J.H.; Slezak, S.E.; & Pasedag, W.F.; Ex-vessel boiling experiments: laboratory-and reactor-scale testing of the flooded cavity concept for in-vessel core retention Part II: Reactor-scale boiling experiments of the flooded cavity concept for in-vessel core retention. *Nuclear engineering and design*, **1997**, 169, 89-99.

4. Rouge S.; Dor I., Geffraye G.; Reactor Vessel External Cooling for Corium Retention SULTAN Experimental Program and Modelling with CATHARE Code, *Workshop on in-vessel core debris retention and coolability*, **1998**.

5. Rouge, S.; SULTAN test facility for large-scale vessel coolability in natural convection at low pressure. *Nuclear engineering and design*, **1997**, 169, 185-195.

6. Rempe, J.L.; Knudson, D.L.; Condie, K.G.; Suh, K.Y.; Cheung, F.B. & Kim, S.B.; Corium retention for high power reactors by an in-vessel core catcher in combination with External Reactor Vessel Cooling. *Nuclear engineering and design*, **2004**, 230, 293-309.

7. Yang, J.; Cheung, F.B.; Rempe, J.L.; Suh, K.Y. & Kim, S.B.; Critical heat flux for downward-facing boiling on a coated hemispherical vessel surrounded by an insulation structure. *Nucl. Eng. Technol*, **2006**, 38

8. Yang, J.; Dizon, M.B.; Cheung, F.B.; Rempe, J.L.; Suh, K.Y. & Kim, S. B.; CHF enhancement by vessel coating for external reactor vessel cooling. *Nuclear engineering and design*, **2006**, 236, 1089-1098.

9. Rempe, J.L.; Suh, K.Y.; Cheung, F.B. & Kim, S. B.; In-vessel retention of molten corium: lessons learned and outstanding issues. *Nuclear technology*, **2008**, 161, 210-267.

10. Theofanous, T.G.; Liu, C.; Additon, S.; Angelini, S.; Kymäläinen, O. & Salmassi, T.;.In-vessel coolability and retention of a core melt. *Nuclear Engineering and Design*, **1997**, 169, 1-48.

11. Theofanous, T.G. & Syri, S.; The coolability limits of a reactor pressure vessel lower head. *Nuclear engineering and design*, **1997**, 169, 59-76.

12. Dinh, T.N.; Tu, J.P. & Theofanous, T.G.; Two-phase natural circulation flow in AP-1000 in-vessel retention-related ULPU-V facility experiments. *In Proceedings of the 2004 international congress on advances in nuclear power plants-ICAPP'04*, **2004**

13. Park, H.M.; Jeong, Y.H. & Heo, S.; The effect of the geometric scale on the critical heat flux for the top of the reactor vessel lower head. *Nuclear Engineering and Design,* **2013**, 258, 176-183.

14. Jeong, Y.H., Chang, S.H., & Baek, W.P.; Critical heat flux experiments on the reactor vessel wall using 2-D slice test section. *Nuclear technology*, **2005**, 152, 162-169.

15. Vishnev, I.; Effect of orienting the hot surface with respect to the gravitational field on the critical nucleate boiling of a liquid. *J. Eng. Phys. Thermophys*. **1973**, 24, 43–48.

16. Lyon, D.; Boiling heat transfer and peak nucleate boiling fluxes in saturated liquid helium between critical temperatures. *Intern. Adv. Cryog. Eng*. 1965, 10, 371–379.

17. El-Genk, M.S.; Guo, Z.; Transient boiling from inclined and downward-facing surfaces in a saturated pool. *Int. J. Refrig*. **1993**, 16, 414–422.

18. Kwark, S.M.; Amaya, M.; Moon, H. & You, S.M.; Effect of soluble additives, boric acid (H_3BO_3) and salt (NaCl) in pool boiling heat transfer. *Nucl. Eng. Technol*, **2011**, 43, 195-204.

19. Jeong, Y.H.; Chang, W.J. & Chang, S.H.; Wettability of heated surfaces under pool boiling using surfactant solutions and nano-fluids. *Int. J. Heat Mass Transfer*, 2008, 51, 3025-3031.

20. Milanova, D. & Kumar, R.; Role of ions in pool boiling heat transfer of pure and silica nanofluids. *Applied Physics Letters*, **2005**, 87, 233107.

21. Lee, J. & Chang, S. H.; An experimental study on CHF in pool boiling system with SA508 test heater under atmospheric pressure. *Nuclear Engineering and Design*, **2012**, 250, 720-724.

22. You, S.M.; Kim, J.; Kim, K.; Effect of nanoparticles on critical heat flux of water in pool boiling heat transfer. *Applied Physics Letters*, **2003**, 83, 3374.

23. Bang, I.C.; Jeong, J.H.; Nanotechnology for advanced nuclear thermal hydraulics and safety: boiling and condensation. *Nucl. Eng. Technol*. **2011**, 43, 217–242.

24. Bang, I.C.; Chang, S.H.; Boiling heat transfer performance and phenomena of Al2O3–water nano-fluids from a plain surface in a pool. *Int. J. Heat Mass Transfer*, **2005**, 48, 2407–2419.

25. Park, S.D.; Lee, S.W.; Kang, S.; Bang, I.C.; Kim, J.H.; Shin, H.S.; Lee, D.W.; Effects of nanofluids containing graphene/graphene-oxide nanosheets on critical heat flux. *Appl. Phys. Lett.*, **2010**, 97, 023103.

26. Kim, S.J.; Bang, I.C.; Buongiorno, J.; Hu, L.; Surface wettability change during pool boiling of nanofluids and its effect on critical heat flux. *Int. J. Heat Mass Transfer*, **2007**, 50, 4105–4116.

27. Bang, I.C.; Kim, J.H.; Thermal-fluid characterizations of ZnO and SiC nanofluids for advanced nuclear power plants. *Nucl. Technol.*, **2010**, 170, 281.

28. Buongiorno, J.; Hu, L.W.; Apostolakis, G.; Hannink, R.; Lucas, T.; Chupin, A.; A feasibility assessment of the use of nanofluids to enhance the in-vessel retention capability in light-water reactors. *Nuclear Engineering and Design*, **2009**, 239, 941–948.

29. Li, D.; Müller, M. B.; Gilje, S.; Kaner, R. B. & Wallace, G. G.; Processable aqueous dispersions of graphene nanosheets. *Nature nanotechnology*, **2008**, 3, 101-105.

30. Kutateladze S.; A hydrodynamic theory of changes in the boiling process under free convection conditions, *Izv. Akad. Nauk SSSR, Otd. Tech. Nauk 4*, **1951**, 529-536.

31. Zuber N.; Hydrodynamic aspects of boiling heat transfer*, (Thesis), California. Univ., Los Angeles; and Ramo-Wooldridge Corp., Los Angeles*, **1959**.

32. Ferjančič K. & Golobič I.; Surface effects on pool boiling CHF, *Experimental thermal and fluid science*, **2002**, 25, 565-571.

33. Golobič I. & Ferjančič K.; The role of enhanced coated surface in pool boiling CHF in FC-72, *Heat and mass transfer*, **2000**, 36, 525-531.

34. Haramura Y. & Katto Y.; A new hydrodynamic model of critical heat flux, applicable widely to both pool and forced convection boiling on submerged bodies in saturated liquids, *Int. J. Heat Mass Transfer*, **1983**, 26, 389-399.

35. Sadasivan P.; Chappidi P., Unal, C.; Nelson R.; Possible mechanisms of macrolayer formation, *International communications in heat and mass transfer*, **1992**, 19, 801-815.

36. Theofanous T.G.; Dinh T.N.; High heat flux boiling and burnout as microphysical phenomena: mounting evidence and opportunities, *Multiphase Science and Technology*, **2006**, 18, 1-26

37. Theofanous T.G.; Dinh T.N.; Tu, J. P. & Dinh A. T.; The boiling crisis phenomenon: Part II: dryout dynamics and burnout, *Experimental Thermal and Fluid Science*, **2002**, 26, 793-810.

38. Rohsenow W.M.; Griffith P.; Correlation of maximum heat flux data for boiling of saturated liquids, *Cambridge, Mass.: Massachusetts Institute of Technology, Division of Industrial Cooperation*, **1955**.

39. Kolev N.; How accurately can we predict nucleate boiling?, *Experimental Thermal and Fluid Science*, **1995**, 10, 370-378.

40. Bang I.C. & Jeong J.H.; Nanotechnology for advanced nuclear thermal-hydraulics and safety: boiling and condensation, *Nucl. Eng. Technol*, **2011**, 43, 217-242.

41. You, S. M.; Kim, J. H. & Kim, K. H.; Effect of nanoparticles on critical heat flux of water in pool boiling heat transfer, *Applied Physics Letters*, **2003**, 83, 3374-3376.

42. Kim, S. J.; Bang, I. C.; Buongiorno, J. & Hu, L. W.; Effects of nanoparticle deposition on surface wettability influencing boiling heat transfer in nanofluids, *Applied Physics Letters*, **2006**, 89, 153107.

43. Kim H.; Kim J. & Kim M.H.; Effect of nanoparticles on CHF enhancement in pool boiling of nano-fluids, *Int. J. Heat Mass Transfer*, **2006**, 49, 5070-5074

44. Kandlikar S.G.; A theoretical model to predict pool boiling CHF incorporating effects of contact angle and orientation, *Transactions-american Society of Mechanical Engineers Journal of Heat Transfer*, **2001**, 123, 1071-1079.

45. Duangthongsuk W. & Wongwises S.; Effect of thermophysical properties models on the predicting of the convective heat transfer coefficient for low concentration nanofluid, *International Communications in Heat and Mass Transfer*, **2008**, 35, 1320-1326.

46. Liter S.G. & Kaviany M.; Pool-boiling CHF enhancement by modulated porous-layer coating: theory and experiment, *Int. J. Heat Mass Transfer*, **2001**, 44, 4287-4311.

47. Polezhaev Y.V. & Kovalev S., Modelling heat transfer with boiling on porous structures, *Thermal engineering*, **1990**, 37, 617-621.

48. Lienhard J.H. and Dhir V.K.; On the Prediction of the Minimum Pool Boiling Heat Flux, *Journal of Heat Transfer*, **1980**, 102, 457-460.

49. Duluc M.C. and François M.X.; Steady-state transition boiling on thin wires in liquid nitrogen. The role of Taylor wavelength, *Cryogenics*, **1998**, 38, 631-638.

50. Park, S.D.; Lee, S.W.; Kang, S.; Kim, S.M.; Bang, I.C.; Pool boiling CHFenhancement by graphene-oxide nanofluid under nuclear coolant chemicalenvironments, *Nuclear Engineering and Design,* **2012**, 252, 184–191.

51. Lee, J.; Jeong, Y.H. & Chang, S.H.; CHF enhancement in flow boiling system with TSP and boric acid solutions under atmospheric pressure, *Nuclear Engineering and Design*, **2010**, 240, 3594-3600.

52. Jeong, Y. H.; Sarwar, M.S. & Chang, S.H.; Flow boiling CHF enhancement with surfactant solutions under atmospheric pressure. *Int. J. Heat Mass Transfer*, **2008**, 51, 1913-1919.

53. Kim, T. I.; Park, H. M. & Chang, S. H.; CHF experiments using a 2-D curved test section with additives for IVR-ERVC strategy. *Nuclear engineering and design*, **2012**, 243, 272-278.

54. Kim, S.J.; McKrell, T.; Buongiorno, J.; Hu, L.W.; Alumina nanoparticles enhance the flow boiling critical heat flux of water at low pressure. *Journal of Heat Transfer*, **2008**, 130, 044501.

55. Kim, S.J.; Mckrell, T.; Buongiorno, J.; Hu, L.W.; Experimental study of flow critical heat flux in alumina-water, zinc-oxide-water, and diamond-water nanofluids. *Journal of Heat Transfer*, **2009**, 131, 043204.

56. Kim, T.I.; Jeong, Y.H.; Chang, S.H.; An experimental study on CHF enhancement in flow boiling using Al_2O_3 nano-fluid, *Int. J. Heat Mass Transfer*, **2010**, 53, 1015-1022.

57. Vafaei, S. & Dongsheng, W.; Critical Heat Flux (CHF) of Subcooled Flow Boiling of Alumina Nanofluids in a Horizontal Microchannel, *Journal of Heat Transfer*, **2010**, 132, 102404.

58. Lee, S.W.; Park, S.D.; Kang, S.; Kim, S.M.; Seo, H.; Lee, D.W.; Bang, I.C.; Critical heat flux enhancement in flow boiling of Al_2O_3 and SiC nanofluids under low pressure and low flow conditions. *Nucl. Eng. Technol*, **2012**, 44, 429-436.

59. Ha, K.S.; Cheung, F.B.; Park, R.J.; Kim, S.B.; Evaluations of two-phase natural circulation flow induced in the reactor vessel annular gap under ERVC conditions, *Nuclear Engineering and Design,* **2012**, 253, 114-124

60. Park, H.M.; Jeong, Y.H.; Heo, Sun.; The effect of the geometric scale on the critical heat flux for the top of the reactor vessel lower head. *Nuclear Engineering and design*, **2013**, 258, 176-183.

61. Carey, V.P.; Liquid–Vapor Phase-Change Phenomena. *Hemisphere Publishing Corporation*, **1992**

62. Arik, M. & Bar-Cohen, A.; Effusivity-based correlation of surface property effects in pool boiling CHF of dielectric liquids. *Int. J. Heat Mass Transfer*, **2003**, 46, 3755-3764

63. Berna G.A.; Beyer G.; Davis K.; Lanning D.; FRAPCON-3: A computer code for the calculation of steady-state, thermal-mechanical behavior of oxide fuel rods for high burnup, *Nuclear Regulatory Commission*, **1997**

64. Holt M.; Campbell R.J.; Nikitin M.B.; Fukushima nuclear disaster, *Congressional Research Service*, **2012**

65. Park S.D. & Bang I.C.; Feasibility of flooding the reactor cavity with liquid gallium coolant for IVR-ERVC strategy, *Nuclear Engineering and Design*, **2013**, 258, 13-18

66. Oh S. & Kim H.; Effectiveness of external reactor vessel cooling (ERVC) strategy for APR1400 and issues of phenomenological uncertainties, *Evaluation of uncertainties in relation to severe accidents and level,* **2005**, 2.

Acknowledgement (감사의 글)

UNIST에 입학하여 5년 반의 짧으면서도 긴 기간을 거쳐 석박사 통합과정을 마치게 되었습니다. 학위과정 중에는 새로운 것에 대한 호기심과 고민의 연속으로 시간이 짧게만 느껴졌습니다. 돌이켜 생각해보니, 긴 시간 동안 항상 옆에서 같이 고민해주고, 생각을 공유해준 많은 분들과의 끝나지 않는 추억으로 채워진 것 같습니다. 항상 옆에서 응원해주시고, 도움을 주신 많은 분들에게 이 자리를 빌려 감사의 마음을 전합니다.

우선 석박사 통합과정 동안 아버지처럼 항상 사랑과 열정을 가지고 많은 관심과 조언을 주신 방인철 교수님께 머리 숙여 감사 드립니다. 항상 어떤 문제에 대해서 고민하고, 새로운 아이디어와 해결책을 제시하시는 것을 보고 연구자가 가야 할 방향과 자세에 대해 많은 것을 배웠습니다. 아직까지 제가 많은 부분에서 부족하여 죄송스럽습니다. 지도해 주신 것을 기초로 하여 더욱 노력하여 발전하도록 하겠습니다. 그리고 바쁘신 가운데 논문을 지도해주시고 격려해주신 김지현 교수님, 박형욱 교수님, 방광현 교수님, 최기용 박사님. 감사합니다.

그리고 연구실 가족들에게도 감사의 마음을 전합니다. 지금은 졸업하고 한 가족의 가장과 훌륭한 연구자로써의 길을 걷고 있는 승원이형, 직장에서 인정받고 있는 성만이. 같이 연구실에 있을 때, 받았던 많은 도움들이 기억나네요. 그리고, 내 동기인 사라. 항상 꼼꼼함과 후배들을 잘 이끌어 주는 걸 보면서 많이 배웠어. 유일한 서울남자인 한이. 많은 일을 열심히 하면서 재미난 결과를 내면서도 후배들을 잘 이끌어 줘서 고맙다. 그리고 경모, 성보, 석빈, 인국, 효, 영신. 다들 자기의 연구분야에서 너무 열심히 해줘서 고마워. 그리고 핵재료 연구랩의 상훈이형, 종진이형, 정석이형, 주앙이형, 경준이, 상일이. 방사선 연구랩의 동한이형, 핵연료 연구랩에 있는 병진이형, 노심 연구랩에 있는 태우. 부족한 제가 졸업하는데 다들 도움을 주셔서 감사합니다.

내 대학 동기인 희규, 동형, 희원, 인현, 영락아. 다들 고민도 잘 받아주고, 충고도 해줘

서 고맙다. 지금은 졸업했지만 KAIST에서 저를 도와주신 태일씨, 종혁씨, 해민씨 고맙습니다. 그리고 해양대에 있는 형탁씨. 나중에 졸업하고 한번 볼까요? 그리고 제가 학위과정을 무사히 마치는데 큰 도움을 주신 프리마테크의 김만영 사장님과 테스의 이종수 사장님 및 업체 관계자 분들에게 감사인사 드립니다.

마지막으로 항상 저를 믿어주시고, 저에게 힘을 주시는 부모님에게 감사하고 사랑한다는 말을 전합니다. 항상 부모님에 해주신 좋은 말씀을 가슴에 새겨 누구에게도 부끄럽지 않는 장한 아들이 되도록 하겠습니다. 별로 신경 안쓰는 듯 하면서도 잘 챙겨주시는 누나와 매형에게도 감사의 말을 전달합니다.